

Primitive asymptotics in ϕ^4 vector theory

Paul-Hermann Balduf*, Johannes Thürigen†

December 12, 2024

A longstanding conjecture in ϕ^4 theory is that primitive graphs dominate the beta function asymptotically at large loop order in the minimal-subtraction scheme. Here we investigate this issue by exploiting additional combinatorial structure coming from an extension to vectors with $O(N)$ symmetry. For the 0-dimensional case, we calculate the N -dependent generating function of primitive graphs and its asymptotics, including arbitrarily many subleading corrections. We find that the leading asymptotic growth rate becomes visible only above ≈ 25 loops, while data at lower order is suggestive of a wrong asymptotics. Our results also yield the exact asymptotics of Martin invariants.

In 4D, each graph comes with a nontrivial Feynman integral, its period. We give bounds on the degree in N for primitive and non-primitive graphs, and construct the primitive graphs of highest degree explicitly using a bijection method. We calculate the 4D primitive beta function numerically up to 17 loops. The qualitative behaviour turns out to be similar to the 0D series, with a small but systematic tendency for the 4D data to grow faster with N , indicating a correlation between periods and $O(N)$ -symmetry factors. The zeros of the 4D primitive beta function approach their asymptotic locations quickly, but, like in the 0-dimensional case, the growth rate of the 4D primitive beta function does not match its asymptotics even at 17 loops.

Our results improve on the knowledge of asymptotics in QFT by putting individual observables into a broader context of ϕ^4 theory. We provide concrete analytic and numerical values to demonstrate that both in the 0D and 4D theory, the reliability of asymptotic expansions greatly depends on the quantity in question. Even if certain quantities are in excellent agreement with the asymptotics already below 10 loops, this must not be mistaken as evidence that overall an asymptotic regime has been reached.

*Mathematical Institute, University of Oxford, Andrew Wiles Building, Woodstock Road, Oxford, OX2 6GG, United Kingdom

†Institute for Analysis and Numerics, University of Münster, Orleans-Ring 10, 48149 Münster, Germany

Contents

1. Introduction	3
1.1. Background and Motivation	3
1.2. Outline and results	4
1.3. Discussion and Outlook	8
2. Setup	10
2.1. $O(N)$ -symmetric ϕ^4 theory	10
2.2. Renormalization, primitive graphs, and periods	14
2.3. The beta function	15
2.4. Martin invariant	18
3. QFT in zero dimensions	18
3.1. Vacuum graphs	19
3.2. External edges, connected and 1PI graphs	20
3.3. Counterterms, primitive graphs, Martin invariants	24
3.4. Asymptotics	25
3.5. Asymptotics of primitive graphs	28
3.6. Asymptotics of Martin invariants	31
3.7. The large- N limit	31
4. Classification of leading N dependence	32
4.1. Dual graphs	32
4.2. The duals of leading-order primitive graphs	35
4.3. Enumeration of graphs at low loop order	42
4.4. Non-primitive graphs	43
5. ϕ^4 theory in four dimensions	46
5.1. Coefficients and evaluations of β_L^{prim} in four dimensions	47
5.2. N dependence of the beta function in zero and four dimensions	47
5.3. Asymptotic growth rate of the beta function at large loop order	49
A. Combinatorial properties of the circuit partition polynomial	52
B. Tables	57

1. Introduction

1.1. Background and Motivation

In the renormalization of perturbative quantum field theory (QFT), one can view *primitive* graphs as the building blocks of the theory. These are the Feynman graphs without subdivergences, and as such one can generate all other Feynman graphs by recursive insertion of primitive graphs into each other. This can be used to define a particular form of Dyson-Schwinger type equations [1, 2] based on the Hopf-algebraic description [3] of perturbative renormalization. In realistic QFTs, the number Feynman graphs grows factorially with the loop order, and the number of primitive graphs grows to leading order at the same rate, which implies that primitive graphs asymptotically represent a constant fraction of all Feynman graphs [4]. In the case of scalar ϕ^4 theory in four dimensions, this fraction is $e^{-\frac{15}{4}} \approx 2.3\%$, but it is conjectured that primitive graphs dominate the large-loop asymptotics of the beta function in the minimal subtraction scheme [5, 6]. However, there seems to be no proof yet and numerical calculations even up to 18 loops did not show clear quantitative agreement with the expected asymptotics [7].

One way to improve the control of scalar field theory is to extend the field to an N -dimensional vector and demand invariance of the theory under $O(N)$ symmetry transformations. Famously, this allows for another perturbative expansion using $\frac{1}{N}$ as expansion parameter; it often yields interesting results since low-order contributions in one expansion can reappear as nonperturbative effects in the other expansion. The large- N expansion of $O(N)$ -symmetric theories has been studied extensively starting from the 1970s [8–13], reviews include [14, 15]. The limit is dominated by “bubble” graphs, which are chains of 1-loop multiedges (*fish* graphs). Large- N expansions have also been fruitful with respect to the number N_f of fermions, such as in the Gross-Neveu model [16], see e.g. [17, 18]. In quantum chromodynamics [19] and matrix models [20], planar graphs dominate the large- N expansion. Generalizing to higher rank tensors leads to certain restricted classes of graphs in the large- N limit [21, 22]. These so-called melonic diagrams have an iterative structure, too. In particular, insertion of melonic diagrams does not change the degree [23] and reducing all melonic subdiagrams leads to so-called schemes [24]. This is similar to the recursive structure of subdivergences, but the notion of primitive graphs is finer than that of schemes: inserting a scheme into a scheme yields again a scheme; but inserting a primitive into a primitive gives by definition a non-primitive graph. In particular, schemes are not necessarily primitive.

Here we will focus on the properties of primitive graphs of $O(N)$ -symmetric ϕ_4^4 theory. Being subleading in the large- N limit, they have not received particular attention in the literature yet. The present article is meant to fill that gap. There are a number of reasons to undertake this endeavor:

Firstly, for the perturbative expansion of ϕ^4 theory in small coupling constant, the asymptotics at large loop order has been determined from instanton calculations [6]. As mentioned above, it is an open problem to what extent this prediction matches perturbation theory at low loop order, and which loop order marks the transition to

the “asymptotic regime”. In [7], the first author observed that the absolute value of certain quantities starts to behave asymptotically from $L \geq 10$ loops, but there still is a discrepancy between the observed and the expected growth rate for the primitive beta function even at $L = 18$ loops. The $O(N)$ symmetry can help to clarify this situation because it supplies additional quantities, and a functional dependence on N , whose asymptotics can be studied.

Secondly, the large- N limit of the vector model is given by chains of 1-loop *fish* graphs. The 1-loop graph, at the same time, determines the leading term of the log-expansion in perturbative renormalization and certain classes of chained and nested 1-loop graphs can be solved analytically to all orders [25–28]. On the Hopf algebra side, it is well understood how the subleading orders of the log-expansion are determined by primitive graphs of higher loop order [29–32]. The N dependence of primitive graphs therefore has direct bearing on the N dependence of the leading-log expansion.

Thirdly, recent years have seen much progress with understanding the Feynman integrals of primitive graphs in ϕ^4 theory, called *Feynman periods*. In particular, the *Martin invariant* [33], which is the (analytic continuation of the) $O(N)$ symmetry factor evaluated at $N = -2$, respects all known symmetries of the period and is furthermore strongly correlated with the numerical value of the Feynman integral [34]. It therefore appears that the $O(N)$ symmetry factors of primitive graphs have a meaning for Feynman integrals *as such*, beyond being a weighting factor in the perturbative expansion.

Fourthly, the case of $O(N)$ symmetry, which is a comparably simple group, could serve as an illustrative case for the interplay of renormalization and symmetries in the form of Hopf ideals [1, 35, 36]. Factorization relations of $O(N)$ symmetry factors in that sense take the role of Ward identities, which guarantee renormalizability.

1.2. Outline and results

In the present subsection, we give a brief summary of all major findings of the article, with references to the corresponding later sections. The subsequent subsection (section 1.3) is a discussion of the takeaways and remaining open questions.

Section 2 introduces $O(N)$ -symmetric ϕ^4 theory and the central objects to be examined in the article: Each Feynman graph comes not only with the symmetry factor of automorphisms $\frac{1}{|\text{Aut}|}$ but also has an $O(N)$ -symmetry factor $T(G, N)$ (definition 2). This is a polynomial in N which one can construct graphically by decomposing every vertex of the graph into pairs of edges. It factorizes under insertion of subgraphs (section 2.1). The *beta function* β describes the theory’s scale-dependence and can be computed from a sum of all vertex-type Feynman integrals. The *primitive beta function* β^{prim} is the sum restricted to primitive vertex-type graphs (eq. (2.15)), it is given by a sum over *periods* $\mathcal{P}(G) \in \mathbb{R}$ (section 2.2) weighted by the symmetry factors $\frac{1}{|\text{Aut}|}$ and $T(G, N)$. Expanding in the number of loops L , the coefficients of the beta function β_L grow factorially in L . According to conjecture 1 [5], its primitive part, β_L^{prim} , grows at the same rate and dominates the beta function at large loop order. Finally, we introduce the *Martin invariant* $M^{[1]}(G) \in \mathbb{N}$ which can be expressed as $T(G, -2)$. It is known

to respect period symmetries, and its numerical value is strongly correlated with the numerical value of the period (section 2.4).

In section 3, we use 0-dimensional QFT to enumerate the Feynman graphs of $O(N)$ -symmetric ϕ^4 theory, weighted by their automorphism- and $O(N)$ -symmetry factors. We determine the exact N -dependent $L \rightarrow \infty$ asymptotics, including subleading corrections.

- The vacuum path integral in 0-dimensional QFT is an ordinary integral. Its power series solution for arbitrary (not necessarily integer) N can be found exactly with the help of a *Hubbard-Stratonovich transformation* (eq. (3.3)), which is a transformation of the integration variable from the multi-component field ϕ to a single intermediate field σ . This series enumerates vacuum graphs, weighted by $T(G, N)$ and $\frac{1}{|\text{Aut}(G)|}$ (fig. 4, section 3.1).
- We generalize this to a generating function $Z(\hbar, j)$ (eq. (3.10)) with sources such that the series coefficients $[\hbar^n j^{2k}]Z(\hbar, j)$ yield the sum of all graphs with a given number of vertices and external edges (figs. 5 and 6). Further algebraic transformations give restriction of the sums to connected and one-particle-irreducible (1PI) graphs (section 3.2) which are polynomial in N and can be computed explicitly with the help of a computer algebra system¹.
- Following the method [37], we obtain the generating function of primitive graphs (section 3.3) with L -loop coefficients $p_L(N)$ (eq. (3.17)). We derive the asymptotics of different classes of graphs¹. For primitive graphs at L loops, we find eq. (3.27):

$$p_L \sim \frac{3^{\frac{N-1}{2}} e^{-\frac{12+3N}{4}}}{\frac{4}{3}\sqrt{2\pi}\Gamma(\frac{N+4}{2})} \left(\frac{2}{3}\right)^{L+\frac{N+5}{2}} \Gamma\left(L + \frac{N+5}{2}\right) \left(36 - \frac{9(3N^2 - 4N - 80)}{4(L + \frac{N+3}{2})} + \dots\right).$$

- The asymptotic expansions are exact, and arbitrarily many subleading terms can be obtained algebraically. The sequence of subleading terms again grows factorially. This means that for finite loop order L , the asymptotic expansion gets closer to the true value only for the first few terms, see fig. 7b.
- The numerical reliability of the asymptotic expansion for finite L varies substantially, depending on the class of graphs. For the sum of all (not necessarily connected) vertex-type graphs, the leading asymptotics differs from the true value by 1% at order 16, and including the first subleading term reduces the error to $\ll 1\%$ already at order 2(!) (fig. 7). Conversely, for the primitive graphs (p_L), the discrepancy between the true value and the leading asymptotics is larger than 20% even at loop order 20, the error of the first subleading correction reaches 1% only at 9 loops, and further subleading corrections increase accuracy only above 20 loops (fig. 8).
- At finite L , $p_L(N)$ grows polynomially with $N > 0$. The asymptotic large- L expansion describes this N dependence fairly well for not too large N (fig. 9a). It

¹Files are available from the first author's website www.paulbalduf.com

strongly depends on N which loop order and how many subleading corrections to the asymptotics are required to reach a given accuracy (fig. 9b).

- The growth ratio r_L of the sum of primitive graphs, for $L \rightarrow \infty$, converges to $\frac{2}{3}$, independent of N (eq. (3.28)). The limiting slope depends linearly on N , as $\frac{N+5}{3} \frac{1}{L}$. We observe that already for $10 \leq L \leq 18$, the numerical values for r_L (for fixed N) lie almost on a straight line, where the limit is independent of N and the slope linear in N (fig. 10a). However, neither the limit nor the slope coincide with the true asymptotic values. Data at $10 \leq L \leq 18$ suggests a wrong asymptotics, and the true asymptotic growth rate of p_L is observed starting from $L \geq 25$ loops.
- We determine the exact all-order asymptotics of the sum of Martin invariants, and its growth ratio (section 3.6).
- A transform of variables $U = N\hbar$ leads to power series in U instead of \hbar , which represent the large- N limit. These series are not factorially divergent (section 3.7).
- The sum of primitive graphs $p_L(N)$, at fixed L , is a polynomial in N . The degree of this polynomial grows like $\frac{2}{3}L$ (lemma 5). We determine the exact asymptotics of the average order of the coefficients, it grows like $\frac{1}{2} \ln(L)$ (eq. (3.31)). This explains why the large- N expansion is convergent while the large- L expansion is not: At fixed L , the highest coefficients in N of the polynomials $p_L(N)$ are vanishingly small compared to the low-order coefficients in N .

While the 0-dimensional QFT in section 3 gives closed formulas for generating functions of certain classes of graphs, these are of limited value for the 4-dimensional theory because every graph is further weighted by its Feynman integral there. Thus, in section 4 we turn to the N dependence of individual graphs. We identify those primitive graphs which have largest degree in N , and give bounds on the degree of non-primitive graphs:

- Section 4.1 introduces certain *dual* graphs G^* . These are the Feynman graphs of the field variable σ introduced through the Hubbard-Stratonovich transformation in section 3.2. Their decisive feature is that every vertex in the dual graph corresponds to a factor of N , and therefore a classification of dual graphs allows for a classification of N dependence of original graphs.
- For an L -loop primitive vertex-type graph, the degree in N is bounded by $\lfloor \frac{2}{3}L - \frac{2}{3} \rfloor$ (lemma 5).
- In general, the map from original graphs to dual graphs is not invertible. A special case are the primitive graphs of leading degree in N with $L = 3n + 1$ loops. They are in bijection with 3-regular 3-connected dual graphs (theorem 1); then the *line graph* construction (definition 6) defines a unique inverse.
- When $L = 3n$ (section 4.2.2) or $L = 3n + 2$ (section 4.2.3), the dual graphs G^* are almost 3-regular. The corresponding leading-degree graphs G can be constructed

algorithmically by a slight variation of the line graph. We have generated all primitives that contribute to leading order in N up to $L = 25$ loops (table 1)¹.

- The L -loop zigzag graph has degree $\lfloor \frac{1}{2}L + 2 \rfloor$, and therefore does not contribute at leading order in N (lemma 8). But there is an infinite family of leading-order primitive graphs similar to zigzags which consist of two layers of triangles.
- In table 2, we give the number of primitive graphs of certain degree in N up to 16 loops. The average degree grows slower than the degree bound $\lfloor \frac{2}{3}L + \frac{2}{3} \rfloor$ (fig. 20a); that is, at large loop order most graphs do not saturate the bound.
- By factorization properties, the degree bounds of primitive graphs imply degree bounds for all other graphs (section 4.4). If no multiedges are present, the degree bound decreases by $\frac{2}{3}$ for every insertion of vertex-type subgraphs (lemma 9), and by $\frac{1}{3}$ for every insertion of propagator-type subgraphs (theorem 3). In particular, in a theory without 1-loop multiedges, all graphs at leading order in N are primitive.

In section 5, we turn to numerical results for the 4-dimensional theory, where each graph obtains a non-trivial value, given by its Feynman period $\mathcal{P}(G)$ (eq. (2.8)).

- The primitive beta function β_L^{prim} is a polynomial in N of degree $\lfloor \frac{2}{3}L - \frac{2}{3} \rfloor$. We give numerical values for the coefficients of these polynomials up to $L = 16$ in table 3 and for the evaluation of β_L^{prim} at integer N in table 4. The leading-order graphs identified above have been integrated numerically¹ for $14 \leq L \leq 16$ to obtain high-accuracy values for the leading coefficients (section 5.1).
- In section 5.2, we examine the ratio $b_L(N) \propto \beta_L^{\text{prim}}(N)/p_L(N)$, normalized to unity at $N = 1$, which measures to what extent the N dependence of 0-dimensional and 4-dimensional agree. Finding it to be a slowly and monotonically growing function in N for $N > -4$, this indicates that $p_L(N)$ gives a reasonably good description for the N dependence of $\beta_L^{\text{prim}}(N)$ at finite L .
- Like the 0-dimensional function $p_L(N)$, also $\beta_L^{\text{prim}}(N)$ has zeros for negative N . In both cases, their location converges to negative integers ≤ -4 very rapidly with growing loop order (fig. 20b).
- The growth ratio $r_L(N)$ of $\beta_L^{\text{prim}}(N)$ shows a strikingly similar pattern to the growth ratio of $p_L(N)$: It appears to converge towards an N -independent value, with a slope that depends linearly on N . However, the limiting value is smaller than expected (fig. 22a). We conclude that this value, extrapolated from our results for $L \leq 18$, probably does not represent the true growth rate (section 5.3). Hence, we cannot explicitly confirm conjecture 1. Still, comparison with the asymptotic behaviour in the 0-dimensional theory suggests that the conjecture is compatible with our data.
- Not just β_L^{prim} but also the average period per graph appears to converge to a limit that is smaller than expected as $L \rightarrow \infty$ (fig. 22b). Hence, the observed mismatch

between data and expected asymptotics of β_L^{prim} is not entirely explained by the behaviour of the 0-dimensional $p_L(N)$, but there appears to be an additional effect of the Feynman integrals themselves. Both for the primitive beta function and for the average period, an extrapolation of numerical data suggests that one will need at least 25 loops to observe the correct leading asymptotics (figs. 22a and 22b).

1.3. Discussion and Outlook

In terms of our numerical data, we have not been able to clearly confirm or refute [conjecture 1](#) stating that primitive graphs dominate the beta function in ϕ_4^4 theory. Rather, we found that for primitive graphs in the 0-dimensional theory, the transition towards the leading asymptotic regime in terms of growth rates occurs around 25 loops (fig. 10a), and for the 4-dimensional theory, the extrapolated growth rate intersects the expected asymptotics around 25 loops, too (fig. 22a). Unfortunately, this is beyond the 18 loops that we can currently reach numerically. However, the N dependence (for N not too large) of these growth rates shows an “asymptotic-like” pattern before the growth rate assumes its asymptotic value. Moreover, the zeros of the N -dependent beta function converge towards their asymptotic values $N \in \{-4, -6, \dots\}$ very rapidly already at $L < 10$ (fig. 20b). In view of this, there really is no such thing as *the* asymptotic regime, and even for different aspects of the same quantity, such as the N dependence and the absolute value of the primitive beta function, the asymptotics sets in at different points.

It is furthermore remarkable that the reliability of the asymptotic expansion is very different for different classes of graphs: while the growth rate of primitive graphs is captured by the leading asymptotics only beyond 25 loops, the sum of all graphs, or all connected graphs, behaves asymptotically at much lower loop order (fig. 7). We have seen in [section 5.2](#) that for primitive graphs, the 4-dimensional theory behaves quite similar to the 0-dimensional one. However, it is not clear if that should be expected for non-primitive generating functions, too, because the renormalization of non-primitive graphs introduces an additional degree of freedom, which has no counterpart in the 0-dimensional theory. Therefore, we can not infer from our findings whether the non-primitive asymptotic expansion in four dimensions is as reliable as it is in zero dimensions.

By [lemma 3](#), a generating function of graphs vanishes at $N = -2j$ if it contains a sum of all orientations (channels) of a $(2j + 2)$ -valent subgraph. Asymptotically, the primitive generating function $p_L(N)$, and all other generating functions of [section 3.4](#), have such zeros for arbitrary large j . This can be interpreted that asymptotically, almost all orientations of suitable subgraphs are present. For the sum of *all* graphs, this statement is trivial: A sum of all graphs in particular contains all possible orientations of every subgraph. However, in general some of these orientations will yield graphs which are not connected, not 1PI, or not primitive. It would be interesting to understand this situation from the perspective of probabilistic graph theory: What is the precise relation between the fact that asymptotically a non-zero fraction of graphs are primitive, and that their generating function has zeros at all negative integer N ?

Regarding the classification of the N dependence of non-primitive graphs ([section 4.4](#)),

we reproduce the known fact that “bubble” graphs (fish chains) dominate. Conversely, the fish-free graphs of highest degree in N at every L are indeed primitive, because inserting any subgraph that is not a multiedge effectively lowers the degree in a large- N expansion. In that respect, our results are analogous to the dominance of *melonic* graphs [23, Sect. 4] [38] in tensor theories. The classification of N dependence in terms of Gurau degree identifies *schemes* as building blocks, analogously to the primitive graphs in our case, but details are different: Primitiveness and the coradical degree only implies bounds on the N dependence (theorem 3), but not an exact classification. Conversely, the coradical degree amounts to the exact classification in terms of leading-log expansions. One of the main results of the present work is that these two, seemingly unrelated, expansions in fact have a lot in common. We leave a precise classification of the N dependence of the leading-log expansion for future work. It would of course also be interesting to find a concrete theory that has Feynman graphs similar to $O(N)$ symmetric ϕ^4 theory, but without multiedge graphs.

Regarding the role of degree bounds, it is worth stressing that the exact asymptotics of the average order in N , $\langle k \rangle_L$ from eq. (3.31), gives a very nice and explicit understanding of the interplay between loop expansion and large- N expansion: For the large- N expansion, one is concerned with degree bounds of classes of graphs, which are linear in the loop order L . However, the average order is only logarithmic in L , which implies that at large fixed L , the overwhelming majority of terms in the $O(N)$ symmetry factors is of very low order in N , much lower than the degree bound. Consequently, it is no contradiction that the loop expansion diverges, while the large- N expansion does not.

The fact that the $O(N)$ symmetry factor $T(G, N)$ factorizes for insertion of subgraphs of *arbitrary* valence (lemma 2), not just 4-valent ones, is an example of how the symmetry of the theory is reflected in an infinite set of identities. In fact, one could include arbitrary interaction terms of the form $(\vec{\phi})^{2k}$ into the Lagrangian without spoiling the factorization. Such vertices would render the theory non-renormalizable by power counting (unless the spacetime dimension is changed), but the counterterms of higher valence would still have the same $T(G, N)$ as the vertices. Moreover, the vertices of higher valence would be “proportional” to products of vertices of lower valence in the sense that the sum of trees produces the same $T(G, N)$ as a single vertex. This behaviour is a very simple, but thereby instructive, example of how a symmetry imposes relation between arbitrarily many terms, analogous to the mechanism that has been suggested for gravity [1, 35, 36]. The case of gravity is of course more complicated since for a *local* symmetry, the identities involve derivatives and thereby the kinematics of the vertices, which is not the case for the present global $O(N)$ symmetry.

2. Setup

2.1. $O(N)$ -symmetric ϕ^4 theory

We consider a Euclidean scalar ϕ^4 theory where the scalar field $\vec{\phi}$ has an internal $O(N)$ symmetry. For now, we assume N to be a positive integer such that $\vec{\phi}$ is an N -component vector (ϕ_1, \dots, ϕ_N) , and the Lagrangian density reads

$$\mathcal{L} = -\frac{1}{2}(\partial_\mu \phi_1 \partial^\mu \phi_1 + \partial_\mu \phi_2 \partial^\mu \phi_2 + \dots + \partial_\mu \phi_N \partial^\mu \phi_N) - \frac{\lambda}{4!}(\phi_1^2 + \phi_2^2 + \dots + \phi_N^2)^2. \quad (2.1)$$

For various N , eq. (2.1) represents different universality classes of critical phenomena. More background and a review of the physical significance of $O(N)$ symmetry can be found in [39]. Perturbation theory of $O(N)$ -symmetric ϕ^4 theory, with example calculations and further generalizations, can be found in the literature, for example [40, 41].

Feynman graphs of ϕ^4 theory are 4-regular up to vertices which are connected to external edges. The structure of the $O(N)$ -symmetric interaction term in eq. (2.1) implies that each 4-valent vertex gives rise to a sum of three terms in Feynman amplitudes, corresponding to the three different possibilities to partition the four edges into pairs. Graphically, such a partition can be interpreted as a *decomposition* of the vertex into two lines connecting the four adjacent edges² as shown in fig. 1.

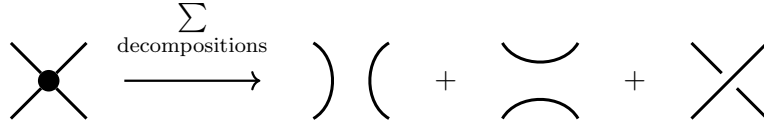


Figure 1: A 4-valent vertex allows for three non-isomorphic *decompositions*, each of which consists of a pair of edges. To compute a Feynman amplitude, all three decompositions need to be summed.

Then, a decomposition of a graph G is a choice of decomposition of all of its vertices. A decomposition of G yields a set of disjoint circuits and paths, where the paths begin and end at external edges of G .

Definition 1. *The circuit partition polynomial J assigns a factor N to each circuit in the sum of all decompositions of a graph,*

$$J(G, N) := \sum_{\text{decompositions of } G} N^{\#\text{circuits}}. \quad (2.2)$$

²These vertex decompositions have also been called *vertex states* in [42], and *transitions* in [33].

Alternatively, one can view each such decomposition as a strand graph [43–45], that is a graph with the additional structure of pairings (green lines) between edges,

The resulting circuits define faces such that a strand graph becomes a 2-complex. The case of vector fields gives rise to a single strand adjacent to each edge such that the 2-complex is only 0-connected, i.e. faces meet only at vertices. In this sense, the stranding is a “decomposition” in this case. In contrast, matrix and order- r tensor multi-scalar fields have 2 or $r > 2$ strands per edge resulting in 2-complexes which are connected surfaces [19] or r -dimensional pseudo manifolds [46], respectively.

If $f(N)$ is a formal power series in N , we use the notation $[N^k]f(N)$ to denote extraction of the coefficient of N^k . For the circuit partition polynomial, $[N^k]J(G, N)$ counts how many different ways there are to obtain exactly k circuits from the graph G .

The polynomial $J(G, N)$ yields a symmetry factor for each Feynman graph G . Due to the factor $\frac{1}{4!}$ in the interaction term in the Lagrangian density (eq. (2.1)), ordinary ϕ^4 theory is restored in the case $N = 1$ but it implies that the sum of all three decompositions of a vertex is scaled by $1/3$:

Definition 2. Let $J(G, N)$ be the circuit partition polynomial (definition 1) of a Feynman graph G with vertices V_G . The $O(N)$ -symmetry factor of ϕ^4 theory is defined as

$$T(G, N) := \frac{J(G, N)}{J(G, 1)} = \frac{1}{3^{|V_G|}} J(G, N).$$

For the latter equality, we have used that in ϕ^4 theory, every vertex is 4-valent. For arbitrary vertex valence $\text{val}(v)$, the factor 3 needs to be replaced by $(\text{val}(v) - 1)!!$, which is the number of non-isomorphic vertex decompositions.

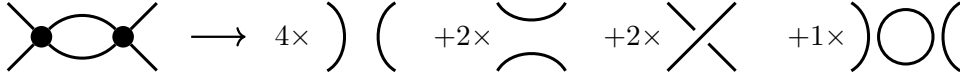


Figure 2: The *fish* graph (also known as double edge, 1-loop multiedge, banana, or bubble) has two vertices. In a sum over all decompositions, both vertices produce three terms according to fig. 1 which yields nine terms in total, only one of which contains a circuit. Thus, the circuit partition polynomial of this graph is $N + 8$. Notice that the circuit partition polynomial depends on whether the four external edges are open or pairwise connected, compare example 1.

Example 1. A Feynman graph that will be relevant in many computations later on is the *fish*, shown in fig. 2. As an example for how definitions 1 and 2 allow to compute $J(G, N)$ by repeatedly decomposing vertices, consider chains of *fish* graphs. These chains are also called “bubble” graphs. We consider four different ways to terminate the two ends of the chain. In all cases, the number of loops is L .

1. For a chain of $(L - 1)$ *fish* graphs with the two edges on one of the sides joined into a self loop,

$$J(\text{fish chain with self loop}, N) = (N + 2)^L. \quad (2.3)$$

This follows by induction as $J(\text{fish}, N) = N + 2$ and extending $\text{fish chain with self loop}$ from L to $L + 1$ loops yields an additional factor $N + 2$ (decompose the last vertex and find that in two cases the decomposition yields the same as for L loops while one case yields a new disconnected loop, thus a factor N).

2. Closing also the other two open edges into a self loop simply yields a factor N , thus such a vacuum graph with L loops has

$$J(\text{vacuum graph with } L \text{ loops}, N) = N(N + 2)^{L-1}. \quad (2.4)$$

3. A ring consisting of $(L - 1)$ fish graphs is an L -loop vacuum graph with

$$J\left(\text{ring of } (L-1) \text{ fish graphs}, N\right) = 2^{L-2}(N-1)(N+2) + (N+2)^{L-1}. \quad (2.5)$$

The argument is again by induction, starting with $J(\text{fish graph}, N) = 3N(N+2)$ (see also eq. (A.1)) and noting that decomposition of any one vertex in the ring yields either the tadpole chain (2.4) or in the other two cases again the ring polynomial (2.5) of one loop less.

4. A chain of L fish graphs, where the edges on both ends are open, has

$$J(\text{chain of } L \text{ fish graphs}, N) = \frac{(N-1)2^{L+1} + (N+2)^{L+1}}{N}. \quad (2.6)$$

In this case, induction starts with $J(\text{fish graph}, N) = N+8$ (fig. 2) and decomposing the last vertex gives two copies of $J(\text{chain of } L-1 \text{ fish graphs}, N)$ with $L-1$ loops and one tadpole chain eq. (2.3).

In the present article, we typically let N be arbitrary, but [example 1](#) already makes it clear that one can eliminate specific graphs from the theory by choosing certain values of N . In particular, all self-loops (tadpoles) are canceled at $N = -2$ and this value determines the *Martin invariant*, see [section 2.4](#).

The circuit partition polynomial, and the related *interlace polynomial* and *Martin polynomial* (to be discussed later in [section 2.4](#)), have long been known in graph theory [[42](#), [47–51](#)]. In the following, we briefly introduce some further definitions, as well as elementary combinatorial properties of the polynomials $T(G, N)$ and $J(G, N)$. Proofs and examples are deferred to [appendix A](#).

Lemma 1. A $(2p - 1)$ -loop multiedge graph without external edges has

$$J(\text{multiedge graph}, N) = (2p-1)!! \prod_{j=0}^{p-1} (N+2j), \quad T(\text{multiedge graph}, N) = \frac{\prod_{j=0}^{p-1} (N+2j)}{(2p-1)!!}.$$

Definition 3. Let g_1 and g_2 be graphs, each of which has exactly $(2p)$ external edges. The joining operation $g_1 \uplus g_2$ is defined as the average of all $(2p)!$ matchings between the external edges of g_1 and g_2 ,

$$g_1 \uplus g_2 := \frac{1}{(2p)!} \sum_{G \text{ matching of } (g_1, g_2)} G.$$

A graph is called n -valent if it has n external edges. In particular, a *vertex-type graph* is 4-valent, a *propagator-type graph* is 2-valent, and a *vacuum graph* is zero-valent. Vacuum graphs in ϕ^4 theory are 4-regular, which means that every vertex has valence four.

Definition 4. Let g be a connected graph with n external edges. The completion $G = g \uplus \{v\}$ of g is the graph where the external edges of g have been joined to a new n -valent vertex v . Conversely, if g arises from G upon removing any one vertex $v \in V_G$, then $g = G \setminus \{v\}$ is called a decompletion of G .

Notice that the sum of matchings in [definition 3](#) contains exactly $(2p)!$ graphs, which may be isomorphic. If $g_2 = v$ is a single vertex, then all $(2p)!$ graphs are isomorphic and the completion $g \uplus \{v\} = G$ is a single graph. We use the term *L -loop completion* to refer to a vacuum graph with $L + 2$ vertices, such that its decompositions are vertex-type graphs of L loops, see [fig. 3](#).

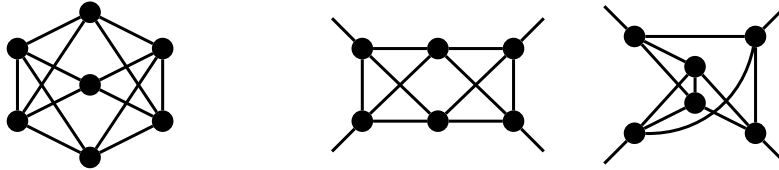


Figure 3: A 5-loop completion (left) has seven vertices. Removing one of the vertices yields a 5-loop decompletion. In this case, only two of the seven possible decompositions are non-isomorphic.


The automorphism symmetry factor $\frac{1}{|\text{Aut}(G)|}$ is compatible with completion and decompletion ([definition 4](#)). Let G be a 4-regular L -loop completion, then

$$\frac{L + 2}{|\text{Aut}(G)|} = \sum_{g \text{ decompletion of } G} \frac{1}{|\text{Aut}(g)|}. \quad (2.7)$$

The sum extends over non-isomorphic decompositions g of G , and the automorphisms $\text{Aut}(g)$ allow permutations of the external legs. To obtain symmetry factors where external edges are fixed, but different channels are summed over (which is the usual convention in QFT), both sides of [eq. \(2.7\)](#) need to be multiplied by $4!$.

Example 2. For the graphs in [fig. 3](#) from left to right, [eq. \(2.7\)](#) reads $\frac{7}{48} = \frac{1}{16} + \frac{1}{12}$. In the traditional QFT convention, the graph in the middle of [fig. 3](#) has three non-isomorphic channels, and a symmetry factor (with external legs fixed) of $\frac{1}{2}$. Indeed, $3 \cdot \frac{1}{2} = \frac{24}{16} = 4! \cdot \frac{1}{16}$, that is, we can reproduce the QFT convention by multiplying with $4!$. The graph at the right has four channels and a leg-fixed symmetry factor $\frac{1}{2}$, and $4 \cdot \frac{1}{2} = 2 = 4! \cdot \frac{1}{12}$.

The operation $g_1 \uplus g_2$ of joining along external edges ([definition 3](#)) can equivalently be interpreted as insertion of g_1 into the completion $G_2 = g_2 \cup \{v_2\}$ in place of a $(2p)$ -valent vertex v_2 , denoted by $g_1 \circ_{v_2} G_2 := g_1 \uplus g_2$. This notation can be extended to insertion of 2-valent subgraphs into edges with the convention that an edge is formally identified with a 2-valent vertex of the graph. In [appendix A](#), we show that the circuit partition polynomial $J(G, N)$ factorizes under joining of graphs ([lemma 13](#)). Recall the comment below [definition 2](#), namely for a $(2p)$ -valent vertex we divide by $(2p - 1)!!$ to account for its $(2p - 1)!!$ decompositions analogous to [fig. 1](#).

Lemma 2. 1. Let g_1 be a $(2p)$ -valent graph, $G_1 = g_1 \uplus \{v\}$ its completion (*definition 4*), and  the multiedge graph with $(2p - 1)$ loops (*lemma 1*). Then

$$T(G_1, N) = T(\text{multiedge}, N) \cdot T(g_1, N) = \frac{\prod_{j=0}^{p-1} (N + 2j)}{(2p - 1)!!} \cdot T(g_1, N).$$

2. Let g_1 be a $(2p)$ -valent graph, and let v_2 be a $(2p)$ -valent vertex in a graph g_2 (which may or may not be a completion). Then $g_1 \circ_{v_2} g_2$ is a sum of graphs which have the same valence as g_2 , and

$$T(g_1 \circ_{v_2} g_2, N) = T(\text{multiedge}, N) \cdot T(g_1, N) \cdot T(g_2 \setminus \{v_2\}, N) = T(g_1, N) \cdot T(g_2, N).$$

The factorization of $O(N)$ -symmetry factors upon insertion of subgraphs (*lemma 2*) can also be interpreted “in the opposite direction”: The $(2p - 1)$ -loop multiedge has vertices of valence $(2p)$, and its circuit partition polynomial has zeros at negative even integers $N \in \{0, -2, \dots, -2p - 2\}$ (*lemma 1*). Namely, the presence of such zeros indicates the presence of either a vertex of valence $(2p)$, or of a sum of $(2p)$ -valent subgraphs.

Lemma 3. 1. Let G be a completion which contains a vertex of valence $2p$. Then $J(G, N)$ and $T(G, N)$ have zeros at $N \in \{0, -2, \dots, -2p + 2\}$.

2. Let g_1, g_2 be $(2p)$ -valent, and let $g = G \setminus \{v\}$ be a sum of vertex-type graphs, where the corresponding sum of completions $G = g_1 \uplus g_2$ (*definition 3*) arises from joining g_1 and g_2 in all possible orientations (channels). Then $J(g, N)$ and $T(g, N)$ have zeros at $N \in \{-4, -6, \dots, -2p + 2\}$.

2.2. Renormalization, primitive graphs, and periods

The renormalization of Feynman graphs has the structure of a Hopf algebra [3, 52, 53], where the *primitive* elements are the Feynman integrals without subdivergences, and the coproduct of the Hopf algebra realizes the Zimmermann forest formula [54] of extracting and renormalizing subdivergences. We remind the reader of the following facts which will be used in the rest of the paper:

- As ϕ^4 theory is renormalizable in four dimensions, a graph is superficially divergent if and only if it has four or less external edges.
- A graph is primitive if it is *cyclically 6-edge connected*, that is, if it has no proper subgraphs of valence less than 6, except for trees.
- Every propagator-type graph except the 2-loop multiedge (the “sunrise” graph) has a vertex-type subgraph upon removing a vertex adjacent to an external edge.
- Consequently, except for the 2-loop multiedge, all primitive graphs of ϕ^4 theory are vertex-type graphs.

- The 2-loop multiedge itself is primitive if one chooses renormalization conditions such that tadpole graphs vanish, otherwise the 2-loop multiedge has 1-loop multiedges (*fish*, [fig. 2](#)) as divergent subgraphs.

The Feynman integral of primitive vertex-type graphs depends logarithmically on the momentum scale. The coefficient of this dependence is the *Feynman period* [[7](#), [55–57](#)], given by the parametric Feynman integral of the first Symanzik polynomial ψ_g of g :

$$\mathcal{P}(g) := \left(\prod_{e \in E_g} \int_0^\infty da_e \right) \delta\left(1 - \sum_{e \in E_G} a_e\right) \frac{1}{\psi_g^2}. \quad (2.8)$$

The period is defined for vertex-type graphs g , but the periods of all decompletions of the same completion G ([definition 4](#)) have the same value, denoted by $\mathcal{P}(G) := \mathcal{P}(g)$.

2.3. The beta function

2.3.1. Definition and asymptotics

The beta function describes the running of the effective coupling with the energy scale. It is related to critical exponents [[41](#), [58](#), [59](#)]. For ϕ^4 theory regularized in $D = 4 - 2\epsilon$ dimensions, it is given by the derivative of the counterterm $z^{(\alpha)} = z^{(4)}/(z^{(2)})^2$ of the invariant charge, where $z^{(4)}$ is the vertex- and $z^{(2)}$ the propagator counterterm,

$$\beta(\alpha, \epsilon, N) := \frac{-\epsilon}{\partial_\alpha \ln(\alpha \cdot z^{(\alpha)}(\alpha, \epsilon, N))} = \sum_{L \geq 1} (-\alpha)^{L+1} \beta_L(\epsilon, N). \quad (2.9)$$

The expansion parameter is $\alpha := -\lambda\mu^{-2\epsilon}(4\pi)^{-2}$, where λ is the coupling constant of our Lagrangian ([eq. \(2.1\)](#)), and μ is an energy reference scale. In the following, we will only be interested in the beta function at $\epsilon = 0$. For every fixed order L , the coefficient $\beta_L(N) := \beta_L(0, N)$ is a polynomial in N . The counterterm in [eq. \(2.9\)](#) is determined by 1PI graphs, the beta function receives contributions from primitive ([section 2.2](#)) and from non-primitive graphs, $\beta_L(N) = \beta_L^{\text{prim}}(N) + \beta_L^{\text{nonprim}}(N)$. The second summand depends on the renormalization scheme, for a recent review see the first author's PhD thesis [[60](#)]. The full beta function in the minimal-subtraction scheme is known up to $L = 7$ loops [[61–63](#)], and starts with

$$\begin{aligned} \beta(\alpha, N) = & -2\epsilon\alpha + \frac{N+8}{3}\alpha^2 - \frac{3N+14}{3}\alpha^3 \\ & + \frac{96(5N+22)\zeta_3 + 33N^2 + 922N + 2960}{216}\alpha^4 + \dots, \end{aligned} \quad (2.10)$$

The leading asymptotics of β_L for $L \rightarrow \infty$ has been obtained from an instanton computation in [[64–67](#)]. The review [[6](#)] gives a consolidated result, with slightly different conventions, namely in $D = 4 - \epsilon$ dimensions for an interaction term $\frac{g}{4}\phi^4$. There, $\beta = -\epsilon g + \frac{(N+8)}{8\pi^2}g^2 + \dots = \sum_k g^k b_k$, and the leading asymptotics of b_k as $k \rightarrow \infty$ is \bar{b}_k ,

$$\bar{b}_k = C_\beta (-1)^k k! k^{\frac{7}{2}} \left(\frac{3}{8\pi^2}\right)^k, \quad C_\beta = 2^{\frac{13}{2}} \cdot 3^{\frac{2}{2}} e^{\frac{3\zeta'(2)}{\pi^2} - \frac{7}{2}\gamma_E - \frac{15}{4}}.$$

The N dependence of this asymptotics can be found in [66]. One can write $e^{\frac{\zeta'(2)}{\pi^2}} = (2\pi e^{\gamma_E})^{\frac{1}{6}}/A^2$ with the Glaisher-Kinkelin constant [68] $A \approx 1.28242713$. In our convention (eq. (2.9)), \bar{b}_k amounts to the leading asymptotics of β_{k-1} . Hence, β_L grows asymptotically as $\beta_L(N) \sim \tilde{\beta}_L(N) (1 + \mathcal{O}(\frac{1}{L}))$, where

$$\tilde{\beta}_L = (L+1)! (L+1)^{\frac{N+6}{2}} \frac{36 \cdot 3^{\frac{N+1}{2}}}{\pi \Gamma(2 + \frac{N}{2}) A^{2N+4}} e^{-\frac{3}{2} - \frac{N+8}{3}(\frac{3}{4} + \gamma_E)}. \quad (2.11)$$

Factorial asymptotic growth can be expressed in many equivalent forms by redefining subleading coefficients. It turns out that eq. (2.11) is not the most suitable form for our purpose. Instead, we will use the notation of [37, 69] throughout the article:

$$\begin{aligned} \beta_L &\underset{L \rightarrow \infty}{\sim} \sum_{r=0}^{\infty} \Gamma(L + c_s - r) a^{-L - c_s + r} c_r \\ &= \left(\frac{1}{a}\right)^{L+c_s} \cdot \Gamma(L + c_s) \left(c_0 + \frac{ac_1}{(L + c_s - 1)} + \frac{a^2 c_2}{(L + c_s - 1)(L + c_s - 2)} + \dots \right). \end{aligned} \quad (2.12)$$

Here, the parameters $a, c_s, \{c_j\}_{j \in \mathbb{N}_0}$ are independent of L , but possibly functions of N . In order to determine the growth parameters of a factorially growing quantity, it is often useful to consider a growth ratio which has a finite limit as $L \rightarrow \infty$. We use

$$r_L(\beta) := \frac{\beta_{L+1}}{L \cdot \beta_L} \underset{L \rightarrow \infty}{\sim} \frac{1}{a} + \frac{c_s}{a} \frac{1}{L} - \frac{c_1}{c_0} \frac{1}{L^2} + \left((c_s - 1) \frac{c_1}{c_0} + a \left(\frac{c_1}{c_0} \right)^2 - 2a \frac{c_2}{c_0} \right) \frac{1}{L^3} + \dots \quad (2.13)$$

By construction, $r_L(\beta)$ is invariant under rescaling of β with an overall factor; $r_L(\beta)$ depends on a and c_s individually, but on the subleading corrections only through the ratios $\frac{c_j}{c_0}$. Notice in particular that knowing the *leading* factorial asymptotics amounts to knowing the limit *and* the $\frac{1}{L}$ correction of the growth ratio.

For the asymptotic growth of the beta function in eq. (2.11), a simple computation yields

$$\frac{\tilde{\beta}_{L+1}}{L \cdot \tilde{\beta}_L} = \frac{(L+2)!(L+2)^{\frac{N+6}{2}}}{L(L+1)!(L+1)^{\frac{N+6}{2}}} = \frac{(L+2)}{L} \left(\frac{L+2}{L+1} \right)^{\frac{N+6}{2}} = \left(1 + \frac{2}{L} \right) \left(1 + \frac{1}{L+1} \right)^{\frac{N+6}{2}}.$$

Expanding the last factor in orders of $\frac{1}{L}$ and comparing with eq. (2.13), we can read off the growth parameters that correspond to eq. (2.11): The beta function in minimal subtraction is expected to grow according to eq. (2.12), with

$$a = 1, \quad c_s = \frac{N+10}{2}, \quad c_0 = \frac{36 \cdot 3^{\frac{N+1}{2}} e^{-\frac{3}{2} - \frac{N+8}{3}(\frac{3}{4} + \gamma_E)}}{\pi \Gamma(2 + \frac{N}{2}) A^{2N+4}}. \quad (2.14)$$

It is important to realize that eq. (2.11) only specifies the *leading* asymptotic growth, and eq. (2.14) represents the same leading asymptotic growth, but they differ in terms $\propto \frac{1}{L}$. For example, for $N = 1$ at $L = 13$, eq. (2.14) is larger than eq. (2.11) by approximately 65%. Without information about subleading coefficients in eq. (2.11), it is impossible to know which of the two conventions is numerically closer to the true value at finite L .

2.3.2. Primitive beta function

The *primitive* beta function β^{prim} consists of the contributions of primitive vertex-type graphs g only, which is given by their Feynman periods $\mathcal{P}(g)$ (eq. (2.8)). Owing to the completion invariance of the period and lemma 2 and eq. (2.7), β^{prim} can equivalently be written as a sum over completions:

$$\beta^{\text{prim}}(N) = 2 \sum_{g \text{ decomp.}} \frac{4! T(g, N)}{|\text{Aut}(g)|} \cdot \mathcal{P}(g) = 2 \sum_{G \text{ comp.}} \frac{4!(L_G + 2) 3T(G, N)}{|\text{Aut}(G)| N(N+2)} \mathcal{P}(G). \quad (2.15)$$

β_L^{prim} is independent of the renormalization scheme, while the full β_L is not. It has been conjectured [6] that the leading asymptotic growth of β_L^{prim} coincides, for $L \rightarrow \infty$, with that of β_L in minimal subtraction:

Conjecture 1. *The leading growth of the primitive beta function is given by eq. (2.11),*

$$\beta_L^{\text{prim}} \sim \bar{\beta}_L \left(1 + \mathcal{O}\left(\frac{1}{L}\right)\right), \quad \bar{\beta}_L := \Gamma\left(L + \frac{N+10}{2}\right) \frac{36 \cdot 3^{\frac{N+1}{2}}}{\pi \Gamma\left(2 + \frac{N}{2}\right) A^{2N+4}} e^{-\frac{3}{2} - \frac{N+8}{3}\left(\frac{3}{4} + \gamma_E\right)}.$$

By eq. (2.15), the conjecture would imply a certain leading growth of the *average* period. Let p_L be the sum of automorphism- and vector-symmetry factors, such that $\beta_L^{\text{prim}}|_{\mathcal{P} \rightarrow 1} = 2p_L$. Dividing $\beta_L^{\text{prim}}(N)$ by $2p_L(N)$, we obtain the average period per graph:

$$\langle \mathcal{P} \rangle_{\frac{T}{\text{Aut}}, L}(N) := \frac{\sum_{G \text{ compl}} \frac{T(G, N) \mathcal{P}(G)}{|\text{Aut}(G)|}}{\sum_{G \text{ compl}} \frac{T(G, N)}{|\text{Aut}(G)|}} = \frac{\beta_L^{\text{prim}}(N)}{2p_L(N)}. \quad (2.16)$$

Notice that $\langle \mathcal{P} \rangle_{T/\text{Aut}, L}$ is the average of a sample weighted proportional to $\frac{T}{\text{Aut}}$, which is not exactly the same as the average of $\frac{T \cdot \mathcal{P}}{\text{Aut}}$ in a uniform sample, see the appendix of [7]. In section 3.5 below, we compute the $L \rightarrow \infty$ asymptotics of $p_L(N)$ (eq. (3.27)). Consequently, conjecture 1 amounts to an asymptotics of $\langle \mathcal{P} \rangle_{T/\text{Aut}}$ according to

$$\langle \mathcal{P} \rangle_{\frac{T}{\text{Aut}}, L} \sim \left(\frac{3}{2}\right)^L L^{\frac{5}{2}} \cdot \delta^N \cdot \frac{9 \left(\frac{3}{2}\right)^{\frac{1}{2}} e^{-\frac{1}{2} - \frac{8\gamma_E}{3}}}{A^4 \sqrt{2\pi}} \left(1 + \mathcal{O}\left(\frac{1}{L}\right)\right), \quad \delta = \frac{\sqrt{\frac{3}{2}} e^{\frac{1}{2} - \frac{\gamma_E}{3}}}{A^2}. \quad (2.17)$$

Notice³ that $\delta \approx 1.013$ such that the N dependence of the leading asymptotics is relatively gentle. $\langle \mathcal{P} \rangle_{\frac{T}{\text{Aut}}, L}$ grows exponentially, not factorially, with L . To investigate its growth, we consider a ratio similar to eq. (2.13), but without the denominator L , namely

$$f_L(\langle \mathcal{P} \rangle_{\frac{T}{\text{Aut}}}) := \frac{\langle \mathcal{P} \rangle_{\frac{T}{\text{Aut}}, L+1}(N)}{\langle \mathcal{P} \rangle_{\frac{T}{\text{Aut}}, L}(N)} = \frac{3}{2} + \frac{15}{4} \frac{1}{L} + \mathcal{O}\left(\frac{1}{L^2}\right). \quad (2.18)$$

Thereby, if conjecture 1 is true, the first two coefficients of f_L in eq. (2.18) should be independent of N . In the following sections, we will first examine $p_L(N)$ and related quantities in detail from the perspective of 0-dimensional *phi*⁴ theory. We return to numerical values of β_L^{prim} in the 4-dimensional theory in section 5.3.

³Erik Panzer drew our attention to the numerical value of this quantity.

2.4. Martin invariant

The *Martin polynomial* [47] is a simple transformation of the circuit partition polynomial (definition 1), $M(G, N) := \frac{J(G, N-2)}{N-2}$. Using lemma 2, the Martin polynomial can be related to the $O(N)$ symmetry factor of the decompletion $g = G \setminus \{v\}$:

$$T(g, N) = \frac{1}{3^{|V_G|-1}} \frac{M(G, N+2)}{N+2}, \quad \text{where } G \text{ is a primitive completion.} \quad (2.19)$$

The linear coefficient of the Martin polynomial is the (first) *Martin invariant* [33],

$$M^{[1]} := \frac{1}{6} \frac{\partial}{\partial N} M(G, N) \Big|_{N=0} = \frac{3^L}{2} \frac{\partial}{\partial N} \left(N \cdot T(g, N-2) \right) \Big|_{N=0} = \frac{3^L}{2} T(g, -2). \quad (2.20)$$

At a fixed loop order, we use eq. (2.7) to relate the sum of all Martin invariants, weighted by symmetry factor, to the sum of all primitive decompletions:

$$M_L^{[1]} := \sum_{\text{completions } G} \frac{(L+2) M^{[1]}(G)}{|\text{Aut}(G)|} = \frac{3^L}{2} \sum_{\text{decomp. } g} \frac{T(g, -2)}{|\text{Aut}(g)|}. \quad (2.21)$$

Example 3. At $L = 1$ loop, the unique decompletion g (the fish graph from fig. 2) has $T(g, N) = \frac{N+8}{9}$. Thus, its completion has the Martin polynomial

$$M(G, N) = 3^2 \cdot N \cdot T(G \setminus \{v\}, N-2) = N(N+6),$$

and the Martin invariant is $M^{[1]} = 1$. The completion has symmetry factor $|\text{Aut}(G)| = 3! \cdot 2^3 = 48$, and the decompletion (the fish) has $|\text{Aut}(g)| = 2^4 = 16$. The sums in eq. (2.21) at $L = 1$ contain only one term each, namely

$$\frac{(1+2) \cdot 1}{48} = \frac{3^1}{2} \left(\frac{N+8}{9 \cdot 16} \right) \Big|_{N=-2} = \frac{1}{16}.$$

For $L \in \{1, \dots, 6\}$, explicit computation yields the sums of Martin invariants:

$$M_L^{[1]} \in \left\{ \frac{1}{16}, 0, \frac{1}{4}, \frac{7}{4}, \frac{89}{4}, \frac{1255}{4} \right\}.$$

3. QFT in zero dimensions

In section 2, we have introduced the $O(N)$ symmetry factors $T(G, N)$ in a “bottom up” fashion, from their definition as sums over circuits (definition 1) and their behaviour upon inserting and joining graphs.

QFT in zero dimensions provides a complimentary perspective on the N dependence of the coefficients of the perturbation series, which is “top down” in the sense that it only considers the sum of all graphs in question. For a recent overview with emphasis on enumeration of graphs, we refer to [4], the analytical properties of the vacuum path integral in 0-dimensional $O(N)$ -dependent ϕ^4 theory have been examined in [70].

3.1. Vacuum graphs

The vacuum path integral of N -dependent zero dimensional ϕ^4 theory is the N -fold ordinary integral

$$Z(\hbar) := \int_{\mathbb{R}^N} \frac{d^N \vec{\phi}}{(2\pi\hbar)^{\frac{N}{2}}} e^{\frac{1}{\hbar} \left(-\frac{\vec{\phi}^2}{2} + \frac{(\vec{\phi}^2)^2}{4!} \right)}. \quad (3.1)$$

For fixed integer N , a power series expansion of this integral can in principle be computed by expanding all dot products $\vec{\phi}^2 = \vec{\phi} \cdot \vec{\phi} = \sum_{j=1}^N \phi_j^2$ in terms of their components, and repeatedly using the Gaussian integral formula

$$\int_{\mathbb{R}} \frac{dx}{\sqrt{2\pi\hbar}} e^{-\frac{x^2}{2\hbar}} x^{2n} = (2n-1)!! \hbar^n. \quad (3.2)$$

However, it is more convenient to make use of the identity

$$\int_{\mathbb{R}} \frac{d\sigma}{\sqrt{2\pi a}} e^{\frac{1}{a} \left(-\frac{\sigma^2}{2} + b\sigma \right)} = e^{\frac{b^2}{2a}}. \quad (3.3)$$

Choosing $b = \vec{\phi}^2/\sqrt{12}$ and $a = \hbar$, this transformation eliminates the $(\vec{\phi}^2)^2$ interaction term from eq. (3.1), and the remaining integral over $d^N \vec{\phi}$ is Gaussian. Equation (3.3) is called *Hubbard-Stratonovich transformation* [71–73], and it can be interpreted physically as introducing an auxiliary “mean field” $\sigma = \vec{\phi}^2$, which turns the Lagrangian of ϕ^4 theory into that of a σ -model [74] (see also e.g. [15, 18, 75]). We discuss the perturbative expansion of σ in section 4.1. For an arbitrary constant c , eq. (3.3) yields

$$\int_{\mathbb{R}^N} \frac{d^N \vec{\phi}}{(2\pi\hbar)^{\frac{N}{2}}} e^{\frac{1}{\hbar} \left(-\frac{\vec{\phi}^2}{2c} + \frac{(\vec{\phi}^2)^2}{4!} \right)} = \int_{\mathbb{R}} \frac{d\sigma}{\sqrt{2\pi\hbar}} \frac{1}{\left(\frac{1}{c} - \frac{\sigma}{\sqrt{3}} \right)^{\frac{N}{2}}} e^{-\frac{\sigma^2}{2\hbar}}. \quad (3.4)$$

To expand this as a power series, use eq. (3.2) and the binomial series

$$(1-t)^{-\frac{N}{2}} = \sum_{n=0}^{\infty} \binom{-\frac{N}{2}}{n} (-t)^n = \sum_{n=0}^{\infty} \binom{\frac{N}{2} + n - 1}{n} t^n = \sum_{n=0}^{\infty} \frac{\Gamma(n + \frac{N}{2})}{\Gamma(n+1)\Gamma(\frac{N}{2})} t^n. \quad (3.5)$$

The vacuum path integral eq. (3.1) amounts to $c = 1$ and becomes

$$Z(\hbar) = \sum_{n=0}^{\infty} \frac{\Gamma(2n + \frac{N}{2})}{\Gamma(\frac{N}{2})\Gamma(n+1)6^n} \hbar^n = \sum_{n=0}^{\infty} \frac{\hbar^n}{\Gamma(n+1)24^n} \prod_{k=0}^{2n-1} (N+2k). \quad (3.6)$$

Note that the N dependence in eq. (3.6) is extremely simple. In fact, this finding is the “analogue” of lemma 2: $Z(\hbar)$ enumerates the sum of *all* vacuum graphs of a given loop order. Those graphs can be viewed as arising from gluing subgraphs in all possible ways, where each gluing produces factors of the form $(N+2j)$ for $j \in \mathbb{N}_0$.

3.2. External edges, connected and 1PI graphs

To enumerate graphs with external edges, we need a source term. We will only be interested in $O(N)$ -invariant observables where two external edges share the same index and the index is being summed over. To this end, it is convenient to introduce a (scalar) source η for $\vec{\phi}^2$ (instead of one for each individual component ϕ_k , $k \in \{1, \dots, N\}$):

$$Z(\hbar, \eta) := \int_{-\infty}^{\infty} \frac{d^N \vec{\phi}}{(2\pi\hbar)^{\frac{N}{2}}} e^{\frac{1}{\hbar} \left(-\frac{\vec{\phi}^2}{2} + \frac{(\vec{\phi}^2)^2}{4!} + \frac{\eta}{\hbar} \vec{\phi}^2 \right)} = \int_{-\infty}^{\infty} \frac{d^N \vec{\phi}}{(2\pi\hbar)^{\frac{N}{2}}} e^{\frac{1}{\hbar} \left(-\frac{\vec{\phi}^2}{2} (1 - 2\frac{\eta}{\hbar}) + \frac{(\vec{\phi}^2)^2}{4!} \right)}. \quad (3.7)$$

We have included an extra factor \hbar^{-1} to be consistent with the ordinary power counting, namely the power of \hbar in the series expansion of $Z(\hbar, \eta)$ counts (vertices minus edges), and a 1-particle source term is one source vertex, the η source term must therefore count like two vertices and have an overall factor \hbar^{-2} in the exponent. Of course, having a source term for $\vec{\phi}^2$ is equivalent to marking exactly one of the propagators in a graph. To solve the integral in eq. (3.7), we apply the Hubbard-Stratonovich transformation eq. (3.3), use eq. (3.4) with $c = \frac{1}{1-2\frac{\eta}{\hbar}}$, and finally use eq. (3.5):

$$Z(\hbar, \eta) = \int_{\mathbb{R}} \frac{d\sigma}{\sqrt{2\pi\hbar}} \frac{1}{\left(1 - 2\frac{\eta}{\hbar} - \frac{\sigma}{\sqrt{3}}\right)^{\frac{N}{2}}} e^{-\frac{\sigma^2}{2\hbar}} = \sum_{n=0}^{\infty} \sum_{k=0}^{\infty} \frac{\Gamma(k + 2n + \frac{N}{2}) 2^k}{\Gamma(\frac{N}{2}) \Gamma(n+1) \Gamma(k+1) 6^n} \eta^k \hbar^{n-k}. \quad (3.8)$$

By construction, the η -derivatives of the generating function $Z(\hbar, \eta)$ in eq. (3.8) enumerate Green functions with pairs of external edges, whose indices are summed. This is a common setup in field theory, compare for example the so-called *generalized effective actions* [76–78]. However, for the following steps it is useful if we can directly compare to the examination of ϕ^4 theory (without $O(N)$ symmetry) in [37], therefore we prefer a source term j that generates a *single* external line. This is possible by replacing η^k in eq. (3.8), but one needs to carefully adjust combinatorial factors since now a $2k^{\text{th}}$ derivative with respect to j replaces a k^{th} derivative with respect to η . Furthermore, we divide by the N dependence at $n = 0$ to cancel summation over vector indices of external edges that was implied in the η -formalism. All in all, the required replacement is

$$\eta^k \mapsto \frac{\Gamma(\frac{N}{2}) \Gamma(k + \frac{1}{2})}{\Gamma(\frac{1}{2}) \Gamma(k + \frac{N}{2})} \frac{\Gamma(k+1)}{\Gamma(2k+1)} j^{2k}. \quad (3.9)$$

We remark that this is a purely formal replacement, j is not a “source term” for any field that exists in this theory. Conceptually, j would be a source term for $\sqrt{\phi^2}$, which is not the same as a (vector-valued) source \vec{j} for the field $\vec{\phi}$. We redefine the summation index n to expose the dependence on \hbar , the resulting transformation of eq. (3.8) is

$$Z(\hbar, j) = \sum_{k=0}^{\infty} \sum_{n=-k}^{\infty} \frac{\left(k + \frac{N}{2}\right)_{2n+2k} \left(\frac{1}{2}\right)_k}{6^n 3^k (n+k)! (2k)!} j^{2k} \hbar^n, \quad (3.10)$$

where we have used Pochhammer symbols $(x)_k = x(x+1)\dots(x+k-1) = \Gamma(x+k)/\Gamma(x)$ to illustrate that the dependence on N is a polynomial for finite n and k .

Now, the coefficient of Z at j^{2k} is a formal power series that enumerates graphs with exactly $2k$ external edges, for example

$$\begin{aligned} \partial_j^0 Z(\hbar, j) \Big|_{j=0} &= Z(\hbar, 0) = 1 + \frac{N(N+2)}{24} \hbar + \frac{N(N+2)(N+4)(N+6)}{1152} \hbar^2 + \dots \\ \partial_j^2 Z(\hbar, j) \Big|_{j=0} &= \frac{1}{\hbar} + \frac{(N+2)(N+4)}{24} + \frac{(N+2)(N+4)(N+6)(N+8)}{1152} \hbar + \dots \\ \partial_j^4 Z(\hbar, j) \Big|_{j=0} &= \frac{3}{\hbar^2} + \frac{(N+4)(N+6)}{8\hbar} + \frac{(N+4)(N+6)(N+8)(N+10)}{384} + \dots \end{aligned} \quad (3.11)$$

Here, the power of \hbar counts (edges minus vertices), where each external edge counts as a 1-valent ϕ -vertex.

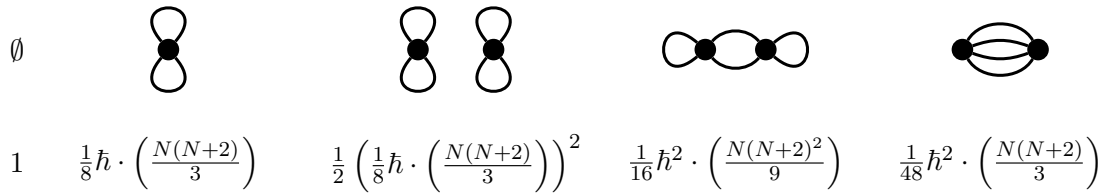


Figure 4: Feynman graphs representing the first three summands of $Z(\hbar, 0)$. This partition function enumerates vacuum graphs. The first line shows the graph, where the solid dot is a vertex to be decomposed according to [fig. 1](#). The second line is the automorphism symmetry factor and the power of \hbar , multiplied by the circuit partition polynomial.

The derivation of $Z(\hbar, \eta)$ did not make explicit reference to circuit partition polynomials ([definition 1](#)), but the resulting series is consistent with the Feynman graph expansion. We give the correspondence for the first few terms of the series expansion. The vacuum partition function $Z(\hbar, 0)$ is a sum of vacuum Feynman graphs as shown in [fig. 4](#), the polynomials $J(G, N)$ for some of the graphs had been computed in [example 1](#).

Example 4. *The sum of the terms at order \hbar^2 in [fig. 4](#) is*

$$\frac{1}{2} \left(\frac{1}{8} \left(\frac{N(N+2)}{3} \right) \right)^2 + \frac{1}{16} \left(\frac{N(N+2)^2}{9} \right) + \frac{1}{48} \left(\frac{N(N+2)}{3} \right) = \frac{N(N+2)(N+4)(N+6)}{1152},$$

which coincides with the first line of [eq. \(3.11\)](#) as claimed. This short calculation already illustrates that the circuit partition polynomials of individual graphs will often appear much more “random” than the $O(N)$ -dependence of the sum of all graphs, as remarked below [eq. \(3.6\)](#).

The power series $\partial_j^2 Z \Big|_{j=0}$ enumerates graphs with two external ϕ -edges, or equivalently vacuum graphs with one marked internal edge. In the latter perspective, the marking amounts to a 2-valent vertex with Feynman rule $\frac{2}{\hbar}$, and cycles containing 2-valent vertices do not give rise to a factor N . Note that this 2-valent vertex influences the automorphism symmetry factor. Of course, the outcome in both perspectives is equivalent. [Figure 5](#) shows the first terms of $\partial_j^2 Z(\hbar, j) \Big|_{j=0}$.

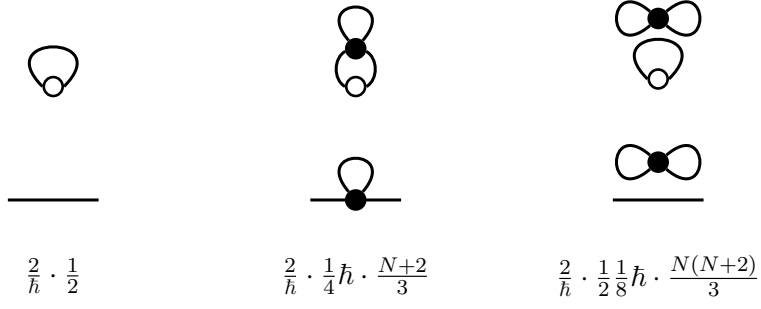


Figure 5: Feynman graphs representing the first two summands of $\partial_j^2 Z(\hbar, j)$. These are vacuum graphs with one marked edge, indicated with a white 2-valent vertex in the first row. Equivalently, upon cutting the white vertex, one obtains graphs with exactly two external edges, shown in the second row. The replacement eq. (3.9) guarantees that there is no sum over the $O(N)$ index j of the external ϕ_j .

Example 5. The sum at order \hbar^0 in fig. 5 reproduces the term in the second line of eq. (3.11),

$$\frac{2}{\hbar} \cdot \frac{1}{4} \hbar \frac{(N+2)}{3} + \frac{2}{\hbar} \frac{1}{16} \hbar \cdot \frac{N(N+2)}{3} = \frac{(N+2)(N+4)}{24}. \quad (3.12)$$

Analogously, the higher derivatives $\partial_j^{2k} Z(\hbar, j)$ enumerate graphs with $2k$ external edges, or with k 2-valent vertices. To be consistent with usual definitions, these 2-valent vertices may not be exchanged by automorphisms, which can be realized by giving an extra factor $k!$ to the graph in question. Figure 6 shows the first graphs of $\partial_j^4 Z(\hbar, j)$.

While the partition function Z enumerates *all* Feynman graphs, the free energy $W := \hbar \ln(Z)$ enumerates the *connected* Feynman graphs. Notice that connectedness here refers to the graphs with external edges, not the vacuum graphs with marked vertices, and that the extra factor \hbar ensures that the order in \hbar coincides with the loop order of the graphs. The series start with

$$\begin{aligned} \partial_j^0 W \Big|_{j=0} &= 1 + \frac{N(N+2)}{24} \hbar + \frac{N(N+2)(N+3)}{144} \hbar^2 + \frac{N(N+2)(60+34N+5N^2)}{2592} \hbar^3 + \dots \\ \partial_j^2 W \Big|_{j=0} &= 1 + \frac{N+2}{6} \hbar + \frac{(N+2)(N+3)}{18} \hbar^2 + \frac{(N+2)(60+34N+5N^2)}{216} \hbar^3 + \dots \\ \partial_j^4 W \Big|_{j=0} &= 1 + \frac{16+5N}{6} \hbar + \frac{92+50N+7N^2}{12} \hbar^2 + \frac{2784+2000N+493N^2+42N^3}{108} \hbar^3 + \dots \end{aligned} \quad (3.13)$$

Example 6. The first terms of $\partial_j^0 W$ in eq. (3.13) correspond to the three connected graphs shown in fig. 4, where one confirms that

$$\frac{1}{16} \hbar^3 \cdot \left(\frac{N(N+2)^2}{9} \right) + \frac{1}{48} \hbar^3 \cdot \left(\frac{N(N+2)}{3} \right) = \frac{N(N+2)(N+3)}{144} \hbar^3.$$

Similarly, the connected graphs from figs. 5 and 6 yield the expected terms of eq. (3.13). Note that of the vertex-type graphs (fig. 6), only the very last one is connected, and it corresponds to the leading term $1 \cdot \hbar^0$ of $\partial_j^4 W$ in eq. (3.13).

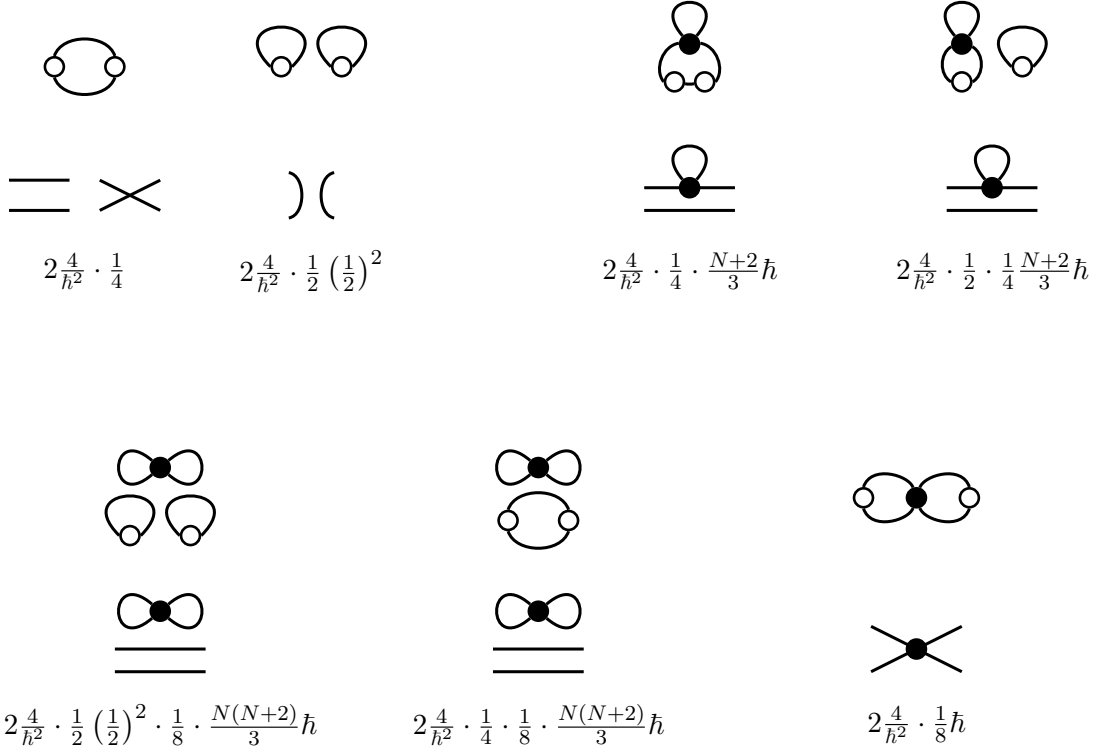


Figure 6: Feynman graphs representing the first two summands of $\partial_j^4 Z(\hbar, j)$. Notice that the three decompositions of the vertex (fig. 1) are generated from two topologically distinct vacuum graphs; together they form the first term of the third line of eq. (3.11). A similar effect occurs at higher loop order, but we do not draw all permutations of external edges explicitly. Only the very last one of the shown graph is connected and contributes as leading summand “1” to the series expansion of W (eq. (3.13)).

In order to enumerate 1PI graphs, one would conventionally introduce the “classical” field variable $\varphi := \partial_j W(\hbar, j)$, invert that series to obtain $j(\hbar, \varphi)$, and define the generating function $G(\hbar, \varphi) := W(\hbar, j(\hbar, \varphi)) - j(\hbar, \varphi)\varphi$. However, it is computationally faster to directly relate the derivatives of G to those of W , namely

$$\partial_\varphi^0 G|_{\varphi=0} = \partial_j^0 W|_{j=0}, \quad \partial_\varphi^2 G|_{\varphi=0} = \frac{-1}{\partial_j^2 W|_{j=0}}, \quad (3.14)$$

$$\partial_\varphi^4 G|_0 = \frac{\partial_j^4 W|_0}{(\partial_j^2 W|_0)^4} = 1 + \frac{N+8}{6} \hbar + \frac{140+46N+3N^2}{36} \hbar^2 + \frac{(N+4)(384+97N+5N^2)}{108} \hbar^3 + \dots$$

3.3. Counterterms, primitive graphs, Martin invariants

Using the 1PI Green functions from eq. (3.14), we compute the invariant charge,

$$Q(\hbar) := \frac{\partial_\varphi^4 G|_{\varphi=0}}{(\partial_\varphi^2 G|_{\varphi=0})^2} = 1 + \frac{N+4}{2}\hbar + \frac{5(N+4)(N+5)}{18}\hbar^2 + \frac{7(N+4)(148+54N+5N^2)}{216}\hbar^3 + \dots$$

The invariant charge defines the running coupling. In our setup, the expansion parameter \hbar takes the role of the coupling, hence we obtain a “renormalized” expansion parameter by $\hbar_{\mathcal{R}}(\hbar) := \hbar \cdot Q(\hbar)$. Inverting this power series, we find

$$\hbar(\hbar_{\mathcal{R}}) = \hbar_{\mathcal{R}} - \frac{N+4}{2}\hbar_{\mathcal{R}}^2 + \frac{(N+4)(4N+11)}{18}\hbar_{\mathcal{R}}^3 + \frac{(N+4)(49+27N+5N^2)}{54}\hbar_{\mathcal{R}}^4 + \dots \quad (3.15)$$

Finally, the vertex counterterm is the inverse (under multiplication) of the 1PI four-point function (eq. (3.14)), where we replace \hbar by eq. (3.15),

$$z^{(4)}(\hbar_{\mathcal{R}}) := \frac{1}{\partial_\varphi^4 G|_{\varphi=0}} = 1 - \frac{N+8}{6}\hbar_{\mathcal{R}} + \frac{20+6N+N^2}{36}\hbar_{\mathcal{R}}^2 - \frac{224+64N+8N^2+N^3}{216}\hbar_{\mathcal{R}}^3 + \dots \quad (3.16)$$

The vertex counterterm enumerates the graphs with four external edges which are either primitive or contain an overlapping divergence. As established in [4, Sec. 6], for ϕ^4 theory the only overlapping divergences are the L -loop chains of multiedge graphs. These chains have an automorphism symmetry factor $\frac{1}{2^L}$ and we have computed the $O(N)$ -symmetry factor in example 1. Therefore the generating function of primitive graphs is

$$\begin{aligned} \text{prim}(\hbar_{\mathcal{R}}) &= \sum_L p_L \hbar_{\mathcal{R}}^L := 1 - z^{(4)}(\hbar_{\mathcal{R}}) + \sum_{L=2}^{\infty} (-1)^L \frac{(N-1)2^{L+1} + (N+2)^{L+1}}{6^L N} \hbar_{\mathcal{R}}^L \quad (3.17) \\ &= \frac{N+8}{6}\hbar_{\mathcal{R}} + \frac{22+5N}{27}\hbar_{\mathcal{R}}^3 + \frac{186+55N+2N^2}{81}\hbar_{\mathcal{R}}^4 + \frac{5440+1946N+147N^2}{486}\hbar_{\mathcal{R}}^5 + \dots \end{aligned}$$

The coefficients $p_L = p_L(N)$ are polynomials in N , and p_2 vanishes since there is no primitive two-loop graph in ϕ^4 theory. Setting $N=1$ in eq. (3.17), we reproduce the sum of automorphism symmetry factors given in [37], which had been called $N_L^{(\text{Aut})}$ in [7]:

$$\text{prim}(\hbar_{\mathcal{R}})|_{N=1} = \frac{3}{2}\hbar_{\mathcal{R}} + \hbar_{\mathcal{R}}^3 + 3\hbar_{\mathcal{R}}^4 + \frac{31}{2}\hbar_{\mathcal{R}}^5 + \frac{529}{6}\hbar_{\mathcal{R}}^6 + \dots \quad (3.18)$$

We give further coefficients $3^{L+1}p_L$ in table 5 in the appendix. These numbers are in general not integers because the automorphism symmetry factors give rise to a denominator. Conversely, in table 6, we give the sum of $O(N)$ -symmetry factors *without* the weighting by automorphism symmetry factors. In both cases, we observe that the coefficients of low order in N are typically larger than the coefficient of the higher orders in N . To quantify this, we define the *average order*

$$\langle k \rangle_L := \frac{1}{p_L|_{N=1}} \sum_{k=0}^{\infty} k \left[N^k \right] p_L(N) = \frac{\partial}{\partial N} p_L(N) \Big|_{N=1} = \frac{\partial \log p_L(N)}{\partial \log N} \Big|_{N=1}. \quad (3.19)$$

This quantity is positive by construction, but it grows with loop order only slowly, staying below $\frac{1}{2}$ for all $L \leq 9$. This indicates that $p_L(N)$ is, for small N , mostly determined by the coefficients of the low-order monomials N^0, N^1 , and not by the highest-order monomial (which, of course, dominates as $N \rightarrow \infty$).

The generating function of primitives (eq. (3.17)) equals, up to a factor $4!$, the sum on the right hand side of eq. (2.21). Consequently, we can read off the sum of the Martin invariants at L loops,

$$M_L^{[1]} := \sum_{\substack{\text{completion } G \\ \text{with } L \text{ loop dec.}}} \frac{(L+2)}{|\text{Aut}(G)|} M^{[1]}(G) = \frac{3^L}{2 \cdot 4!} [\hbar_{\mathcal{R}}^L] \text{prim}(\hbar_{\mathcal{R}}) \Big|_{N=-2} = \frac{3^L}{48} p_L(-2).$$

The factor 3^L can be absorbed into the argument of $\text{prim}(\hbar_{\mathcal{R}})$, namely

$$\sum_{L=0}^{\infty} M_L^{[1]} \hbar_{\mathcal{R}}^L = \frac{1}{48} \text{prim}(3\hbar_{\mathcal{R}}) \Big|_{N=-2}. \quad (3.20)$$

We reproduce the explicit computation from example 3, and find for $L \in \{1, \dots, 10\}$:

$$M_L^{[1]} \in \left\{ \frac{1}{16}, 0, \frac{1}{4}, \frac{7}{4}, \frac{89}{4}, \frac{1255}{4}, \frac{20405}{4}, \frac{372139}{4}, \frac{7510709}{4}, \frac{166012747}{4} \right\}.$$

3.4. Asymptotics

So far, we have obtained generating functions for certain sums of graphs, which deliver their exact counts at low loop order. Now, we turn to the asymptotic expansion around infinite order. One way to obtain the asymptotics of the 0-dimensional path integral $Z(\hbar, j)$ is to start from closed formula eq. (3.10) for the n^{th} coefficient,

$$[\hbar^n j^{2k}] Z(\hbar, j) = \frac{\Gamma(2n + 3k + \frac{N}{2})}{\Gamma(n + k + 1)} \frac{\Gamma(k + \frac{1}{2})}{6^n 3^k \Gamma(k + \frac{N}{2}) \Gamma(\frac{1}{2}) \Gamma(2k + 1)} \quad (3.21)$$

Here, k is a fixed number, while the asymptotic expansion concerns $n \rightarrow \infty$. Using the multiplication identity for the gamma function, $\Gamma(2n + A) = \Gamma(n + \frac{A}{2}) \Gamma(n + \frac{A}{2} + \frac{1}{2}) \frac{4^n 2^A}{2\sqrt{\pi}}$, we can directly apply the known asymptotic expansion [79]

$$\frac{\Gamma(n+x)\Gamma(n+y)}{\Gamma(n+z)} \underset{n \rightarrow \infty}{\sim} \sum_{r=0}^{\infty} \Gamma(n+x+y-z-r) (-1)^r \frac{(z-x)_r (z-y)_r}{r!}.$$

In our case, $x = \frac{3}{2}k + \frac{N}{4}$, $y = \frac{3}{2}k + \frac{N+2}{4}$, and $z = k + 1$. The Pochhammer symbols $(A)_r := \Gamma(A+r)/\Gamma(A)$ in the formula can be simplified,

$$\left(1 - \frac{1}{2}k - \frac{N}{4}\right)_r \left(\frac{1}{2} - \frac{1}{2}k - \frac{N}{4}\right)_r = \frac{1}{16^r} \prod_{t=1}^{2r} (N + 2k - 2t) = \frac{\Gamma(1 - k - \frac{N}{2} + 2r)}{4^r \Gamma(1 - k - \frac{N}{2})}.$$

Combining all parts, the right hand side of eq. (3.21) has the expansion

$$n \underset{\rightarrow \infty}{\sim} \sum_{r=0}^{\infty} \Gamma\left(n + 2k + \frac{N-1}{2} - r\right) \frac{(-1)^r 2^n 8^k 2^{\frac{N}{2}} \Gamma(1 - k - \frac{N}{2} + 2r) \Gamma(k + \frac{1}{2})}{2\pi r! 3^n 3^k 4^r \Gamma(1 - k - \frac{N}{2}) \Gamma(k + \frac{N}{2}) \Gamma(2k + 1)} \quad (3.22)$$

We transform this expression to the notation of [37, 69] that we already used in eq. (2.12):

$$\left[\hbar^n j^{2k}\right] Z(\hbar, j) \underset{n \rightarrow \infty}{\sim} \sum_{r=0}^{\infty} c_r a^{-n-c_s+r} \Gamma(n + c_s - r), \quad (3.23)$$

$$\text{where } a = \frac{3}{2}, \quad c_s = 2k + \frac{N-1}{2}, \quad (3.24)$$

$$c_r = \frac{(-1)^{k+r} 3^k 3^{\frac{N-1}{2}} \sin\left(\frac{N}{2}\pi\right) \Gamma(1 - k - \frac{N}{2} + 2r)}{6^r 2^k \sqrt{2} \pi^{\frac{3}{2}} r! \Gamma(k+1)} = c_0 \cdot \frac{(-1)^r}{6^r} \left(1 - k - \frac{N}{2}\right)_{2r}.$$

Example 7. The coefficient $k = 0$ of the path integral, hence the power series $Z(\hbar, 0) = \sum \hbar^n z_n$, has the asymptotics

$$z_n \sim \frac{3^{\frac{N-1}{2}} \left(\frac{3}{2}\right)^{-n - \frac{N-1}{2}} \Gamma(n + \frac{N-1}{2})}{\sqrt{2\pi} \Gamma(\frac{N}{2})} \left(1 - \frac{(N-2)(N-4)}{24(2n+N-3)} + \frac{(N-2)(N-4)(N-6)(N-8)}{1152(2n+N-3)(2n+N-5)} + \dots\right).$$

A plot of the coefficients for $k = 2$, that is, the 4-point function $[\hbar^n j^4]Z(\hbar, j)$, is shown in fig. 7a. We see that already the leading asymptotics $c_0 A^{-n-c_s} \Gamma(n + c_s)$ matches the data points quite well, the deviation is $\approx 1\%$ at $n = 15$. If one divides by this leading asymptotics, the remaining difference is captured well by the subleading terms in eq. (3.23). Note that eq. (3.23) is an *asymptotic* expansion: Including higher terms in the sum improves the description for $n \rightarrow \infty$, but the sum does not converge for any finite n , as is clearly visible for the small values of n in fig. 7b.

The mapping from $Z(\hbar, j)$, viewed as a formal power series in \hbar , to its asymptotics (eq. (3.23)) is the alien derivative operator \mathcal{A}_\hbar^a of [37, 69],

$$\mathcal{A}_\hbar^{\frac{3}{2}} Z(\hbar, j) := \hbar^{-c_s} \sum_{r=0}^{\infty} \sum_{k=0}^{\infty} c_r(k, N) \hbar^r j^{2k}. \quad (3.25)$$

This operator has well-defined product- and chain rules, and it commutes with the ordinary derivative ∂_j . To compute the asymptotics of the generating function of connected graphs, $W(\hbar, j) = \hbar \ln Z(\hbar, j)$, we use the chain rule and note that the power series of $\ln(x)$ is not divergent, therefore $\mathcal{A}_x^{\frac{3}{2}} \ln(x) = 0$ and

$$\mathcal{A}_\hbar^{\frac{3}{2}} W(\hbar, j) = \frac{\hbar}{Z(\hbar, j)} \mathcal{A}_\hbar^{\frac{3}{2}} Z(\hbar, j).$$

The first four terms of this power series are given in table 7 in appendix B. Note that by eq. (3.25), the exponent of \hbar in the prefactor encodes the constant c_s (which thereby

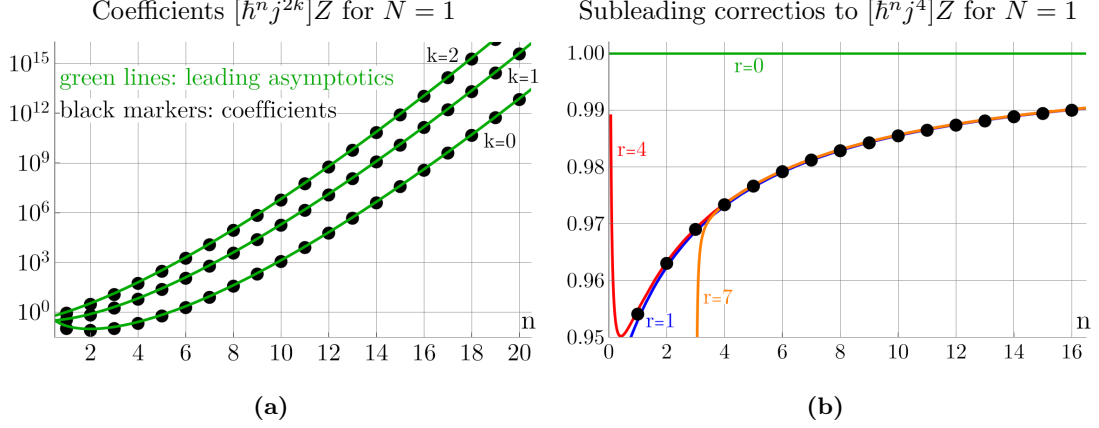


Figure 7: (a) First 20 coefficients of $[\hbar^n j^{2k}]Z(\hbar, j)$, for $N = 1$ and $k \in \{0, 1, 2\}$, logarithmic plot. The green line shows the leading asymptotics according to eq. (3.23), only including the term $r = 0$ (b) The data points for $k = 2$, scaled to the leading asymptotics. Colored lines show the subleading corrections up to the indicated r . Note that this asymptotic expansion matches the data remarkably well even at very low orders n .

does not always take the value of eq. (3.24), whereas $a = \frac{3}{2}$ in all cases). Setting $N = 1$ reproduces the coefficients given in [37] for ϕ^4 theory without $O(N)$ symmetry.

The asymptotics of the generating function $G(\hbar, \varphi)$ of 1PI graphs follows from eq. (3.14),

$$\begin{aligned} \mathcal{A}_{\hbar}^{\frac{3}{2}} \partial_{\varphi}^0 G|_{\varphi=0} &= \mathcal{A}_{\hbar}^{\frac{3}{2}} \partial_j^0 W|_{j=0}, & \mathcal{A}_{\hbar}^{\frac{3}{2}} \partial_{\varphi}^2 G|_{\varphi=0} &= \frac{1}{\left(\partial_j^2 W|_{j=0}\right)^2} \mathcal{A}_{\hbar}^{\frac{3}{2}} \partial_j^2 W|_{j=0}, \\ \mathcal{A}_{\hbar}^{\frac{3}{2}} \partial_{\varphi}^4 G|_{\varphi=0} &= \frac{1}{\left(\partial_j^2 W|_{j=0}\right)^4} \mathcal{A}_{\hbar}^{\frac{3}{2}} \partial_j^4 W|_{j=0} - \frac{4 \partial_j^4 W|_{j=0}}{\left(\partial_j^2 W|_{j=0}\right)^5} \mathcal{A}_{\hbar}^{\frac{3}{2}} \partial_j^2 W|_{j=0}. \end{aligned}$$

Again, the first coefficients of these power series are given explicitly in table 5. Similarly, we use the product rule to compute the asymptotics of the invariant charge:

$$\mathcal{A}_{\hbar}^{\frac{3}{2}} Q = \mathcal{A}_{\hbar}^{\frac{3}{2}} \left(\frac{\partial_j^4 W|_{j=0}}{\left(\partial_j^2 W|_{j=0}\right)^2} \right) = \frac{\mathcal{A}_{\hbar}^{\frac{3}{2}} \partial_j^4 W|_{j=0}}{\left(\partial_j^2 W|_{j=0}\right)^2} - \frac{2 \partial_j^4 W|_{j=0}}{\left(\partial_j^2 W|_{j=0}\right)^3} \mathcal{A}_{\hbar}^{\frac{3}{2}} \partial_j^2 W|_{j=0}.$$

This is the asymptotics of the renormalized coupling $\mathcal{A}_{\hbar}^{\frac{3}{2}} \hbar_{\mathcal{R}} = \hbar \mathcal{A}_{\hbar}^{\frac{3}{2}} Q$. To obtain the asymptotics of the inverse function, let x be the variable of the inverse series $\hbar_{\mathcal{R}}^{-1}$, then

$$\mathcal{A}_{\hbar_{\mathcal{R}}}^{\frac{3}{2}} \hbar(\hbar_{\mathcal{R}}) = \mathcal{A}_x^{\frac{3}{2}} \hbar_{\mathcal{R}}^{-1}(x) = -e^{\frac{3}{2} \left(\frac{1}{x} - \frac{1}{\hbar_{\mathcal{R}}^{-1}(x)} \right)} \frac{\mathcal{A}_{\hbar}^{\frac{3}{2}} \hbar_{\mathcal{R}}(\hbar)}{\partial_{\hbar} \hbar_{\mathcal{R}}(\hbar)} \Big|_{\hbar=\hbar_{\mathcal{R}}^{-1}(x)}.$$

We provide their coefficients in table 7. Finally, we need the asymptotics of the vertex counterterm $z^{(4)}$, expressed as a power series of $\hbar_{\mathcal{R}}$. With $\mathcal{A}_{\hbar}^{\frac{3}{2}} z^{(4)}(\hbar) = -\left(\partial_{\varphi}^4 G|_0\right)^{-2} \mathcal{A}_{\hbar}^{\frac{3}{2}} \partial_{\varphi}^4 G|_0$,

and, since both $G(\hbar)$ and $\hbar(\hbar_{\mathcal{R}})$ have factorially divergent series,

$$\mathcal{A}_{\hbar_{\mathcal{R}}}^{\frac{3}{2}} z^{(4)}(\hbar(\hbar_{\mathcal{R}})) = \partial_{\hbar} z^{(4)}|_{\hbar=\hbar(\hbar_{\mathcal{R}})} \cdot \mathcal{A}_{\hbar_{\mathcal{R}}}^{\frac{3}{2}} \hbar(\hbar_{\mathcal{R}}) + e^{\frac{3}{2}\left(\frac{1}{\hbar_{\mathcal{R}}} - \frac{1}{\hbar(\hbar_{\mathcal{R}})}\right)} \mathcal{A}_{\hbar}^{\frac{3}{2}} z^{(4)}|_{\hbar=\hbar(\hbar_{\mathcal{R}})}. \quad (3.26)$$

3.5. Asymptotics of primitive graphs

The asymptotics of the primitive graphs is unchanged by the addition of multiedge chains, and coincides with eq. (3.26) as given in table 7. Concretely, the asymptotic growth of p_L as $L \rightarrow \infty$ in the series $\text{prim}(\hbar_{\mathcal{R}}) =: \sum p_L \hbar_{\mathcal{R}}^L$ (eq. (3.17)) is

$$p_L \sim \frac{3^{\frac{N-1}{2}}}{\frac{4}{3}\sqrt{2\pi}\Gamma\left(\frac{N+4}{2}\right)} e^{-\frac{12+3N}{4}} \left(\frac{2}{3}\right)^{L+\frac{N+5}{2}} \Gamma\left(L+\frac{N+5}{2}\right) \cdot \left(36 - \frac{9(3N^2 - 4N - 80)}{4\left(L+\frac{N+3}{2}\right)} + \frac{9(9N^4 - 40N^3 - 488N^2 - 416N + 1664)}{128\left(L+\frac{N+1}{2}\right)\left(L+\frac{N+3}{2}\right)} + \dots\right). \quad (3.27)$$

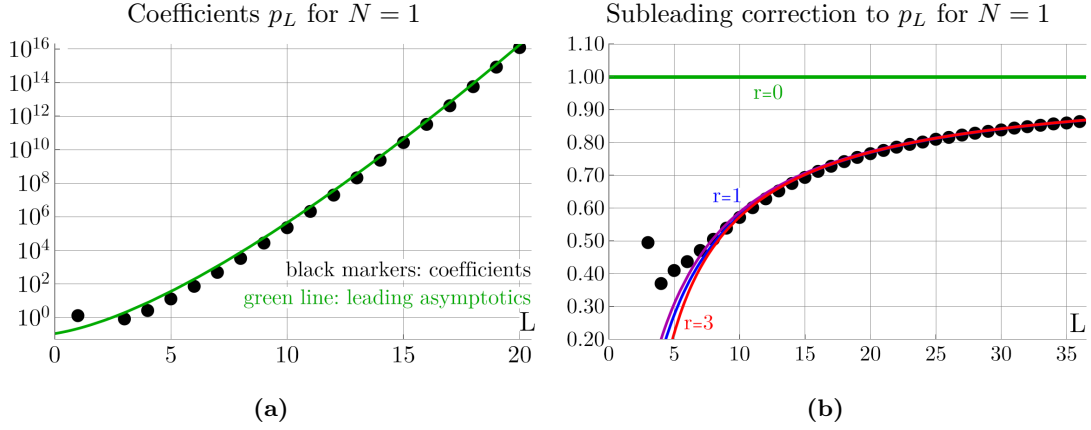


Figure 8: (a) First 20 coefficients p_L of $\text{prim}(\hbar_{\mathcal{R}})$, for $N = 1$, logarithmic plot. The green line shows the leading asymptotics according to eq. (3.27), only including the first term in the parenthesis. (b) The same data points, but scaled to the leading asymptotics. They converge to unity as $L \rightarrow \infty$. Colored lines show the first three subleading corrections. Compare to fig. 7b and note the different plot scale.

For low loop orders, the exact terms p_L from eq. (3.17) are shown together with the leading term of eq. (3.27) in fig. 8a. Comparing this to the analogous plot for $\partial_j^4 Z(\hbar, j)$ (fig. 7a), we note that the asymptotic expansion of primitive graphs is much less accurate in capturing the terms at low order, compared to the asymptotic expansion of $\partial_j^4 Z$. For example, at $L = 16$ loops, the leading asymptotics for p_{16} is roughly 30% off the true value, while for $[\hbar^{16}]\partial_j^4 Z$, the difference is only about 1%. A similar picture holds for the subleading corrections: From fig. 7b, we see that the first subleading order, $r = 1$, starts to capture the data only for $L > 8$ loops. A closer investigation of the remaining residue indicates that the second subleading order, $r = 2$, reliably improves the accuracy only at $L > 25$. Both these thresholds depend on the value of N . In fig. 9b,

we show the minimum loop order required to reach a certain accuracy with the leading, first subleading, 5th subleading, or 9th subleading order. The qualitative takeaway is that below roughly 25 loops, the asymptotic expansion is unreliable and accurate results are mostly coincidence of cancellations for particular values of N .

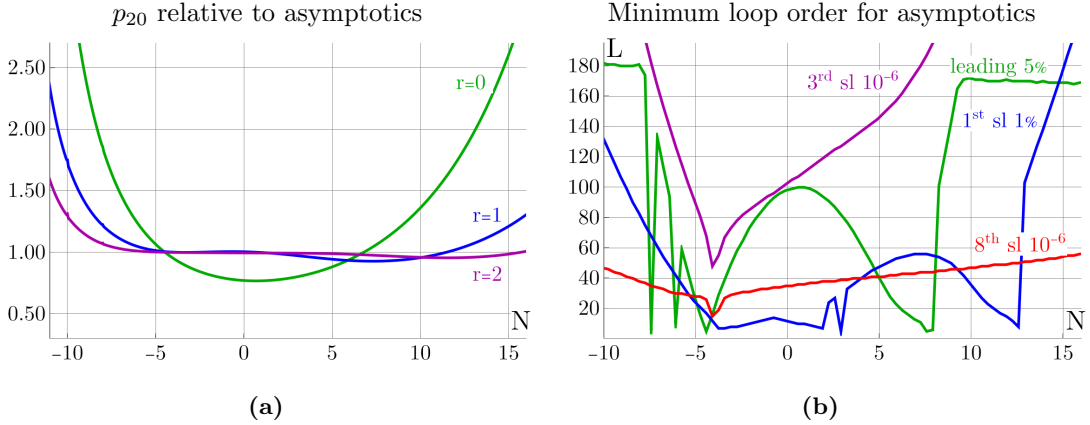


Figure 9: (a) $p_{20}(N)$ from eq. (3.17) divided by the asymptotics eq. (3.27), where both are functions of N . The leading asymptotics ($r = 0$) captures the N dependence up to a factor ~ 2 in this regime, higher corrections are close to unity for not too large $|N|$. The accuracy might appear poor at first, but $p_L(N)$ is strongly dependent on N , we have $p_{20}(15)/p_{20}(1) > 10^3$. (b) Minimum loop order where the asymptotic expansion coincides with the true count of primitive graphs to a given accuracy. The leading asymptotics might need as much as $L \geq 180$ to reach 5% accuracy. From $L \geq 30$ loops, one can expect that including the first subleading terms improves accuracy, as evidenced from the lines where the 3rd respective 8th corrections reach 10^{-6} accuracy.

To investigate the N dependence, we divide $p_{20}(N)$ by the asymptotic series eq. (3.27) for $L = 20$ up to a certain maximum order $r \in \{0, 1, 2\}$, see fig. 9a. We see that the leading asymptotics, $r = 0$, essentially fails at reproducing the actual N dependence, while already $r = 1$ gives a reasonable result for $-5 \leq N \leq 10$, and $r = 2$ is even more accurate, but still differs visibly for $N \approx 10$. Despite the agreement, note that the limit $N \rightarrow \infty$ does not commute with the asymptotic expansion: Every term in the perturbation series is a polynomial, and therefore diverges as $N \rightarrow \infty$ (at fixed order L). On the other hand, the asymptotic expansion eq. (3.27) vanishes as $N \rightarrow \infty$ due to the factor $\frac{1}{\Gamma(\frac{N+4}{2})}$.

The asymptotics eq. (3.27) has zeros at all negative integer N smaller than -2 , due to the factor $\Gamma(\frac{N+4}{2})$ in the denominator. In view of lemma 3, a zero at $N = -2j$ represent a summation over all channels of a $(2j + 2)$ -valent subgraph. A priori, not all such channels would give rise to a primitive graph, but in the limit $L \rightarrow \infty$, indeed almost all channels are present. This is a curious alternative perspective on the known fact that asymptotically, almost all simple graphs are primitive, that is, the leading asymptotic number of primitive graphs coincides with the leading asymptotic number of all simple graphs. Moreover, despite the rather slow convergence of the absolute value of p_L to its asymptotics (fig. 8b), the location of these zeroes converges rapidly towards negative even

integers, see fig. 20b. This effect was called *superfast convergence* in [80]. An alternative perspective is that $p_L(N)$ is not factorially divergent when N is exactly a negative even integer ≤ 4 [81].

Later, when we compare to numerical data of 4-dimensional ϕ^4 theory, we will consider the growth ratio r_L defined in eq. (2.13). By eq. (3.27), this ratio is an asymptotic power series in $\frac{1}{L}$, starting with

$$r_L(p) := \frac{1}{L} \frac{p_{L+1}}{p_L} \sim \frac{2}{3} + \frac{N+5}{3} \frac{1}{L} - \frac{3N^2 - 4N - 80}{24} \frac{1}{L^2} + \frac{5N^3 + 8N^2 + 40N + 352}{48} \frac{1}{L^3} + \dots \quad (3.28)$$

Consequently, if we plot the exact data (eq. (3.17)) as a function of $\frac{1}{L}$, we expect to see a finite limit $\frac{2}{3}$ as $\frac{1}{L} \rightarrow 0$, and a linear convergence towards this limit with a slope $\frac{N+5}{3}$. This is indeed what we observe in fig. 10a, but it is striking that this behaviour only sets in for $L \geq 25$. Conversely, for smaller L , the data points almost lie on a linear function, too, but with a *wrong* slope and limit which does not reflect the true behaviour as $L \rightarrow \infty$. Not only that, but these wrong would-be asymptotics even mimics the N dependence of eq. (3.28): For various values of N , one obtains a slope that linearly depends on N , and the y -axis intercept is almost independent of N , close to 0.64. This value is $\approx 5\%$ smaller than the true limit $\frac{2}{3}$. To illustrate this effect, we did linear fits to the data points r_L for $10 \leq L \leq 18$, (marked red in fig. 10a), and extrapolated their slopes to $L = \infty$ (red lines). For comparison, the true asymptotics (eq. (3.28)) is drawn as green lines.

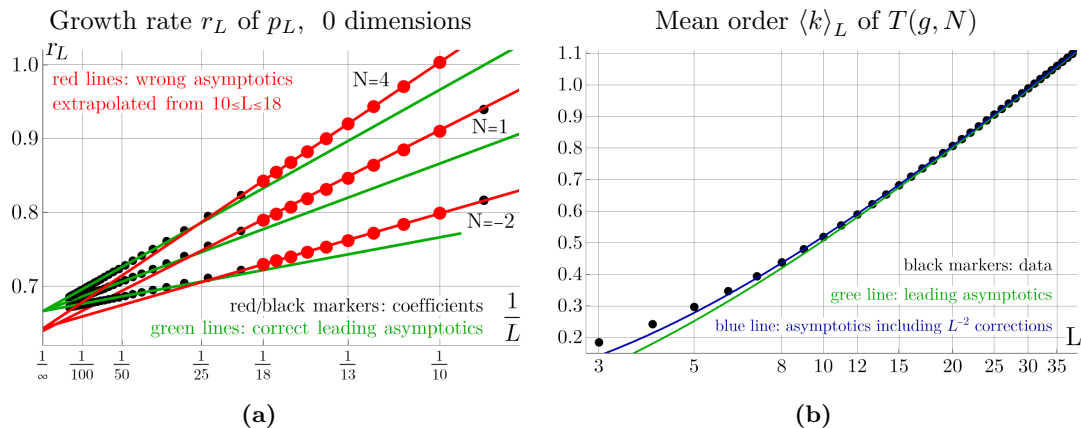


Figure 10: (a) Growth ratio r_L (eq. (3.28)) for $L \leq 150$, for three selected values of N . Green lines show the exact asymptotics including $\frac{1}{L}$ terms. Red lines show the wrong asymptotics obtained from a linear fit of $10 \leq L \leq 18$ loops (data points marked in red). Note that the red points give rise to the expected N dependence (i.e. convergence to a N -independent limit at $L \rightarrow \infty$, with a slope that grows linearly in N , but the numerical value of these constants is not the true asymptotic one. The data starts to match the true asymptotics at $L \approx 25$. (b) Mean order $\langle k \rangle_L$ of the polynomial $p_L(N)$ (eq. (3.19)), together with its asymptotics (eq. (3.31)). The asymptotics grows logarithmically, which is a straight line in this log linear plot.

3.6. Asymptotics of Martin invariants

By eq. (3.20), the sum of all Martin invariants at L loops, $M_L^{[1]}$, is a simple transformation of the generating function of primitive graphs. We can infer its asymptotics from eq. (3.27),

$$M_L^{[1]} \sim \frac{2^L e^{-\frac{3}{2}}}{24\sqrt{\pi}} \Gamma\left(L + \frac{3}{2}\right) \left(1 - \frac{15}{4(L + \frac{1}{2})} + \frac{63}{32(L + \frac{1}{2})(L - \frac{1}{2})} - \frac{1263}{128(L + \frac{1}{2})(L - \frac{1}{2})(L - \frac{3}{2})} + \dots\right).$$

The growth rate is three times the one of primitives (eq. (3.28)) at $N = -2$,

$$r_L(M^{[1]}) := \frac{M_{L+1}^{[1]}}{L \cdot M_L^{[1]}} \sim 2 + 3\frac{1}{L} + \frac{15}{2}\frac{1}{L^2} + \frac{33}{2}\frac{1}{L^3} + \frac{753}{8}\frac{1}{L^4} + \frac{3243}{4}\frac{1}{L^5} + \dots \quad (3.29)$$

In fig. 10a, we see that the sum of Martin invariants shows the same effect as the sum of primitive graphs, namely the growth rate r_L assumes the true asymptotic behaviour only above 25 loops. Dividing $M_L^{[1]}$ by $N_L^{(\text{Aut})}$, we obtain the average Martin invariant of an L -loop primitive, where the graphs are weighted by their automorphism symmetry factor. Its asymptotics at $L \rightarrow \infty$ is

$$\frac{M_L^{[1]}}{N_L^{(\text{Aut})}} = 3^L L^{-\frac{3}{2}} \frac{e^{\frac{9}{4}} \sqrt{\pi}}{128\sqrt{2}} \left(1 - \frac{21}{16}\frac{1}{L} + \frac{673}{512}\frac{1}{L^2} + \frac{82809}{8192}\frac{1}{L^3} + \dots\right). \quad (3.30)$$

3.7. The large- N limit

Unlike the large- L limit, the large- N limit is not factorially divergent. To see this, introduce a variable $U = \hbar N$, so that each occurrence of \hbar in the generating functions in section 3.2 is replaced by $\frac{U}{N}$. The coefficients of $Z(U, j)$ (eq. (3.10)) still contain positive powers of N , but those are entirely due to disconnected graphs. In W , and all subsequent series, the coefficients are polynomials in $\frac{1}{N}$. In a large- N limit (where U is kept fixed), all subleading terms vanish and one obtains a power series in U . In particular, the coefficients of $\text{prim}(\hbar)$ (eq. (3.17)) have no leading contribution beyond order U^1 . This says that to a fixed order $\frac{1}{N^k}$, only finitely many primitive graphs will contribute, and all primitives beyond a certain loop order vanish to that order in $\frac{1}{N}$.

Example 8. By eq. (3.13), the series for connected vertex-type graphs starts with

$$\partial_j^4 W \Big|_{j=0} \left(U, \frac{1}{N}\right) = 1 + \left(\frac{5}{6} + \frac{8}{3}\frac{1}{N}\right)U + \left(\frac{7}{12} + \frac{25}{6}\frac{1}{N} + \frac{23}{3}\frac{1}{N^2}\right)U^2 + \dots$$

The large- N limit of this series is $1 + \frac{5}{6}U + \frac{7}{12}U^2 + \dots$. Conversely, the generating series for primitive graphs starts with

$$\text{prim}\left(U, \frac{1}{N}\right) = \left(\frac{1}{6} + \frac{4}{3}\frac{1}{N}\right)U + \left(0 + \frac{5}{27}\frac{1}{N^2} + \frac{22}{27}\frac{1}{N^3}\right)U^3 + \left(0 + \frac{2}{81}\frac{1}{N^2} + \dots\right)U^4 + \dots$$

In this case, the large- N limit of higher-order terms vanishes, and $\text{prim}(U, 0) = \frac{1}{6}U$.

The replacement $\hbar \mapsto \frac{U}{N}$ leads to an extra factor N^n in eq. (3.22). The asymptotic growth coefficient $a = \frac{3}{2}$ of eq. (3.24) then turns into $a = \frac{3}{2}N$, which diverges in the limit $N \rightarrow \infty$. The asymptotic growth of series coefficients is $\propto a^{-n}\Gamma(n + c_s)$, hence, unbounded growth of a indicates that the large- N series does not diverge factorially. Convergence of the large- N expansion means that with growing L , the coefficient of highest order in N in the polynomial $p_L(N)$ grows much slower than the sum of all terms (which is the evaluation of $p_L(N)$ at fixed N). This causes the sum to diverge factorially with growing L , while every finite order in the large- N expansion is convergent.

We can make this behaviour more explicit by considering the average order $\langle k \rangle_L$ of the polynomials $p_L(N)$, introduced in eq. (3.19). Computing the N -derivative of the asymptotics of $p_L(N)$ from eq. (3.27), we find the asymptotics of $\langle k \rangle_L$:

$$\langle k \rangle_L = \frac{\partial_N p_L}{p_L} \Big|_{N=1} \sim \frac{1}{2} \ln(L) + \frac{1}{2} \gamma_E - \frac{25}{12} + \frac{3}{2} \ln(2) + \frac{11}{8} \frac{1}{L} - \frac{145}{96} \frac{1}{L^2} + \mathcal{O}\left(\frac{1}{L^3}\right). \quad (3.31)$$

Here, γ_E is the Euler-Mascheroni constant. This asymptotics together with data points for $L \leq 40$ is shown in fig. 10b.

The average order $\langle k \rangle_L$ grows only logarithmically with the loop order, whereas the *degree* of $T(G, N)$ grows linearly (see lemma 5 below). This means that, as L increases, the polynomials are more and more dominated by terms of low order in N , that is, the coefficient of largest order in N are vanishingly small compared to the coefficients at low order. It explains why it is possible that each fixed order in the large- N expansion converges, while the full perturbative series (which would be the sum of all orders in the large- N expansion) is factorially divergent. More details of the resummed perturbation series for the case of vacuum graphs can be found in [70].

4. Classification of leading N dependence

4.1. Dual graphs

In studying the 0-dimensional path integral in section 3, we have used the Hubbard-Stratonovich transformation [71–73] as a formal identity between certain integrals that share the same power series expansion (eq. (3.3)). In the present section, we interpret the same transformation as a mapping between the $O(N)$ -symmetric ϕ^4 theory, and a “dual” theory of a field σ with interaction $\frac{N}{2} \hbar \ln\left(1 - \frac{\sigma}{\sqrt{3}}\right)$ whose vacuum path integral (in the 0-dimensional case) is eq. (3.4). This is a common tool also used e.g. in tensor models [82–84], loop vertex expansion [85], or for a duality between 3-dimensional ϕ^4 theory and string theory [86].

Both the original field ϕ and the dual field σ admit a perturbative expansion in terms of Feynman graphs. These expansions produce the same power series when Feynman rules are applied, but the relevant graphs and their Feynman rules are different in both cases. In Feynman graphs of the original ϕ^4 theory (fig. 4), all vertices are 4-valent and contribute \hbar , and the N dependence arises from decompositions of these vertices (fig. 1).

The dual field σ has interaction vertices of all valences $n \geq 1$ for which the Feynman rules give $\frac{(n-1)!}{2 \cdot 3^{\frac{n}{2}}} N$. These vertex Feynman rules do not contain \hbar . Instead, each edge of σ contributes a factor \hbar . The vertices of σ correspond to the circuits in the decompositions of the graphs of ϕ , and the edges of σ correspond to the vertices of ϕ . The mapping between graphs G of ϕ^4 theory and dual graphs G^* of the σ model is therefore one to many, in the sense that it does not map each graph G , but each decomposition of a graph G , to one dual graph G^* .

Definition 5. *Let G be a completion (definition 4). For a fixed decomposition of G into circuits, the Hubbard-Stratonovich dual graph G^* is constructed as follows: Each of the circuits becomes a vertex of G^* and for each vertex in G adjacent to two (possibly identical) circuits there is an edge of G^* connecting the corresponding vertices.*

Visually, each circuit in the decomposition of G is being contracted to a vertex, preserving adjacency, see fig. 11. In particular,

$$|E_{G^*}| = |V_G|. \quad (4.1)$$

Figure 11 shows an example of non-isomorphic duals G^* that are obtained from distinct decompositions of the same ϕ^4 -graph G . The first few connected vacuum graphs of σ are shown in fig. 12, they reproduce the terms of the connected graphs of ϕ in fig. 4.

Since the concept of *planar* duality is an important ingredient to the large- N expansion of many quantum field theories, we want to stress at this point that the duality of definition 5 is *not* planar duality, and neither the graphs G nor their dual graphs G^* are typically planar.

Our goal is to use the dual graphs G^* to understand the leading N dependence of primitive graphs of ϕ^4 theory. To that end, we need to understand how to reconstruct G from a given G^* , and under which conditions the resulting G is primitive (section 2.2). We first establish two elementary lemmata.

Lemma 4. *If G is a primitive completion with $L > 1$ loops, then the dual G^* is connected and does not contain 1-valent or 2-valent vertices.*

Proof. By definition 5, the Hubbard-Stratonovich transformation maps connected graphs to connected graphs. The valence of a vertex in G^* is larger than or equal to the number of vertices in the corresponding circuit in the decomposition of G . If a vertex of G^* had valence two, there would be a circuit in G with at most two vertices. Such circuit is either a tadpole or a double edge, both of which are not allowed since G is primitive. \square

Lemma 5. *Let G be a primitive completion (definition 4), where $L > 1$ is the loop order of the decomposition $g = G \setminus \{v\}$. Then the degree of the $O(N)$ symmetry factor (definition 2) is bounded by*

$$\begin{aligned} \text{Degree in } N \text{ of the polynomial } T(G, N) &\leq N_{\max} := \frac{|E_G|}{3} = \frac{2}{3}L + \frac{4}{3} \\ \text{Degree in } N \text{ of the polynomial } T(g, N) &\leq N_{\max} - 2 = \frac{2}{3}L - \frac{2}{3}. \end{aligned}$$

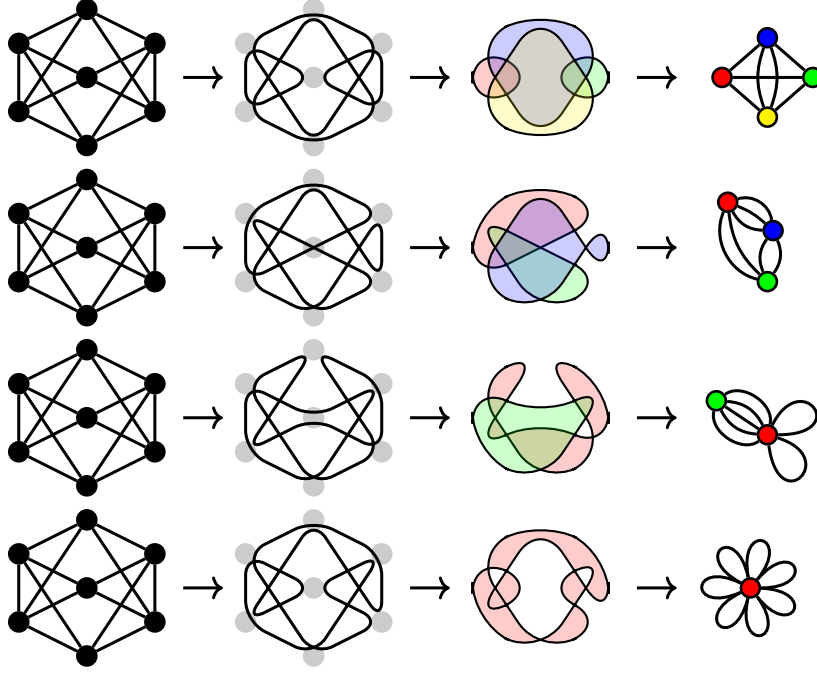


Figure 11: Construction of four distinct duals G^* for four possible choice of circuits of the completion G shown in fig. 3. For the same graph G , the duals G^* can have different numbers of vertices, but in all cases the number of edges in G^* equals the number of vertices in G (eq. (4.1)). In particular, an Eulerian circuit in the original graph amounts to G^* being a rose graph on a single vertex (bottom row).

Proof. In the absence of multiedges, the smallest number of edges in a circuit is three. A completion with L loops has $L + 2$ vertices and $2(L + 2)$ edges. Distributing these edges into circuits of length three gives the claimed formula. The bound for the decompletion $g = G \setminus \{v\}$ follows from lemma 2.

Alternatively, consider the dual G^* (definition 5). The number of vertices in G^* equals the order in N of the corresponding term in $T(G, N)$. By lemma 4, each vertex in G^* has valence at least 3, therefore $|V_{G^*}| \leq \frac{2}{3}|E_{G^*}|$. A 4-regular completion with L loops has $L + 2$ vertices, hence by eq. (4.1) $|E_{G^*}| = L + 2$. \square

Example 9. The graph in fig. 11 has $L = 5$ and hence $\lfloor N_{\max} \rfloor = \lfloor \frac{14}{3} \rfloor = 4$. The top row in the picture shows one choice of circuits that exhausts this bound.

Lemma 5 does not hold for the decompletion at $L = 1$, which is the fish graph (fig. 2). The completion of the fish is a ring of three fish, which, according to example 1, has degree 3 in N . This is larger than $N_{\max} = \frac{2}{3} \cdot 1 + \frac{4}{3} = 2$.

For general G^* , the mapping $G \mapsto G^*$ of definition 5 is not invertible. However, it is possible to construct an inverse mapping for certain restricted classes of dual graphs; these happen to be the ones of leading order in N and we will show that in this case one can construct G from the line graph of G^* .

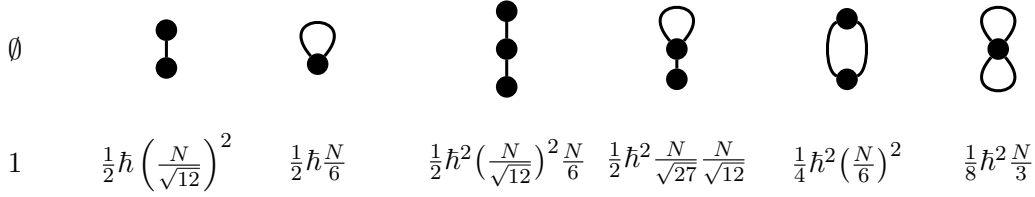


Figure 12: Feynman graphs of the dual field σ , representing the first three terms of $\partial_j^0 W|_0$ (eq. (3.13)). The number of edges determines the order of \hbar , and the number of vertices is the order in N . Hence, this expansion produces the full N dependence, whereas for the corresponding Feynman graphs of ϕ (the connected graphs in fig. 4), one needs to insert the $O(N)$ symmetry factor $T(G, N)$ (definition 2) in addition.

Definition 6. Let G^* be a graph. The line graph $L(G^*)$ is a graph where every edge of G^* is a vertex of $L(G^*)$, and two vertices of $L(G^*)$ are connected by an edge if and only if the corresponding edges in G^* are adjacent to the same vertex in G^* .

Note that for general G^* , the line graph $L(G^*)$ is not 4-regular.

Example 10. Every 4-regular graph G with n vertices has at least one Eulerian circuit, that is, a circuit that traverses every edge exactly once. The dual G^* of such a decomposition is a rose graph with n petals, shown in the last row of fig. 11. Consequently, every 4-regular graph G has a rose graph G^* among its duals. From this G^* , it is not possible to infer any information about G except for the number of vertices.

The line graph $L(G^*)$ of the rose on n petals is the complete graph K_n , which is not 4-regular in general.

4.2. The duals of leading-order primitive graphs

4.2.1. Primitive graphs with $3n + 1$ loops

We first consider those loop orders where the ratio N_{\max} in lemma 5 is an integer, namely $L \in \{4, 7, 10, 13, \dots\}$, or generally $L = 3n + 1$ for $n \in \mathbb{N}$. To exhaust the bound N_{\max} , a dual graph G^* (definition 5) must have the maximum number of vertices for a given number of edges,

$$|V_{G^*}| \stackrel{!}{=} \frac{2L_G + 4}{3} = \frac{2}{3}|E_{G^*}|. \quad (4.2)$$

In the absence of 2-valent vertices (lemma 4), eq. (4.2) implies that all vertices of G^* are 3-valent. Hence, only such completions G can contribute at leading order in N which have a 3-regular dual graph G^* . The interesting part is the converse: Under which conditions can we obtain a primitive completion G from a 3-regular G^* ? We first show that the leading decompositions are unique:

Lemma 6. Let $L = 3n + 1$ for $n \in \mathbb{N}$. Let G be a primitive completion that has a decomposition of leading order N_{\max} (lemma 5). If G is the six-vertex zigzag (the

octahedron graph, *fig. 14*), it has two isomorphic decompositions. In all other cases, there is exactly one decomposition at leading order.

Proof. The decompositions at leading order are such that every circuit has length three. Hence, for there to be more than one such decomposition, it must be possible to decompose G into triangles in more than one way.

Consider a vertex $v \in G$. Assume that all three decompositions (*fig. 1*) of that vertex give rise to a term of leading order in $T(G, N)$. This means that in all three cases, the pairs of edges must belong to triangles. This is only possible if all four neighboring vertices to v are also adjacent to each other, see *fig. 13*. Hence, G is K_5 . But K_5 has five vertices and thus $L = 3$ in contradiction to the assumption $L = 3n + 1$. Consequently, it is impossible that all three decompositions of any vertex contribute at leading order.

Now assume that there are two compositions that contribute at leading order. Then, the four neighboring vertices of v each have to be adjacent to two (but not all three) others. In order to be a decomposition at leading order for the whole graph, these vertices each have to be adjacent another triangle in each of the two configurations, see *fig. 14*. The only way to realize this is to have all four vertices adjacent to one vertex v' . Hence, G is the octahedron. \square

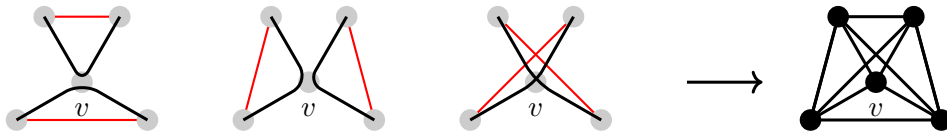


Figure 13: Proof of *lemma 6*: If we assume that each of the three decompositions of a vertex v leads to two triangles, the graph must contain all of the edges indicated in red. This implies that the graph is necessarily K_5 , which has $L = 3$.

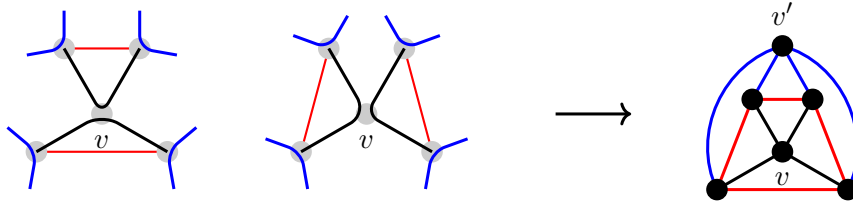


Figure 14: Proof of *lemma 6*: If we assume that two decompositions of a vertex v lead to two triangles each, the graph must contain the red edges. When the four red edges are present, they, together with v , form a 4-valent subgraph. The only way to obtain a primitive (=internally six-edge connected) graph is to connect the four blue edges to a single vertex v' . The resulting graph is the octahedron (=six-vertex zigzag).

Theorem 1. *Let $L = 3n + 1$ for $n \in \mathbb{N}$. The primitive completed graphs G which contribute at leading order in N are the line graphs (*definition 6*) of those 3-regular, simple graphs G^* which are 3-edge-connected.*

Proof. By construction and [lemma 5](#), the dual graphs G^* of the leading contributions in $T(G, N)$ are 3-regular. We need to show two things: 1. When G^* is furthermore three-connected, then its line graph is primitive. And 2. this construction produces all primitive G that contribute at leading order in N .

1. If 3-edge-connected, every edge in G^* is adjacent to two *distinct* vertices. These, in turn, are adjacent to a total of four distinct other edges. Hence, the line graph $L(G^*)$ is 4-regular, and every vertex of $L(G^*)$ is adjacent to another four distinct vertices. In particular, there are no multiedges and no tadpoles. Furthermore, every vertex of G^* corresponds to a triangle of edges in $L(G^*)$. Since every edge in G^* is adjacent to four distinct edges, every vertex of $L(G^*)$ is adjacent to two triangles which have no edges in common (there may be more than two triangles in total if they share edges). This implies that every edge of $L(G^*)$ is part of at least one triangle. Now assume that a subgraph $\gamma \subset L(G^*)$ is connected to its complement through four edges. Since each of the four edges must be part of some triangle, they must be arranged such that two of them share one triangle and the other two share another triangle. Hence, γ is connected to its complement in $L(G^*)$ through two vertices. Removing these two vertices disconnects the two parts. Therefore, removing the two corresponding edges in G^* disconnects G^* . Consequently, if $L(G^*)$ has a subgraph of valence four, then G^* is two-edge-reducible. Analogously, a subgraph of valence two in $L(G^*)$ leads to G^* being one-edge-reducible. We conclude that, if G^* is 3-edge-connected, no such subgraphs can be present in $L(G^*)$. Therefore $L(G^*)$ is primitive.

2. By [lemma 6](#), apart from the special case, each primitive graph G has at most one decomposition at leading order. Conversely, knowing the dual G^* , we can reconstruct all triangles of the original graph G and how they are connected. But for a triangle, knowing its adjacent vertices is enough to fix all edges in the triangle, consequently, all edges of G are fixed. Hence, at leading order in N , knowing G^* is enough to uniquely fix G , and therefore no two distinct G lead to the same G^* .

Note that the bijectivity rests on the vertices of G^* corresponding to *triangles*: For a cycle of larger size, one would have multiple ways to arrange the edges while still being incident to the same set of vertices, compare [fig. 16](#) (a). \square

The number of three-connected cubic graphs on $2n \geq 4$ vertices is [[87](#), A204198],

$$\{1, 2, 4, 14, 57, 341, 2828, 30468, 396150, \dots\}. \quad (4.3)$$

The first three of these graphs are shown in [fig. 15](#). By [theorem 1](#), [eq. \(4.3\)](#) is at the same time the number of primitive completions at $L = 3n + 1$ loops which contribute to leading order. We have written a small program, based on `nauty` [[88](#)], to generate the relevant dual graphs and construct the leading primitives. The counts can be found in [table 1](#) below, confirming [eq. \(4.3\)](#).

4.2.2. Primitive graphs with $3n$ loops

Completions with $3n$ loops have $3n + 2$ vertices, and therefore $6n + 4$ edges. By [lemma 5](#), the leading graphs of $3n$ loops have order $2n + 1$ in N , hence their duals ([definition 5](#))

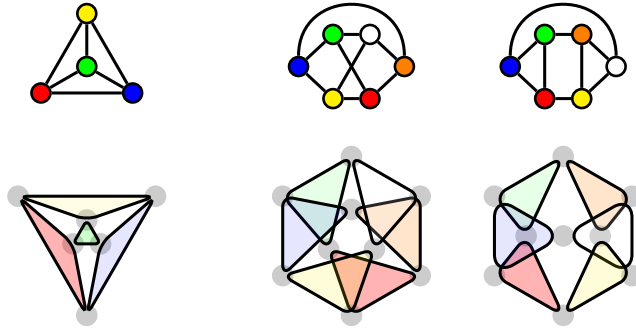


Figure 15: The 3-regular three-connected graphs G^* on four and six vertices. Below them are their line graphs, which are the leading-order decompositions of completions G at four and seven loops.

have $2n + 1$ vertices and $3n + 2$ edges. The leading graphs are those whose cycles are all triangles except for one square. Consequently, the dual graphs have $2n$ 3-valent vertices and a single 4-valent vertex.

In [section 4.2.1](#), the analogous conditions implied that the dual graphs are *simple*, that is, free of multiedges. This is not true in the case of $3n$ loops. By [lemma 4](#), G^* still has no 2-valent vertices and, with the same proof as [theorem 1](#), there are no 2-valent subgraphs. Hence, the dual G^* must be 3-edge-connected. But this leaves the possibility that it can contain a double edge adjacent to the single 4-valent vertex, as shown in [fig. 16](#) (b).

Furthermore, the line graph alone is not suitable to recover G from G^* . When G^* contains a 4-valent vertex, the line graph $L(G^*)$ ([definition 6](#)) contains five-valent vertices. Still, we can use the line graph construction for all edges that are not adjacent to the single 4-valent vertex v and replace v by a circuit of length four. There are exactly three different possibilities of an undirected circuit on four vertices, shown in [fig. 16](#) (a).

Theorem 2. *The leading decompositions at $L = 3n$ loops, $n > 1$, arise from 3-edge-connected dual graphs G^* , consisting of a single 4-valent vertex v , and $2n$ 3-valent vertices, where either one of the following is true:*

1. G^* is simple (and therefore three-vertex connected), then all three decompositions of v shown in [fig. 16](#) (a) contribute.
2. G^* is three-vertex connected and contains one double edge, adjacent to v . Only that decomposition of v contributes which does not lead to a double edge in G , see (b) in [fig. 16](#).
3. G^* is simple and has one 2-vertex cut, where one of the cut vertices is the 4-valent vertex v . Then only that one decomposition of v contributes that joins the two cut components of G with four and not two edges, see [fig. 16](#) (c).

Since [theorem 2](#) potentially involves a sum over distinct decompositions of a given 4-valent vertex, the number n_0 of leading-order graphs generated is in general larger than

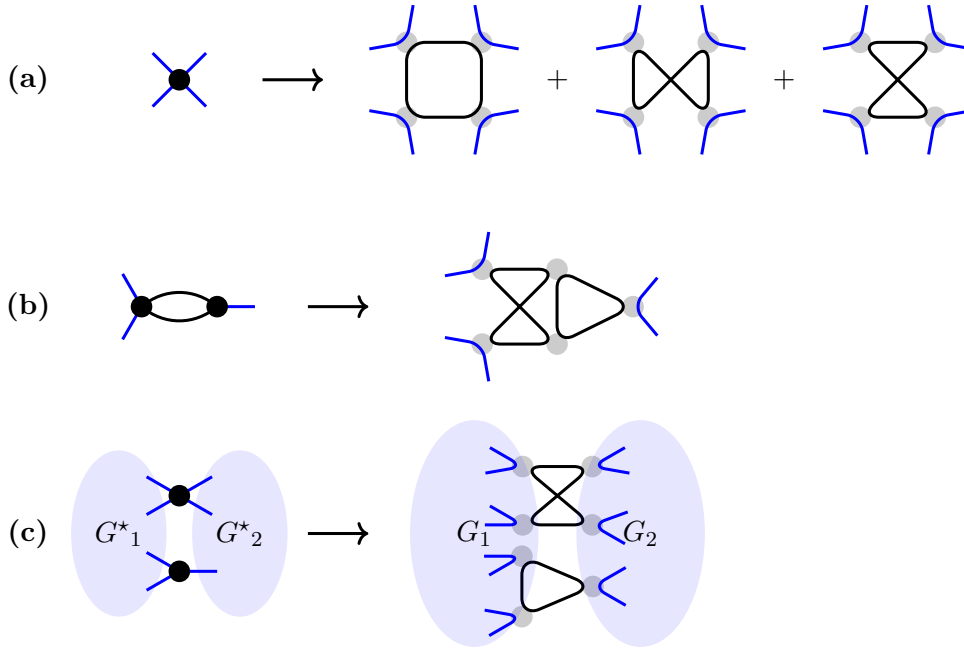


Figure 16: (a) A 4-valent vertex in G^* gives rise to one of three possible circuits. In a three-vertex-connected simple G^* , all three give rise to (potentially distinct) primitives G . (b) If G^* contains a double edge adjacent to a 4-valent vertex, there is only one possibility to decompose this vertex which makes G primitive. (c) Similarly, if the 4-valent vertex of G^* is a cut vertex of a 2-vertex cut, then only one of the three decompositions gives rise to a primitive G , namely the one that produces four edges between the cut components.

the number of non-isomorphic duals G^* . Algorithmically, the graphs in [theorem 2](#) (b) can be generated from 3-regular, 3-edge-connected graphs on $2n$ vertices upon replacing one of the 3-valent vertices by a 4-valent vertex with adjacent double edge. The three distinct choices of where to put the double edge amount to distinct decompositions of the same primitive G . We have generated all suitable G^* and from them all primitive G which contribute at leading order in N up to $L = 24$ loops, see [table 1](#).

Example 11. *The case $n = 1$ is excluded from [theorem 2](#) because the dual graph with one 4-valent and two 3-valent vertices contains two multiedges. This G^* is the dual of K_5 , and the three ways of arranging the four-cycle ([fig. 16](#) (a)) amount to the three isomorphic vertex decompositions of K_5 discussed in the proof of [lemma 6](#), see [fig. 17](#). As all five vertices of K_5 are equivalent, one obtains in total $3 \cdot 5 = 15$ decompositions contributing at leading order in N . An explicit computation yields*

$$T(K_5, N) = 132N + 96N^2 + 15N^3, \quad T(K_5 \setminus \{v\}, N) = 66 + 15N.$$

Notice that a similar sum over isomorphic vertices is not present when G^ is 3-regular because there, all circuits have length three and swapping them results in the same decomposition.*

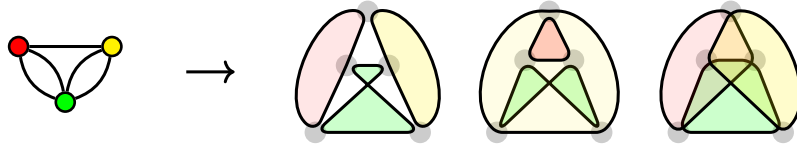


Figure 17: The unique dual G^* with one 4-valent and two 3-valent vertices. The three ways of arranging its four-cycle give rise to three isomorphic three-loop graphs $G = K_5$. Equivalently, this choice can be understood as the three ways of splitting the upper vertex in G according to [fig. 1](#), compare [fig. 13](#).

4.2.3. Primitive graphs with $3n + 2$ loops

In this case, the completed graphs G have $3n + 4$ vertices and $6n + 8$ edges. The leading order in N is $2n + 2$. Consequently, the dual graphs G^* have $2n + 2$ vertices and $3n + 4$ edges. These dual graphs either have two 4-valent vertices and the other $2n$ vertices 3-valent, or one vertex is 5-valent and the other $2n + 1$ are 3-valent. As before, G^* must be 3-edge-connected, but it can have a 2-vertex cut. These conditions imply that G^* must not contain double edges consisting of only 3-valent vertices, but there may be one or two double edges adjacent to a vertex of valence larger than three. It is straightforward to derive the particular constraints on decompositions in each of these cases, analogously to [theorem 2](#), and to implement them in a computer program. However, it is little insightful to enumerate them here, so we merely state the (obvious) necessary condition on G^* .

Lemma 7. *Let $L = 3n + 2$ with $n \in \mathbb{N}$. The primitive graphs G contributing at leading order in N arise from dual graphs G^* which have $2n + 2$ vertices, $3n + 4$ edges, no vertices of degree lower than three, and which are 3-edge-connected.*

For $L = 3n + 1$ ([theorem 1](#)), there is a one-to-one correspondence between dual graphs G^* and the leading-order decompositions of primitive completions G , given by the line graph ([definition 6](#)). Already for $L = 3n$ ([theorem 2](#)), a single dual can give rise to more than one completion, compare [fig. 16](#) (a). In the present case $L = 3n + 2$, the correspondence is even weaker:

1. A given dual G^* can produce multiple non-isomorphic leading-order graphs G .
2. A leading order graph G can have more than one leading-order decomposition, that is, the leading-order coefficient of $T(G, N)$ is not necessarily unity.
3. Not all leading-order decompositions of a fixed G result in isomorphic duals G^* .

[Figure 18](#) shows an example of the latter two effects.

Again, we have generated all relevant G^* and their corresponding primitive graphs G at leading order up to $L = 23$, see [table 2](#). While the necessary constraints on the allowed mappings from dual vertices to circuits are tedious to spell out explicitly, a computer program that checks them is still much faster than the explicit enumeration of *all* primitives and filtering for leading-order decompositions. For example, generating the

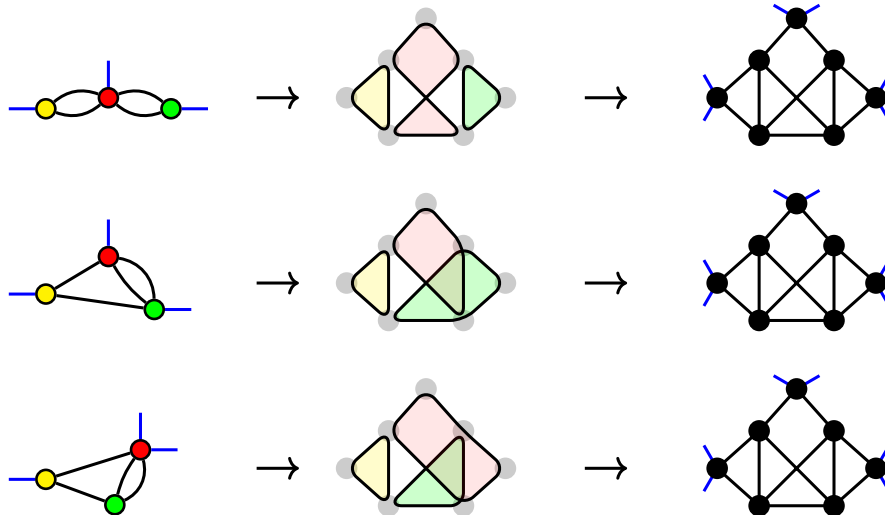


Figure 18: The right column shows a subgraph of some completion G . This subgraph has five non-isomorphic vertex decompositions into three circuits each, three of them are shown in the central column. Each of them gives rise to a distinct, non-isomorphic dual (left column). On the other hand, the four- and five-valent vertices of the duals can not contribute all of their possible circuit orientations since some of them would produce non-primitive graphs.

leading duals at $L = 17$ loops took less than two minutes, while generating and filtering all 16-loop graphs for table 2 took more than one week.

Table 1 shows the count of graphs for all three cases $L \bmod 3 \in \{0, 1, 2\}$. An explicit list of these graphs is available from the first author’s website⁴. We remark that the present construction of completions from their duals can be extended to subleading primitive completions by including dual graphs that have less vertices at a fixed number of edges, and observing an increasing number of restrictions on the allowed mappings from vertices to circuits.

4.2.4. Families of leading primitive graphs

The zigzag-graphs, or $(1, 2)$ -circulants, are famously the only irreducible infinite family of graphs in ϕ^4 theory whose period is known analytically [89].

Lemma 8. *Let Z_L be the zigzag graph whose decompletion has L loops. In the polynomial $T(Z_L, N)$, the coefficient of highest-order in N has order $\lfloor \frac{L}{2} + 2 \rfloor$, and is $(2L + 4)$ when L is odd, and 2 when L is even.*

Proof. We need to identify a vertex decomposition that gives rise to the maximum number of circuits. Concretely, as many circuits as possible need to be triangles. For a zigzag, all vertices can be drawn on a circle such that they are only ever adjacent to their nearest and next-nearest neighbors. In that sense, any potential short cycle must be “local”.

⁴paulbalduf.com/research

$3n$			$3n + 1$			$3n + 2$		
L	$\lfloor N_{\max} \rfloor$	n_0	L	$\lfloor N_{\max} \rfloor$	n_0	L	$\lfloor N_{\max} \rfloor$	n_0
3	3	1	4	4	1	5	4	2
6	5	3	7	6	2	8	6	22
9	7	10	10	8	4	11	8	205
12	9	57	13	10	14	14	10	2,278
15	11	425	16	12	57	17	12	29,840
18	13	4,151	19	14	341	20	14	440,910
21	15	49,136	22	16	2,828	23	16	7,181,335
24	17	673,350	25	18	30,468			

Table 1: Number n_0 of primitive completed graphs contributing at leading order in N . All these graphs have been explicitly generated from their dual; for $L = 3n + 1$, the count equals the number of 3-vertex connected graphs eq. (4.3) as expected.

Starting from any triangle, we see that the next triangle can only touch the current one at a vertex, but they can not share an edge. Hence, the ring of $(L + 2)$ vertices can have at most $\frac{L+2}{2}$ triangles. Every other vertex has two edges which are not in any triangle, they form another “special” circuit, giving a total of $\frac{L}{2} + 2$ circuits.

When L is even, there are exactly two distinct decompositions of this type. When L is odd, there remains a “defect” of one edge which does not fit a triangle. Either the special circuit is extended to cover this edge, or one triangle is sacrificed to make a 4-circuit to cover the edge, leaving the special circuit intact. The defect can be located at any of the $(L + 2)$ vertices, always giving rise to two distinct possibilities to resolve it, for a total of $2L + 4$ decompositions that yield the same maximum number of circuits.

One might suspect that another decomposition of the same, or potentially larger, number of circuits is possible based on squares, but this is not the case. Like the triangles, the squares require one long “special” circuit, and there is effectively only one square for every three vertices, so they result in a number of circuits $\sim \frac{L}{3}$. \square

By lemma 8, the degree of the zigzag coincides with the leading degree $\lfloor \frac{2}{3}L + \frac{4}{3} \rfloor$ (lemma 5) only for $L \in \{4, 5, 6, 8\}$. For other loop orders, the zigzag is not among the leading graphs at large N .

One can find infinite families of completions that contribute to leading order at all loops if one starts from the dual graphs (definition 5). For the case of $L = 3n + 1$ loops, all we have to do is find a family of 3-connected 3-regular graphs. By theorem 1, the line graph of such graph on $2n$ vertices will be a primitive completion in ϕ^4 theory at $3n + 1$ loops. One such infinite family is shown in fig. 19

4.3. Enumeration of graphs at low loop order

To verify and complement the combinatorial construction of leading primitive graphs, we have enumerated all primitive graphs of ϕ^4 theory up to including 16 loops and

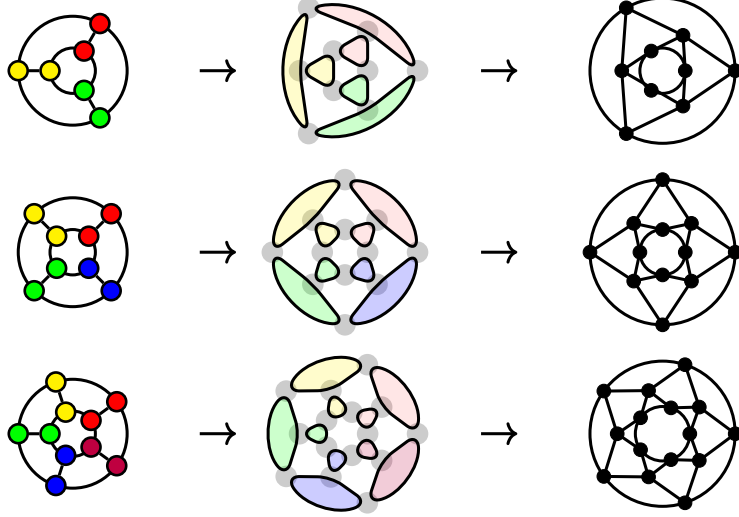


Figure 19: First instances of an infinite family of duals (first column), whose corresponding completed graphs (last column) exhaust the bound [lemma 5](#) at $L = 1 \pmod 3$ loops. The dual on six vertices is the same as in [fig. 15](#), but drawn differently.

determined their $O(N)$ symmetry factors $T(G, N)$. The degree in N is bounded by N_{\max} ([lemma 5](#)), we introduce

$$n_k := \text{Number of graphs where } T(G, N) \text{ has degree } (N_{\max} - k). \quad (4.4)$$

These numbers are shown in [table 2](#). Specifically, n_0 is the number of leading graphs in N , and our findings confirm the count of graphs constructed from dual graphs ([table 1](#)). Furthermore, we observe in [table 2](#) that, as L grows, the degree of most graphs is lower than N_{\max} , or equivalently, the number n_0 of leading graphs is increasingly smaller than the numbers of subleading graphs. This is expected from the asymptotic analysis in [section 3.7](#): The large- N limit is not factorially divergent, therefore, for large enough L , the number n_k for any fixed k grows less than factorially.

In [eq. \(3.19\)](#), we introduced the average *order* in N of the polynomials $T(G, N)$ and found that it grows only logarithmically in L ([eq. \(3.31\)](#)). Analogously, we define the average *degree* as

$$\langle n \rangle_L := \text{Average degree in } N \text{ of } T(G, N) \text{ over all } L\text{-loop completions } G \quad (4.5)$$

Numbers are shown in [table 2](#). In the log-log plot in [fig. 20a](#), the bound $N_{\max} \sim \frac{2}{3}L$ approaches a straight line with slope 1. Similarly, it seems that $\langle n \rangle_L$ approaches a straight line, but with smaller slope, which suggests that that $\langle n \rangle_L$ grows polynomially in L with exponent smaller than 1.

4.4. Non-primitive graphs

Knowing a bound for the order in N of primitive graphs, we can use [lemma 2](#) to obtain a bound for graphs with subdivergences. Recall [lemma 2](#): The $O(N)$ -symmetry factor is

L	$\lfloor N_{\max} \rfloor$	n_0	n_1	n_2	n_3	n_4	n_5	$\langle n_{\max} \rangle_L$
3	3	1	0	0	0	0	0	3
4	4	1	0	0	0	0	0	4
5	4	2	0	0	0	0	0	4
6	5	3	2	0	0	0	0	4.60
7	6	2	12	0	0	0	0	5.14
8	6	22	27	0	0	0	0	5.45
9	7	10	200	17	0	0	0	5.97
10	8	4	373	973	4	0	0	6.28
11	8	205	7,127	2,390	0	0	0	6.78
12	9	57	11,427	68,354	1,467	0	0	7.12
13	10	14	6,850	364,479	384,170	130	0	7.50
14	10	2,278	499,780	6,129,768	1,003,848	3	0	7.93
15	11	425	324,100	21,776,598	59,847,247	749,814	0	8.26
16	12	57	125,057	27,008,312	569,122,747	356,187,442	94,550	8.65

Table 2: Number n_k of (primitive) completions whose degree in N is the k -th subleading order (eq. (4.4)). Bold numbers indicate loop orders L where N_{\max} (lemma 5) is integer. With increasing loop order, most graphs have a degree $n_{k \geq 1}$ which is lower than N_{\max} , i.e. they do not contribute to the leading order n_0 . The last column shows the average degree (eq. (4.5)).

multiplicative under insertion of propagator-type subgraphs. When G is a completion where $T(G, N)$ is of degree n , then removing one edge e produces a propagator-type graph $G \setminus \{e\}$ where $T(G \setminus \{e\}, N) = \frac{T(G, N)}{N}$ is of degree $n - 1$, and removing one vertex v produces a vertex-type graph $g := G \setminus \{v\}$ where $T(g, N) = \frac{3T(G, N)}{N(N+2)}$ is of degree $n - 2$.

Lemma 9. *Let g be a vertex-type graph that arises from inserting a primitive decompletion g_2 with $L_2 > 1$ loops into a primitive decompletion g_1 with $L_1 > 1$ loops. The resulting graph g is a decompletion with $L_1 + L_2$ loops and*

$$\text{Degree in } N \text{ of the polynomial } T(g, N) \leq \frac{2}{3}(L_1 + L_2) - \frac{4}{3}.$$

Proof. The stated loop order of the joined graph trivially follows from counting the edges and vertices, and noting that g is connected.

Let $G_1 = g_1 \cup \{v\}$ be the completion of g_1 , and let $G := G_1 \circ_v g_2$ be the sum of graphs that arises from inserting g_2 in place of a vertex $v \in G_1$ in all possible ways, where $v \neq v_1$. According to lemma 2, $T(G, N) = T(G_1, N) \cdot T(g_2, N)$. By lemma 5, the degree in N of $T(G_1, N)$ is $\leq \frac{2}{3}L_1 + \frac{4}{3}$. Similarly, for g_2 the degree is bounded by $\frac{2}{3}L_2 - \frac{2}{3}$. Hence, the degree of $T(G, N)$ is bounded by

$$\frac{2}{3}L_1 + \frac{4}{3} + \frac{2}{3}L_2 - \frac{2}{3} = \frac{2}{3}(L_1 + L_2) + \frac{2}{3}.$$

This bound refers to G , which is a sum of graphs, but the coefficients of $T(G, N)$ are positive, therefore there can be no cancellations and the bound holds for every graph

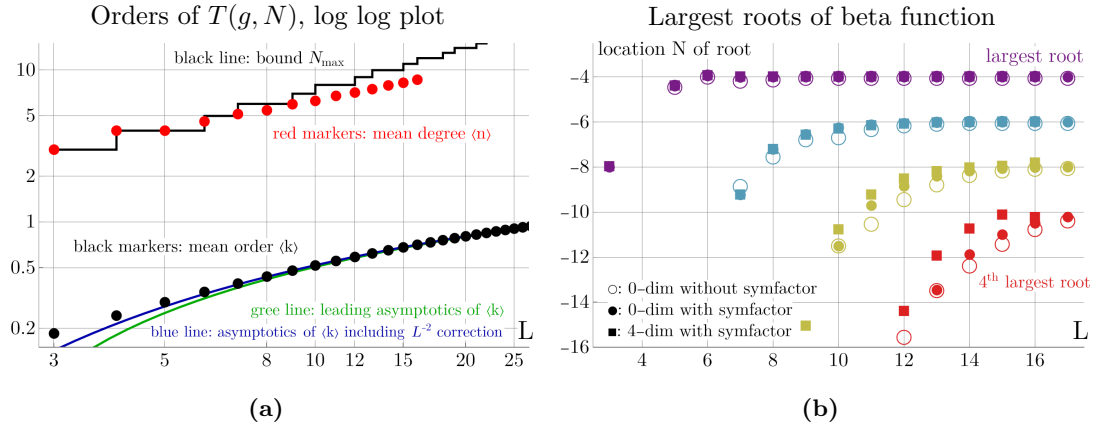


Figure 20: (a) The mean degree $\langle n \rangle_L$ (red markers) appears to lie on a straight line in this log log plot, which suggests that it grows polynomially in L . The bound N_{\max} (black line) grows proportional to L^1 (lemma 5). For comparison, the mean order $\langle k \rangle_L$ (eq. (3.19), black markers) grows only logarithmically in L (eq. (3.31), blue and green lines). Compare fig. 10b. (b) Largest roots of the primitive beta function in 4-dimensions (squares, table 3), of $p_L(N)$ (filled circles, table 5), and of the sum of all primitive $T(G, N)$ without symmetry factor (empty circles, table 6). In all cases, the roots converge towards even negative integers as L grows, as expected from eqs. (2.11) and (3.27), and this convergence is rapid already at low loop orders. It indicates the presence of sums over all channels of subgraphs (lemma 3).

individually. The graph g in the statement of the lemma is a decompletion of one of the graphs in G (where the vertex v is the decompletion vertex). The degree of $T(g, N) = \frac{3T(G, N)}{N(N+2)}$ is two less than the degree of $T(G, N)$, which yields the desired bound. \square

A Feynman graph has *coradical degree* $n + 1$ if it can be obtained from a primitive graph by inserting primitive graphs n times. It is irrelevant whether the inserted graphs are distinct, and whether they are inserted into disjoint locations or into each other. Equivalently, in the Hopf algebra of Feynman graphs [3], the coradical degree is the number of times the coproduct needs to be applied such that all resulting terms contain at least one factor $\mathbb{1}$. A primitive graph has coradical degree one, a graph with one divergent subgraph has coradical degree two, and so on. Dyson-Schwinger equations, when formulated as identities for generating function of Feynman graphs, ensure that every graph can be built by a (not necessarily unique) sequence of insertions of primitive graphs [1].

From lemma 9, one can derive bounds on the degree in N of non-primitive graphs, and the interesting result is that these bounds can be expressed in terms of the coradical degree. The renormalized Feynman amplitude of a superficially divergent graph of coradical degree n depends on the momentum scale s like $\ln(s)^n$. Consequently, bounding the degree of $T(G, N)$ in terms of coradical degree n implies a bound for the N dependence of terms in the leading-log expansion. The precise value of these bounds depends on the class of graphs under consideration (connected/1PI/...), and whether one excludes

certain small graphs (tadpoles/multiedges/...). As an illustration, we derive just one particular bound of this type.

We call a graph *fish free* if neither the underlying primitive graph, nor any of the subgraphs inserted at any stage, are the fish graph (i.e. the 1-loop vertex correction given by a double edge, [fig. 2](#)). Being fish free is a nontrivial assumption, this situation may arise e.g. if a modification of the Feynman rules excludes the presence of double edges, or if double edges have been analytically resummed already. Conversely, the vanishing of tadpole graphs (i.e. graphs with only one external edge, such that they do not depend on momenta) is a choice of renormalization condition that can be made at will, and which is automatic in a massless theory in dimensional regularization.

Theorem 3. *Assume that tadpole graphs vanish. Let g be a 1PI fish free L -loop vertex-type graph of coradical degree n . Then*

$$\text{Degree in } N \text{ of the polynomial } T(g, N) \leq \frac{2}{3}L - \frac{1}{3}n.$$

Proof. For insertions of vertex-type subgraphs, the result follows recursively from [lemma 9](#).

Propagator-type graphs can be obtained from vertex-type graphs by either of two operations: Either by joining two of the external edges to each other, which raises the loop order by one and the degree in N by one, or by joining three external edges to a new vertex, which increases the loop order by two and the degree in N by one. In both cases, the coradical degree of the resulting propagator-type graph is one larger than the one of the vertex-type subgraph. The first operation gives zero contribution if tadpoles vanish because when, during the renormalization process, the vertex-type subgraph is contracted, the resulting cograph is a tadpole and hence the product vanishes. We are left with the second operation. If L is the loop order of the resulting propagator-type graph, the degree of the vertex-type subgraph is bounded by $\frac{2}{3}(L-2) - \frac{2}{3}(n-1) = \frac{2}{3}L - \frac{2}{3}n - \frac{2}{3}$, and the degree of the resulting propagator-type graph is bounded by

$$\frac{2}{3}L - \frac{2}{3}n - \frac{2}{3} + 1 = \frac{2}{3}L - \frac{2}{3}n + \frac{1}{3}.$$

We see that every such iteration raises the degree by $\frac{1}{3}$, compared to the bound $\frac{2}{3}L - \frac{2}{3}n$. Hence, a valid bound is given by $\frac{2}{3}L - \frac{1}{3}n$.

When only vertex-type subgraphs are being inserted, the graph has bound $\frac{2}{3}L - \frac{2}{3}n$, which in particular is stronger than $\frac{2}{3}L - \frac{1}{3}n$. When a propagator subgraph is inserted, the $T(G, N)$ are multiplicative, too ([lemma 2](#)), consequently their degree is additive. Likewise, the coradical degree and the loop number are additive, and therefore, the resulting graph again is bounded by $\frac{2}{3}L - \frac{1}{3}n$. \square

5. ϕ^4 theory in four dimensions

Everything so far has been about identifying and enumerating graphs, and understanding their combinatorial properties. In a realistic theory, the Feynman integral of each graph has some non-trivial value. In this last section, we use the numerical values of

primitive graphs in ϕ^4 theory in four spacetime dimensions, which is the Feynman period (section 2.2), in order to examine to what extent the qualitative combinatorial findings stay true in a more realistic setting.

5.1. Coefficients and evaluations of β_L^{prim} in four dimensions

For $L \leq 13$ loops, the periods $\mathcal{P}(G)$ of all primitive graphs had been computed in [7]⁵. Inserting these values into eq. (2.15),

$$\beta_L^{\text{prim}}(N) = 2 \sum_{\substack{G \text{ comp.} \\ L \text{ loops}}} \frac{4!(L+2)}{|\text{Aut}(G)|} \frac{3T(G, N)}{N(N+2)} \mathcal{P}(G), \quad (5.1)$$

we obtain the coefficients in N of β_L^{prim} . For $14 \leq L \leq 18$ loops, only non-complete uniform random samples of periods are available in [7] due to the large number of graphs. As discussed in section 4.3, not every graph contributes to every order in N , this implies that the statistical uncertainties of the large- N coefficients is large. To improve the statistical situation, we have numerically integrated all leading-degree graphs of $L \in \{14, 15, 16\}$ loops using the methods explained [7], based on the `tropical-feynman-quadrature` program [90, 91]. Consequently, for $L > 13$, the subleading coefficients suffer from sampling uncertainty, but the leading ones do not. Numerical values are shown in table 3 in appendix B.

The beta function at small positive integer values of N is associated with the critical behaviour of various physical models. In table 4 in appendix B, we report the evaluations of β_L^{prim} at integer N . Once more, the data for $L \leq 13$ was taken from [7], and these values are also reported in small print in table 4 for larger L . However, for $14 \leq L \leq 17$, we additionally used the weighted sampling algorithm developed in [34] to obtain more accurate values, reported in larger print in table 4. We did not compute new data at $L = 18$ due to limited computing resources. Note that the sampling algorithm does the weighting for a specific given value of N , hence it needs to run multiple times to compute β_L^{prim} at multiple N , but this is still substantially faster than inferring all the evaluations of β_L^{prim} from a single uniform sample.

As a remark, it is not trivial to relate the uncertainties in table 3 to those in table 4, because both arise from the (numerical and statistical) uncertainties of the periods, while $T(G, N)$ are known exactly. Each column in each of the tables constitutes a different linear combination of periods.

5.2. N dependence of the beta function in zero and four dimensions

The mean of the 4-dimensional period is much larger than unity, and grows with the loop order, numbers had been given in [7]. It is therefore clear that the function $2p_L(N)$ from 0-dimensional QFT is not a good approximation of the 4-dimensional $\beta_L^{\text{prim}}(N)$ in terms

⁵This dataset can be downloaded from DOI 10.5683/SP3/NLEDGH.

of absolute value; however, it might still be a good approximation for the N dependence. This will be investigated in the present section.

A first characteristic feature of the N dependence is the presence of roots (zeros) at negative N . In the limit $L \rightarrow \infty$, both in zero dimensions (eq. (3.27)) and in four dimensions (eq. (2.11)), these roots are asymptotically located at negative even integers $N \leq -4$. For finite L , the largest roots are plotted in fig. 20b. Indeed, we see that both in the 0-dimensional and in the 4-dimensional case, the roots quickly converge to negative even integers as L grows, as had been observed already in [61, 80]. In particular, the largest roots are close to their asymptotic location already at low loop orders, long before the absolute value or the growth rate of the beta function is close to its asymptotics (compare figs. 8b and 10a).

Next, we compare the N dependence of $p_L(N)$ and $\beta_L^{\text{prim}}(N)$ for positive N . To this end, recall that in eq. (2.16), we introduced the N dependent average L -loop period, weighted by symmetry factors, $\langle \mathcal{P} \rangle_{T/\text{Aut},L}(N) = \beta_L^{\text{prim}}(N)/2p_L(N)$. If the N dependence of $p_L(N)$ and $\beta_L^{\text{prim}}(N)$ were identical, then $\langle \mathcal{P} \rangle_{T/\text{Aut},L}(N)$ would be independent of N . We hence examine whether $\langle \mathcal{P} \rangle_{T/\text{Aut},L}(N) \stackrel{?}{\approx} \langle \mathcal{P} \rangle_{T/\text{Aut},L}(1)$. This is equivalent to asking whether

$$\beta_L^{\text{prim}}(N) \stackrel{?}{\approx} \langle \mathcal{P} \rangle_{\frac{T}{\text{Aut}},L}(1) \cdot 2p_L(N) = \beta_L^{\text{prim}}(1) \cdot \frac{p_L(N)}{p_L(1)}. \quad (5.2)$$

We introduce the N dependent ratio between the left- and right-hand side of eq. (5.2),

$$b_L(N) := \frac{\beta_L^{\text{prim}}(N) p_L(1)}{\beta_L^{\text{prim}}(1) p_L(N)} = \frac{\langle \mathcal{P} \rangle_{\frac{T}{\text{Aut}},L}(N)}{\langle \mathcal{P} \rangle_{\frac{T}{\text{Aut}},L}(1)}. \quad (5.3)$$

Example 12. At $L = 5$, the two primitives have almost the same $O(N)$ symmetry factors, $T(g_1, N) = 528 + 186N + 15N^2$ vs $T(g_2, N) = 526 + 189N + 14N^2$, and their periods are very close, $\mathcal{P}(G_1) \approx 52.01$, $\mathcal{P}(G_2) \approx 55.58$. This implies that the ratio $b_5(N)$ is close to unity, and the beta function at 5 loops almost factorizes (eq. (5.2)).

Conversely, for $L = 8$, inserting the numerical values of table 3 for β_L^{prim} and the rational numbers of table 5 for p_L , one finds a function that notably differs from unity,

$$b_6(N) \approx \frac{13603 + 7150.5N + 1221.0N^2 + 75.809N^3 + 1.2273N^4}{13704 + 7097.8N + 1179.6N^2 + 69.410N^3 + 1.0000N^4}.$$

For finite L , $b_L(N)$ is a rational function which has poles at negative N because the zeros of $p_L(N)$ and $\beta_L^{\text{prim}}(N)$ do not exactly coincide. However, $b_L(N)$ is smooth for $N \geq -2$, and it is unity at $N = 1$ by construction. Plots of $b_L(N)$ for different L are shown in fig. 21a. We observe that $b_L(N)$ grows monotonically with N , which indicates that there is a correlation between the $O(N)$ symmetry factor $T(G, N)$ of a graph and the value of its period $\mathcal{P}(G)$.

For finite L , the limit $N \rightarrow \infty$ of $b_L(N)$ is finite, and it measures the average of periods which are leading at large N (section 4.2), divided by the average of all periods. The limit is shown in fig. 21b, it grows with L with what could be a power law. A value of $b_L(\infty)$

larger than unity means that the average of the leading- N -periods is systematically larger than the average of *all* periods. If $b_L(\infty)$ grows only polynomially with L , this means that the large- N expansion of *primitive* graphs is convergent not only in 0-dimensional QFT (section 3.7) but also in 4 dimensions.

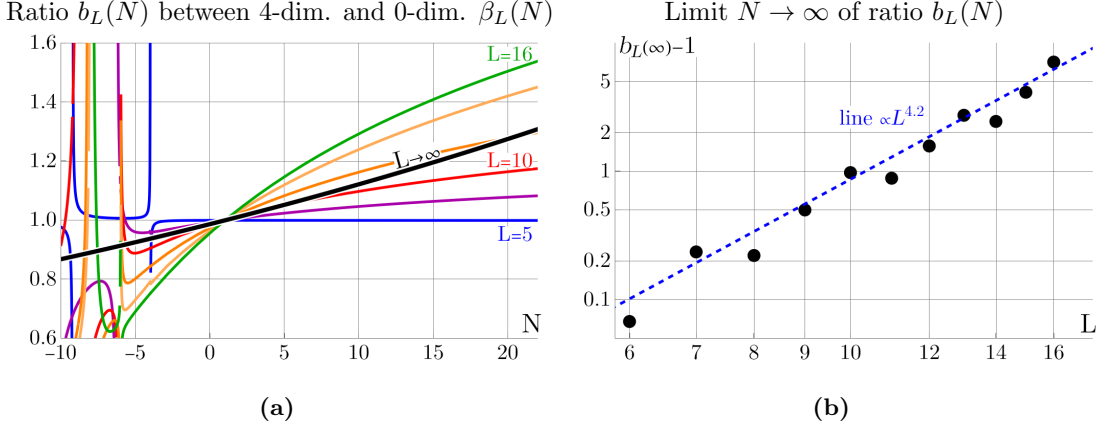


Figure 21: (a) Ratio $b_L(N)$ (eq. (5.3)) between the 4-dimensional and the 0-dimensional primitive beta function, for $L \in \{5, 8, 10, 12, 14, 16\}$. For finite L , the ratio converges to a constant at $N \rightarrow \infty$. The limiting curve for $L \rightarrow \infty$ is shown in black, it is unbounded as $N \rightarrow \infty$. (b) Numerical value of the limit $b_L(\infty)$. Heuristically, the values seem to grow like $L^{4.2}$.

Asymptotically for $L \rightarrow \infty$, we know from eq. (2.17) that $b_L(N) \rightarrow \delta^{N-1}$ with $\delta \approx 1.013$. This function is shown as a black curve in fig. 22a, it does not match the curves for finite L particularly well, even for $L = 16$. In this sense, $L = 16$ is not in the “asymptotic regime”. However, note that both $p_L(N)$ and $\beta_L^{\text{prim}}(N)$ are strongly dependent on N and their values span multiple orders of magnitude for $N \in [-2, 20]$. The ratio $b_L(N)$ is slowly varying in this domain and takes values in $[0.8, 1.5]$, which shows that qualitatively, the N dependence of the 0-dimensional $p_L(N)$ is indeed a rather good model for the N dependence of the 4-dimensional $\beta_L^{\text{prim}}(N)$.

5.3. Asymptotic growth rate of the beta function at large loop order

As stated in section 2.3.2, there is a conjecture that the leading asymptotic growth of the primitive beta function should coincide with the one of the full beta function in MS, and therefore it should grow according to conjecture 1. In [7] we observed a potential discrepancy between conjecture 1 and the numerically computed *primitive* beta function. In that work, limited numerical accuracy for $L > 13$ loops prevented a definite conclusion.

The asymptotic growth ratio r_L (eq. (2.13)) of the primitive beta function behaves as $r_L = a + \frac{c_s}{a} \frac{1}{L} + \mathcal{O}(L^{-2})$, where the conjectured asymptotics implies $a = 1, c_s = 5 + \frac{1}{2}N$ (eq. (2.14)). We have numerical data for β_L^{prim} for $L \leq 18$, which corresponds to r_L for $L \leq 17$. We can determine the growth parameters a and c_s by plotting our numerical values of r_L against $\frac{1}{L}$ and extracting slope and y -intersection of a linear fit. The result is shown in fig. 22a. We observe that the linear fits (red lines) result in $a \approx 0.8$, which

depends only little on the value of N used for the fit. The slope of the empirical fit lines is approximately described by $c_s \approx 8 + 0.8N$. These empirical values of a and c_s for $L \leq 18$ loops are incompatible with the conjectured asymptotics (eq. (2.14)), even when numerical uncertainties are taken into account. This is clearly visible from the fact that the red data points in fig. 22a do not lie on the green lines.

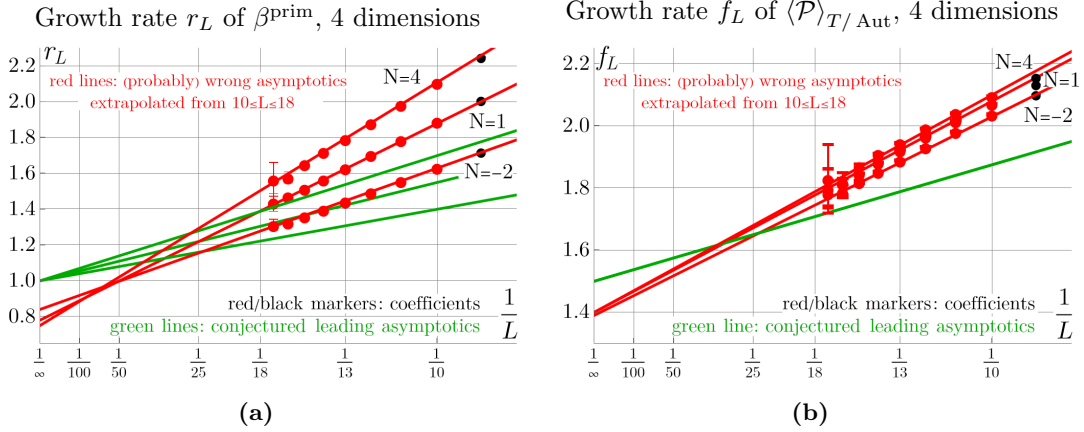


Figure 22: (a) Ratio r_L according to eq. (2.13) for the primitive beta function β^{prim} in four dimensions. Green lines indicate the leading asymptotics of the full beta function in minimal subtraction, which is conjecturally equal to that of β^{prim} . Red lines indicate the numerically measured growth rate from $10 \leq L \leq 18$ loops. If the pattern continues, the data can be expected to reach the true asymptotics at $L \geq 25$ loops. Compare the strikingly similar situation in zero dimensions, fig. 10a. (b) Growth ratio f_L (eq. (2.18)) of the average period for the 4-dimensional theory. This quantity is independent of the sum of symmetry factors $p_L(N)$. Conjecture 1 implies that the data should lie on the green line for large L , for all values of N .

However, the pattern in fig. 22a is strikingly similar to the analogous plot in 0-dimensional QFT, fig. 10a. In the 0-dimensional case, we have verified that the growth rate r_L changes its slope at $L \geq 25$ loops, and starts to converge towards the correct limiting value (green lines), while it appears to converge towards a too low limit when only $10 \leq L \leq 18$ is extrapolated (red lines). Remarkably, even in the 4-dimensional case (fig. 22a), the extrapolated red lines intersect the conjectured asymptotics at $L \approx 25$. In view of these observations, we conclude that the 4-dimensional primitive beta function probably does not show its true asymptotic growth rate even at 18 loops, and we conjecture that to observe the true growth rate requires data at least at $L \geq 25$ loops.

The function p_L in 0-dimensional QFT is just the sum of symmetry factors, which are the same symmetry factors as in 4 dimensions. Since the growth rate of p_L and the growth rate of β^{prim} show the same qualitative behaviour, the question arises whether this effect is caused *entirely* by symmetry factors. To investigate this, we compute the average period per graph, weighted by the symmetry factor (of automorphism and $O(N)$ symmetry), as defined in eq. (2.16). The growth ratio f_L of this average (eq. (2.18)) is expected to behave, asymptotically, as $f_L \sim \frac{3}{2} + \frac{15}{4} \frac{1}{L}$. In a plot where the x -axis is $1/L$, we hence expect a linear function whose slope is $\frac{15}{4}$, independent of N .

Indeed, in the plot [fig. 22b](#), we see that the numerical values of f_L scale almost linearly with $\frac{1}{L}$, and their slope and y -intercept is almost independent of N . Nevertheless, the fit lines from $10 \leq L \leq 18$ result in $f_L \approx 1.40 + 6.7\frac{1}{L}$, which is incompatible with the expected asymptotics. Strikingly, these fit lines (red lines in [fig. 22b](#)) once more intersect the conjectured asymptotics at $L \approx 25$. In this sense, the average of the period exhibits much the same scaling behaviour as the symmetry factors or the beta function itself, namely, at $10 \leq L \leq 18$ they grow too quickly (i.e. f_L or r_L is larger than the conjectured asymptotics), but their growth rate decreases too quickly (i.e. the extrapolation $\frac{1}{L} \rightarrow 0$ results in a too low value). The similarity of these effects is in particular interesting since for the 0-dimensional p_L , it is a purely combinatorial effect that arises from the number of graphs and their symmetry factors, whereas for $\langle \mathcal{P} \rangle_{T/\text{Aut}}$ and f_L , it concerns the numerical value of period integrals. A priori, there would be no reason to expect that the number of graphs and the value of their integrals behave in any way similar.

However, we know from previous work [\[34\]](#) that the numerical value of the period of an individual graph is strongly correlated with its $O(N)$ symmetry factor $T(G, N)$. It would thus be conceivable that, since the periods in $\langle \mathcal{P} \rangle_{T/\text{Aut}}$ are weighted proportionally to their symmetry factor, this correlation is responsible for the observed similarity between the growth of $\langle \mathcal{P} \rangle_{T/\text{Aut}}$ and p_L . This is not the case. Firstly, at $N = 1$ the factor $T(G, N)$ is unity for all graphs and hence does not influence the relative sampling. Secondly, the correlation changes sign for different values of N ⁶. Hence, for $N > 1$, the graphs with large periods are weighted relatively more, while for $N < 1$ they are weighted relatively less, compared to a uniform distribution, but the observed growth rate f_L of $\langle \mathcal{P} \rangle_{T/\text{Aut}}$ ([fig. 22b](#)) is almost independent of N . We thus conclude that, while these correlations certainly have some influence on the weighted mean $\langle \mathcal{P} \rangle_{T/\text{Aut}}$, they are not solely responsible for the observed too large growth rate f_L of $\langle \mathcal{P} \rangle_{T/\text{Aut}}$.

Acknowledgements

We thank Karen Yeats and Erik Panzer for comments and discussions.

PHB did parts of this work while affiliated with the University of Waterloo and Perimeter Institute. Research at Perimeter Institute is supported in part by the Government of Canada through the Department of Innovation, Science and Economic Development and by the Province of Ontario through the Ministry of Colleges and Universities. Work at the University of Oxford was funded through Royal Society grant URF/R1/201473.

JT has been funded by the German research foundation (DFG, grant number 418838388) and in the last stage by the European Union (ERC, GE4SPDE, 101045082), as well as by Germany's Excellence Strategy EXC 2044-390685587, Mathematics Münster: Dynamics–Geometry–Structure.

⁶Empirically, the correlation is roughly $\ln \mathcal{P}(G) \approx \frac{-c_0}{(N-1)} + \frac{c_1}{(N-1)} \ln T(G, N)$, for $c_0 \sim 150$, $c_1 \sim 10$.

A. Combinatorial properties of the circuit partition polynomial

In [section 2.1](#), we stated several facts about the circuit partition polynomial $J(G, N)$ ([definition 1](#)), and the $O(N)$ -symmetry factor $T(G, N)$ ([definition 2](#)). The present section contains derivations and further examples.

One of the crucial properties of the polynomials $T(G, N)$ and $J(G, N)$ is that they factorize under insertion of subgraphs ([lemma 2](#)). To see why this is the case, we first give a proof for a special case of this statement, namely for the completion ([definition 4](#)) of a vertex-type (i.e. 4-valent) graph.

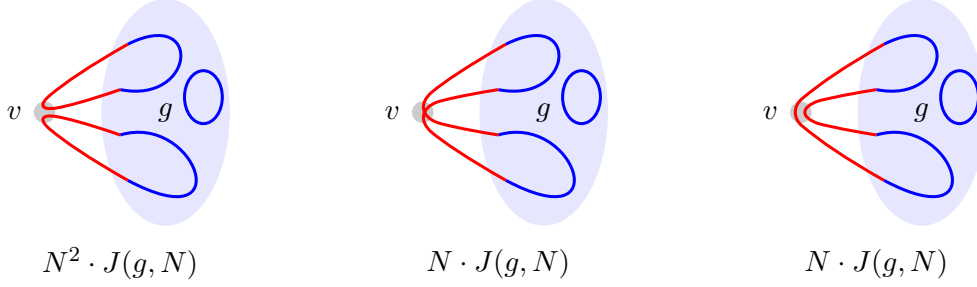



Figure 23: Proof of [lemma 10](#). We fix an arbitrary decomposition in the vertex-type graph g . This decomposition amounts to a choice to connect the four external edges into pairs, indicated by blue arcs, and zero or more circuits in g . The completion vertex v allows for three distinct decompositions, drawn as red lines. One of them (first drawing) produces two circuits and hence a factor of N^2 , the remaining two decompositions produce only one circuit and hence a factor N . Hence, the circuit partition polynomial of the completion is $J(G, N) = (N^2 + 2N) \cdot J(g, N)$.

Lemma 10 ([\[41\]](#) Section 6). *Let g be a vertex-type graph and $G = g \uplus \{v\}$ its completion. Then the circuit partition polynomials satisfy*

$$J(G, N) = N(N + 2) \cdot J(g, N).$$

Proof. Every possible decomposition of g amounts to a choice to connect the four external edges into two pairs, plus a choice to join all remaining edges into circuits. Now consider the completion $G := g \uplus \{v\}$. G has no external edges, therefore, every possible vertex decomposition results in circuits only (and no “open ends”). The sum over all possible decompositions, assigning the value N to every circuit, is by definition the circuit partition polynomial $J(G, N)$ ([definition 1](#)).

On the other hand, every decomposition of G amounts to choosing one of the three possible decompositions of the vertex v together with a choice of decomposition of g . Since every decomposition of g is, especially, a choice of joining the four external edges of g into pairs, of the three decompositions of v exactly one produces two circuits, and the other ones produce one circuit each, regardless of which particular decomposition of g was chosen. This is shown in [fig. 23](#). These three summands hence contribute $(N^2 + N + N) = N(N + 2)$ to the circuit partition polynomial $J(G, N)$. Since this is true for *every* decomposition of g , we conclude that $J(G, N) = N(N + 2) \cdot J(g, N)$. \square

A special case of [lemma 10](#) occurs if the 4-valent graph g is a single vertex. Then, $J(g, N) = 3$ and we obtain the 3-loop multiedge graph  as the completion of g with

$$J(\text{triangle}, N) = 3N(N + 2), \quad (\text{A.1})$$

which is consistent with the $L = 3$ case of (2.5) in [example 1](#). If we transform J into T ([definition 2](#)), the factor 3 in [eq. \(A.1\)](#) is cancelled, and [lemma 10](#) can be written as

$$T(G, N) = T(\text{triangle}, N) T(g, N), \quad T(\text{triangle}, N) = \frac{N(N + 2)}{3}. \quad (\text{A.2})$$

The other way round, starting from a vacuum graph G , we obtain the $O(N)$ symmetry factor of any decomposition $G \setminus \{v\}$ as

$$T(G \setminus \{v\}, N) = \frac{T(G, N)}{T(\text{triangle}, N)} \quad (\text{A.3})$$

This in particular implies that all decompositions g of a vacuum graph G share the same $O(N)$ symmetry factor $T(g, N)$, even if they are non-isomorphic graphs.

Example 13. *The vacuum graph G shown in [fig. 3](#) has*

$$T(G, N) = \frac{1}{3^7} (1056N + 900N^2 + 216N^3 + 15N^4) = \frac{1}{3^6} N(N + 2)(N + 8)(5N + 22).$$

Each of the (non-isomorphic) decompositions shown in [fig. 3](#) has, by explicit calculation,

$$T(G \setminus \{v\}, N) = \frac{1}{729} (176 + 62N + 5N^2) = \frac{1}{3^6} (N + 8)(5N + 22).$$

This is the expected result from [eq. \(A.3\)](#).

To generalize [lemma 10](#) to the full statement of [lemma 2](#), we need decompositions of $(2p)$ -valent vertices, where p is an integer. A 2-valent vertex ($p = 1$) has only a single decomposition, and for $p = 2$ we obtain the three choices shown in [fig. 1](#). In general, the decomposition of a $(2p)$ -valent vertex is the sum over all $(2p - 1)!! = (2p - 1)(2p - 3)(2p - 5) \cdots 1$ choices to match the $(2p)$ adjacent edges into pairs.

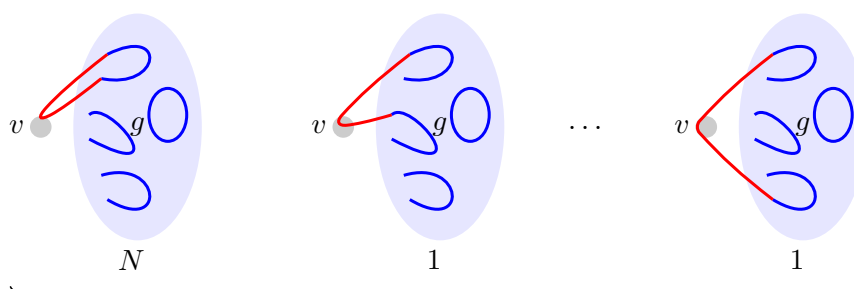
Lemma 11. *Let p be a positive integer and let g be a $(2p)$ -valent graph with completion $G = g \uplus \{v\}$ ([definition 4](#)). Then*

$$J(G, N) = \left(\prod_{j=0}^{p-1} (N + 2j) \right) \cdot J(g, N).$$

Proof. We use induction. For $p = 1$, the completion vertex v is 2-valent and hence has only a single decomposition. This decomposition joins the two external edges of g and gives rise to one new circuit, so $J(G, N) = N \cdot J(g, N)$. For $p = 2$, the statement is [lemma 10](#). Assume that the statement is true for g with $2p - 2$ external edges.

Fix any one decomposition of g . It implies a matching of the $2p$ external edges of g into pairs. Without loss of generality, assume that edge 1 is matched to edge 2 within g as

shown in fig. 24. The decompositions of the completion vertex v are pairs, too. Consider the edge that is matched to edge 1. If it is edge 2, a new circuit arises, giving rise to a factor N . If it is any one of the $2p - 2$ other external edges, no circuit is created and we obtain a factor of $2p - 2$ by summing over these cases, see fig. 24. In all cases, the remaining graph has $2p - 2$ unmatched edges, and its completion can be obtained from the induction hypothesis. We thus have $J(G, N) = (N + 2(p - 1)) \cdot (\prod_{j=0}^{p-2} (N + 2j)) \cdot J(g, N)$ and the claim follows. \square



total factor $N + 1 + \dots + 1 = N + (2p - 2)$, remaining g has $2(p - 1)$ external edges.

Figure 24: Induction step of lemma 11. Fix an arbitrary decomposition in the $(2p)$ -valent graph g . This implies a choice to connect the $(2p)$ external edges into pairs, indicated by blue arcs. In the decompositions of v , there are $(2p - 1)$ ways to connect the first external edge, shown in red. In the first case, a factor N arises (left), but not in the $(2p - 2)$ remaining cases.

When the graph g in lemma 11 is itself a $2p$ -valent vertex, the completion $G = \textcircled{g}$ is a $(2p - 1)$ -loop multiedge. A $(2p)$ -valent vertex has $(2p - 1)!!$ decompositions, consequently the circuit partition polynomial of $J(G, N)$ must have $((2p - 1)!!)^2$ terms. The product in lemma 11 has only $(2p - 1)!!$ factors, therefore every factor occurs $(2p - 1)!!$ times. We obtain lemma 1, $J(\textcircled{g}, N) = (2p - 1)!! \prod_{j=0}^{p-1} (N + 2j)$.

Example 14. *Joining two fish graphs (each of which has four external edges) produces 24 summands. Eight of them are isomorphic to a ring of four double edge graphs, and 16 are isomorphic to another five-loop graph, as shown in fig. 25. Upon identifying isomorphic graphs and dividing by $4! = 24$, we obtain $\textcircled{g} \uplus \textcircled{g} = \frac{1}{3}G_1 + \frac{2}{3}G_2$.*

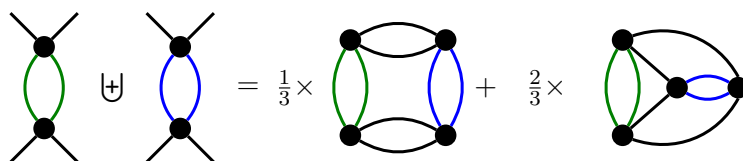


Figure 25: Joining two fish graphs in all possible ways (definition 3) gives rise to eight copies of G_1 and 16 copies of G_2 . Dividing by $4!$ yields the shown multiplicities.

Lemma 11 holds not only for completions $g \uplus \{v\}$, but also for joining two arbitrary $(2p)$ -valent graphs $g_1 \uplus g_2$ according to definition 3. This becomes obvious once one

realizes that it is equivalent to sum over all decompositions of the completion vertex v (as done in the proof of [lemma 11](#)), or to fix one decomposition of v and instead sum over all permutations of the external edges of g . Stated more formally:

Lemma 12. *The sum over all channels, and over all vertex decompositions, of a $(2p)$ -valent graph g has the same external structure (i.e. the same pattern of external edges being joined into pairs) as the sum over all decompositions of a $(2p)$ -valent vertex. The constant of proportionality is the circuit partition polynomial $J(g, N)$.*

Proof. According to [definition 1](#), the circuit partition polynomial is a sum over all decompositions of the vertices of g . Let ζ be one of these decompositions. ξ implies a partition of the external edges of g into pairs, as illustrated in [fig. 2](#). If we join g to another $(2p)$ -valent graph g_2 , the operation $g \uplus g_2$ involves a sum over all permutations of the external edges of g . This sum results in an induced sum for each of the decompositions ζ . Instead of first summing over all decompositions, and then summing each term over the permutations, we may exchange the order of summation. Regardless of the details of the individual decomposition ζ , the sum over its external edges is always the same: It is a symmetric sum over all ways of pairing the external edges. But the latter is exactly what it means to decompose a single vertex, see [fig. 1](#), so we have

$$\begin{aligned} \sum_{\substack{\text{permutations of} \\ \text{external edges of } g}} \sum_{\substack{\text{decompositions } \zeta \\ \text{of permuted } g}} N^{\#\text{circuits}} &= \sum_{\substack{\text{decompositions } \zeta \\ \text{of } g}} \sum_{\substack{\text{permutations of} \\ \text{external edges of } \zeta}} N^{\#\text{circuits}} \\ &= \left(\sum_{\substack{\text{decompositions } \zeta \\ \text{of } g}} N^{\#\text{circuits}} \right) \cdot \sum_{\substack{\text{decompositions} \\ \text{of a } (2p)\text{-valent vertex}}} \end{aligned}$$

The factor in parentheses is the circuit partition polynomial of g . □

$$\begin{aligned} \text{fish graph} + \text{fish graph} + \text{fish graph} &\rightarrow 8 \times \left(\text{blue vertex} + \text{blue vertex} + \text{blue vertex} \right) \\ &+ 1 \times \left(\text{white vertex} \right) \end{aligned}$$

Figure 26: By [lemma 12](#), the sum over all vertex decompositions, and additionally over all channels, is proportional to the decomposition of a single vertex (highlighted in blue). The proportionality factor is $J(g, N)$, which is $(N + 8)$ for the fish graph, compare [fig. 2](#).

[Figure 26](#) illustrates [lemma 12](#). From the viewpoint of renormalization theory, [lemma 12](#) asserts that quantum corrections to a $(2p)$ -valent vertex, at every loop order, can be interpreted as a redefinition of that vertex (and *not* as introduction of a new $(2p)$ -valent vertex with different tensor structure). In that sense, [lemma 12](#) is the analogue of what would be a Ward- or Slavnov-Taylor identity in a gauge theory: It guarantees that

counterterms do not break the symmetry of the theory. For a (local) gauge symmetry, such identities involve kinematic dependences, but this is not the case for the present (global) $O(N)$ symmetry.

Combining [lemma 11](#) with [lemma 12](#), we see that circuit partition polynomials factorize not only upon adjoining a completion vertex v , but whenever two graphs are joined in all possible ways according to [definition 3](#).

Lemma 13. *Let p be a positive integer. Denote by $J(G, N)$ the circuit partition polynomial ([definition 1](#)), and by \uplus the joining operation ([definition 3](#)).*

1. *Let g_1 be a $(2p)$ -valent graph with completion $G_1 = g_1 \uplus \{v\}$ ([definition 4](#)). Then*

$$J(G, N) = \left(\prod_{j=0}^{p-1} (N + 2j) \right) \cdot J(g_1, N).$$

2. *Let g_2 be another $(2p)$ -valent graph (possibly isomorphic to g_1). Then*

$$J(g_1 \uplus g_2, N) = \left(\prod_{j=0}^{p-1} (N + 2j) \right) \cdot J(g_1, N) \cdot J(g_2, N).$$

The union $g_1 \uplus g_2$ of graphs ([definition 3](#)) can equivalently be interpreted as first completing $G_2 = g_2 \uplus \{v\}$, and then inserting g_1 in place of the completion vertex v . This allows for one more level of generalization of [lemma 13](#), namely, one can insert into a vertex of a non-completed graph, and obtain another non-completed graph (whereas the operation \uplus always produces completions). The appropriate factorization formula for that case can be obtained by first completing $g_2 \cup \{v\}$, then inserting into $v_2 \in g_2$, where $v_2 \neq v$, and finally removing v from the resulting completion. If all $J(G, N)$ are transformed into $T(G, N)$, this finally proves [lemma 2](#) from [section 2.1](#). [Lemma 3](#) is then an immediate corollary, upon recalling [lemma 12](#).

Example 15. *Consider the two possibilities of merging two fish graphs. A fish graph has three distinct channels, shown in [fig. 26](#). Merging the two graphs produces the two non-isomorphic graphs shown in [fig. 25](#). One of the three possibilities results in a five-loop “ring” graph G_1 of four fish, whose $O(N)$ -symmetry factor has been computed in [example 1](#),*

$$T(G_1, N) = \frac{N(N+2)(N^2+6N+20)}{81}.$$

The remaining two channels produce isomorphic graphs. Decomposing any of their vertices results in a three-loop multiedge with one tadpole and two copies of four-loop ring graphs. Together, the $O(N)$ -symmetry factor of these graphs is

$$T(G_2, N) = \frac{1}{3} \frac{N+2}{3} N \frac{N+2}{3} + \frac{2}{3} \frac{N(N+2)(N+8)}{27} = \frac{N(N+2)(5N+22)}{81}.$$

By adding these two terms, we confirm [lemma 2](#). Indeed, we find

$$\begin{aligned} \frac{1}{3} T(G_1, N) + \frac{2}{3} T(G_2, N) &= \frac{N(N+2)(N+8)^2}{243} = \frac{N(N+2)}{3} \frac{N+8}{9} \frac{N+8}{9} \\ &= T(\text{fish}, N) T(g, N) T(g, N). \end{aligned}$$

B. Tables

L	N^0	N^1	N^2	N^3	N^4	N^5	N^6	N^7	N^8	N^9	N^{10}
1	2.66667(1)	0.333335(2)									
3	11.75344(3)	2.671236(3)									
4	95.2440(3)	28.16354(8)	1.024129(3)								
5	1.226284(7) ³	438.766(3)	33.1116(2)								
6	16.49034(6) ³	6.87280(3) ³	751.562(3)	16.06524(5)							
7	240.5389(6) ³	113.6758(3) ³	16.03469(4) ³	672.775(2)	2.59286(2)						
8	3.739433(7) ⁶	1.965620(4) ⁶	335.6488(7) ³	20.83929(5) ³	337.3748(8)						
9	61.4643(2) ⁶	35.41073(7) ⁶	7.03789(2) ⁶	572.453(2) ³	16.79838(5) ³	88.9654(4)					
10	1.061828(1) ⁹	662.7130(6)	149.2471(2) ⁶	14.88098(2) ⁶	634.029(1) ³	8.68937(2) ³	9.51925(9)				
11	19.197780(8) ⁹	12.857492(6) ⁹	3.217478(2) ⁹	377.0775(2) ⁶	20.96349(1) ⁶	481.1632(3) ³	2.822003(4) ³				
12	362.13909(8) ⁹	258.20912(6) ⁹	70.73210(2) ⁹	9.465852(2) ⁹	645.2312(2) ⁶	20.914424(6) ⁶	254.8850(2) ³	523.581(2)			
13	7.111467(2) ¹²	5.361932(2) ¹²	1.5889419(4) ¹²	237.73172(6) ⁹	19.076888(5) ⁹	797.4419(3) ⁶	15.244803(7) ⁶	93.2975(2) ³	42.1726(2)		
14	145.3(3) ¹²	115.2(3) ¹²	36.57(9) ¹²	6.02(2) ¹²	553(3) ⁹	28.2(2) ⁶	743(9) ⁶	8.3(3) ⁶	22.5672(1) ³		
15	3.068(8) ¹⁵	2.543(8) ¹⁵	858(3) ¹²	153.3(7) ¹²	15.8(1) ¹²	943(9) ⁹	31.5(5) ⁹	0.53(2) ⁹	3.5(5) ⁶	3.246120(8) ³	
16	67.0(6) ¹⁵	57.7(6) ¹⁵	20.5(3) ¹⁵	3.92(6) ¹⁵	441(8) ¹²	29.7(7) ¹²	1.16(4) ¹²	24(2) ⁹	0.23(4) ⁹	> 9(1) ³	209.836(3)

57

Table 3: Coefficients of N of the primitive beta function in 4 dimensions. The notation $12.34(5)^6$ is a shorthand for $(12.34 \pm 0.05) \cdot 10^6$, where the uncertainty is one standard deviation. The leading coefficients for $L \geq 11$ result from new numerical integration, all other values from the data set of [34]. We confirm the observation of section 4.3, namely that, despite the presence of terms of high order in N , the coefficients of N^0 or N^1 are numerically larger by far.

L	$N = -6$	$N = -4$	$N = -2$	$N = -1$	$N = 0$	$N = 1$	$N = 2$	$N = 3$	$N = 4$	$N = 5$
1	0.66666(1)	1.33334(1)	2.00001(2)	2.33335(2)	2.66668(2)	3.00002(2)	3.33335(3)	3.66668(3)	4.00003(4)	4.33336(2)
3	-4.273978(9)	1.068494(3)	6.41097(2)	9.08220(2)	11.75344(3)	14.42467(4)	17.09591(4)	19.76715(5)	22.43838(5)	25.10962(6)
4	-36.8686(1)	-1.024129(3)	43.0134(2)	68.1046(2)	95.2440(3)	124.4316(4)	155.6676(5)	188.9517(5)	224.2842(6)	261.6649(7)
5	-214.291(2)	1.00792(9)	481.199(3)	820.630(5)	1.126284(7) ³	1.69816(1) ³	2.23626(2) ³	2.84059(2) ³	3.51113(2) ³	4247.90(3)
6	-1.160331(4) ³	-4.0506(2)	5.62246(2) ³	10.35304(4) ³	16.49035(6) ³	24.13078(8) ³	33.3707(2) ³	44.3066(2) ³	57.0347(2) ³	71.6516(3) ³
7	-6.22640(2) ³	-3.235(2)	71.9853(2) ³	142.2276(4) ³	240.5389(6) ³	370.9248(9) ³	537.453(2) ³	744.253(2) ³	995.519(3) ³	1.295503(4) ⁶
8	-34.9763(2) ³	-11.99(1)	989.470(2) ³	2.088956(3) ⁶	3.739425(6) ⁶	6.06186(1) ⁶	9.18536(2) ⁶	13.2471(3) ⁶	18.39233(3) ⁶	24.77452(5) ⁶
9	-206.792(3) ³	-8.6(2)	14.48076(3) ⁶	32.53576(6) ⁶	61.4644(2) ⁶	104.5024(2) ⁶	165.2889(4) ⁶	247.8765(5) ⁶	356.7427(7) ⁶	496.799(1) ⁶
10	-1.26654(2) ⁶	-6.8(5)	224.2097(2) ⁶	534.1068(5) ⁶	1.061829(1) ⁹	1.889313(2) ⁹	3.113716(3) ⁹	4.848456(5) ⁹	7.22427(7) ⁹	10.39026(1) ⁹
11	-7.89133(7) ⁶	31(2)	3.656288(2) ⁹	9.201175(4) ⁹	19.197780(8) ⁹	35.67128(2) ⁹	61.1029(3) ⁹	98.72568(4) ⁹	152.11128(7) ⁹	225.7068(1) ⁹
12	-49.5188(5) ⁶	84(9)	62.59314(2) ⁹	165.82079(4) ⁹	362.13909(8) ⁹	701.2126(2) ⁹	1.2482219(3) ¹²	2.0864662(5) ¹²	3.3201518(7) ¹²	5.077369(2) ¹²
13	-312.076(7) ⁶	110(111)	1.1221927(3) ¹²	3.1190391(8) ¹²	7.111465(2) ¹²	14.319958(4) ¹²	26.424680(7) ¹²	45.66681(2) ¹²	74.96131(2) ¹²	118.02171(3) ¹²
14	0(2) ⁹	-25(16) ⁶	21.04(3) ¹² 21.03(1)¹²	61.2(1) ¹² 61.12(1)¹²	145.3(3) ¹² 145.11(7)¹²	303.6(7) ¹² 303.30(4)¹²	580(2) ¹² 579.3(1)¹²	1.0337(3) ¹⁵ 1.0336(3)¹⁵	1.750(5) ¹⁵ 1.746(1)¹⁵	2.834(9) ¹⁵ 2.831(2)¹²
15	-38(27) ⁹	100(240) ⁶	410.7(8) ¹² 411.47(6)¹²	1.244(3) ¹⁵ 1.2470(2)¹⁵	3.08(2) ¹⁵ 3.081(5)¹⁵	6.64(2) ¹⁵ 6.655(1)¹⁵	13.10(5) ¹⁵ 13.131(9)¹⁵	24.09(9) ¹⁵ 24.14(3)¹⁵	41.9(2) ¹⁵ 42.03(1)¹⁵	69.7(4) ¹⁵ 69.91(4)¹⁵
16	0(2) ¹²	0(8) ⁹	8.34(5) ¹⁵ 8.39(2)¹⁵	26.2(2) ¹⁵ 26.44(3)¹⁵	67.0(6) ¹⁵ 67.5(2)¹⁵	150(2) ¹⁵ 151.14(6)¹⁵	304(4) ¹⁵ 306.9(8)¹⁵	574(7) ¹⁵ 583(1)¹⁵	1.03(2) ¹⁸ 1.043(4)¹⁸	1.75(3) ¹⁸ 1.781(3)¹⁸
17	0(23) ¹²	0(120) ⁹	178(2) ¹⁵	580(6) ¹⁵	1.53(2) ¹⁸	3.53(5) ¹⁸ 3.553(9)¹⁸	7.4(2) ¹⁸	14.4(3) ¹⁸	26.3(5) ¹⁸	46.0(2) ¹⁸
18	-1.1(9) ¹⁵	0(3) ¹²	3.97(8) ¹⁸	13.4(4) ¹⁸	37(2) ¹⁸	87(3) ¹⁸	187(8) ¹⁸	370(20) ¹⁸	700(40) ¹⁸	1.25(8) ²¹

Table 4: Evaluations of the primitive beta function at specific values of N . For $N \geq -2$, the beta function grows monotonically with N . For $L > 1$, the function has a zero close to $N = -4$, this is reflected by a comparably small function value at $N = -4$. The notation $0(a)^b$ indicates that the value is indistinguishable from zero with an uncertainty of $a \cdot 10^b$.

For $L \geq 14$, the values arise from uniform non-complete samples of [7], hence their uncertainty is notably larger than for $L \leq 13$. These values are written in small print. In particular, for $L \in \{17, 18\}$, the samples are so small that the uncertainty estimate might be too optimistic. Bold font indicates that a value has been obtained with the importance sampling algorithm of [34], these are still non-complete samples, but more accurate than the uniform sample (given above the bold value).

L	N^0	N^1	N^2	N^3	N^4	N^5	N^6	N^7	$\langle k \rangle_L$
1	$\frac{1}{2}$	$\frac{1}{16}$							0.111
3	$\frac{11}{4}$	$\frac{5}{8}$							0.185
4	$\frac{93}{4}$	$\frac{55}{8}$	$\frac{1}{4}$						0.243
5	340	$\frac{973}{8}$	$\frac{147}{16}$						0.297
6	5500	$\frac{18259}{8}$	$\frac{3949}{16}$	5					0.347
7	$\frac{405351}{4}$	$\frac{189811}{4}$	656	$\frac{8395}{32}$	$\frac{7}{8}$				0.394
8	$\frac{8297865}{4}$	$\frac{4297721}{4}$	178559	$\frac{336221}{32}$	$\frac{1211}{8}$				0.438
9	46581140	$\frac{105141971}{4}$	$\frac{40380769}{8}$	$\frac{12386715}{32}$	$\frac{654445}{64}$	44			0.480
10	1136329932	$\frac{2761781725}{4}$	$\frac{1193546199}{8}$	$\frac{446298325}{32}$	$\frac{34315811}{64}$	$\frac{49435}{8}$	5		0.519
11	$\frac{119592596531}{4}$	$\frac{155018200259}{8}$	$\frac{9243683059}{2}$	$\frac{16159964821}{32}$	$\frac{405018107}{16}$	$\frac{63513385}{128}$	$\frac{72137}{32}$		0.556
12	$\frac{3374570327461}{4}$	$\frac{4630005232849}{8}$	$\frac{600700832091}{4}$	$\frac{596312684627}{32}$	$\frac{18283668245}{16}$	$\frac{4077699355}{128}$	$\frac{19881095}{64}$	$\frac{3619}{8}$	0.590

Table 5: For every loop order L , this table shows the coefficients of N dependence of $p_L(N)$ according to eq. (3.17), multiplied by $\frac{3^{L+1}}{4!}$. This is the sum of the circuit partition polynomials $J(g, N)$ of primitive decompletions g , weighted by their automorphism symmetry factor (where external vertices are fixed, or equivalently a factor $4!$ is included). Although the degree of these polynomials grows with L (see lemma 5), the average order $\langle k \rangle_L$ (eq. (3.19)) does not even reach unity for $L \leq 12$.

L	N^0	N^1	N^2	N^3	N^4	N^5	N^6	N^7	$\langle k \rangle_L$
1	8	1							0.111
3	66	15							0.185
4	186	55	2						0.243
5	1,054	375	29						0.297
6	7,564	3,048	317	6					0.338
7	59,986	27,839	3,858	169	2				0.393
8	601,600	308,644	51,092	3081	50				0.436
9	7,973,840	4,491,030	868,191	68,983	2,065	14			0.481
10	136,783,626	83,167,949	18,098,205	1,734,427	71,781	1,046	4		0.521
11	2,831,713,102	1,840,518,187	442,488,075	49,304,820	2,588,273	56,598	347		0.558
12	68,493,277,652	47,153,165,436	12,325,920,197	1,552,897,804	98,221,630	2,916,283	32,440	73	0.593

Table 6: Analogous to table 5, but disregarding automorphism symmetry factors. Note the substantial numerical difference with respect to table 5 at small N , indicating a large influence of automorphisms.

Quantity	Prefactor	u^0	u^1	u^2	u^3
$\mathcal{A}_h^{\frac{3}{2}} \partial_j^0 W _{j=0}$	$\frac{\hbar^{-\frac{N-3}{2}} 3^{\frac{N-1}{2}}}{\sqrt{2\pi}\Gamma(\frac{N}{2})}$	1	$-\frac{N^2-2N+4}{12}$	$\frac{96-104N+24N^2-8N^3+N^4}{288}$	$\frac{N^6+18N^5-124N^4+600N^3-3568N^2+6432N-5760}{10368}$
$\mathcal{A}_h^{\frac{3}{2}} \partial_j^2 W _{j=0}$	$\frac{\hbar^{-\frac{N+1}{2}} 3^{\frac{N-1}{2}}}{2\sqrt{2\pi}\Gamma(\frac{N+2}{2})}$	6	$-\frac{N(N+2)}{3}$	$\frac{N(N+2)(N^2-2N-12)}{48}$	$\frac{N(N+2)(N^4-8N^3-16N^2+200N+480)}{1728}$
$\mathcal{A}_h^{\frac{3}{2}} \partial_j^4 W _{j=0}$	$\frac{\hbar^{-\frac{N+5}{2}} 3^{\frac{N-1}{2}}}{\frac{4}{3}\sqrt{2\pi}\Gamma(\frac{N+4}{2})}$	36	$-3(N+2)(N+4)$	$\frac{(N+2)(N^3+6N^2-12N-32)}{8}$	$\frac{(N+2)(N^5+4N^4-64N^3+8N^2+960N+1152)}{288}$
$\mathcal{A}_h^{\frac{3}{2}} \partial_\varphi^2 G _0$	$\frac{\hbar^{-\frac{N+1}{2}} 3^{\frac{N-1}{2}}}{2\sqrt{2\pi}\Gamma(\frac{N+2}{2})}$	6	$\frac{(N+2)(N+4)}{2}$	$\frac{(N+2)(N+4)(N^2+2N-12)}{48}$	$\frac{(N+2)(N+4)(N^4-40N^2+72N+768)}{1728}$
$\mathcal{A}_h^{\frac{3}{2}} \partial_\varphi^4 G _0$	$\frac{\hbar^{-\frac{N+5}{2}} 3^{\frac{N-1}{2}}}{\frac{4}{3}\sqrt{2\pi}\Gamma(\frac{N+4}{2})}$	36	$-3(N+2)(N+12)$	$\frac{N(N+2)(100+22N+N^2)}{8}$	$\frac{-(N+2)(4992-192N+8N^2+176N^3+28N^4+N^5)}{288}$
$\mathcal{A}_h^{\frac{3}{2}} \hbar_{\mathcal{R}}$	$\frac{\hbar^{-\frac{N+3}{2}} 3^{\frac{N-1}{2}}}{\frac{4}{3}\sqrt{2\pi}\Gamma(\frac{N+4}{2})}$	36	$-3(N+2)(N+8)$	$-\frac{(N+2)(N+4)(12-10N-N^2)}{8}$	$\frac{(N+2)(N+4)(1056-120N-40N^2+12N^3+N^4)}{288}$
$\mathcal{A}_{\hbar_{\mathcal{R}}}^{\frac{3}{2}} \hbar$	$\frac{\hbar_{\mathcal{R}}^{-\frac{N+3}{2}} 3^{\frac{N-1}{2}}}{\frac{4}{3}\sqrt{2\pi}\Gamma(\frac{N+4}{2})} e^{-\frac{12+3N}{4}}$	-36	$\frac{-9N^2+60N+336}{2}$	$-\frac{(N+4)(9N^3-172N^2+552N+2368)}{32}$	$-\frac{(N+4)(27N^5-792N^4+6088N^3+3872N^2-144256N-363008)}{2304}$
$\mathcal{A}_{\hbar_{\mathcal{R}}}^{\frac{3}{2}} z^{(4)}$	$\frac{\hbar_{\mathcal{R}}^{-\frac{N+5}{2}} 3^{\frac{N-1}{2}}}{\frac{4}{3}\sqrt{2\pi}\Gamma(\frac{N+4}{2})} e^{-\frac{12+3N}{4}}$	-36	$\frac{-9N^2-12N-240}{2}$	$-\frac{9N^4-40N^3-488N^2-416N+1664}{32}$	$-\frac{27N^6-252N^5-1880N^4+960N^3+21376N^2-59904N-419840}{2304}$

Table 7: Asymptotic growth coefficients of 1PI Green function, renormalized coupling and counterterms computed in [section 3.4](#), see [section 5.1](#). Here $u = \hbar$ or $u = \hbar_{\mathcal{R}}$, depending on the argument as indicated by $\mathcal{A}_u^{\frac{3}{2}}$. Setting $N = 1$, the series reproduce [\[37\]](#). Notice that the prefactor and leading terms of $\partial_j^4 W$, $\partial_\varphi^4 G$, and $z^{(4)}$ coincide up to $e^{-\frac{15+3N}{4}}$. This means that to asymptotic leading order, the number of connected-, 1PI-, and primitive vertex type graphs is the same up to $e^{-\frac{15+3N}{4}}$. The distinction between these classes results in a subleading change in their number.

References

- ¹D. Kreimer, “Anatomy of a gauge theory”, *Annals of Physics* **321**, 2757–2781 (2006).
- ²W. D. van Suijlekom, “Renormalization of Gauge Fields: A Hopf Algebra Approach”, *Communications in Mathematical Physics* **276**, 773–798 (2007).
- ³D. Kreimer, “On Overlapping Divergences”, *Communications in Mathematical Physics* **204**, 669–689 (1999).
- ⁴M. Borinsky, *Graphs in Perturbation Theory: Algebraic Structure and Asymptotics*, Springer Theses (Springer International Publishing, Cham, 2018), <http://link.springer.com/10.1007/978-3-030-03541-9>.
- ⁵A. J. McKane and D. J. Wallace, “Instanton calculations using dimensional regularisation”, *J. Phys. A* **11**, 2285 (1978), <https://dx.doi.org/10.1088/0305-4470/11/11/013>.
- ⁶A. J. McKane, “Perturbation expansions at large order: Results for scalar field theories revisited”, *Journal of Physics A: Mathematical and Theoretical* **52**, 055401 (2019).
- ⁷P.-H. Balduf, “Statistics of Feynman amplitudes in ϕ^4 -theory”, *Journal of High Energy Physics* **2023.11**, 160 (2023).
- ⁸L. Dolan and R. Jackiw, “Symmetry behavior at finite temperature”, *Phys. Rev. D* **9**, 3320–3341 (1974).
- ⁹H. J. Schnitzer, “Hartree approximation in relativistic field theory”, *Phys. Rev. D* **10**, 2042 (1974).
- ¹⁰S. Coleman, R. Jackiw, and H. D. Politzer, “Spontaneous symmetry breaking in the $O(N)$ model for large N ”, *Phys. Rev. D* **10**, 2491 (1974).
- ¹¹A. N. Vasil’ev, Yu. M. Pis’mak, and Yu. R. Khonkonen, “Simple method of calculating the critical indices in the $1/n$ expansion”, *Theor. Math. Phys.* **46**, 104–113 (1981).
- ¹²A. N. Vasiliev, Yu. M. Pismak, and Yu. R. Khonkonen, “ $1/N$ Expansion: Calculation of the exponents η and ν in the order $1/N^3$ for arbitrary number of dimensions”, *Theor. Math. Phys.* **47**, 465–475 (1981).
- ¹³A. N. Vasiliev, Yu. M. Pismak, and Yu. R. Khonkonen, “ $1/N$ expansion: Calculation of the exponent η in the order $1/N^3$ by the conformal bootstrap method”, *Theor. Math. Phys.* **50**, 127–134 (1982).
- ¹⁴J. Zinn-Justin, “Vector models in the large N limit: A few applications”, in *11th Taiwan Spring School on Particles and Fields* (1998).
- ¹⁵M. Moshe and J. Zinn-Justin, “Quantum field theory in the large N limit: A Review”, *Phys. Rept.* **385**, 69–228 (2003).
- ¹⁶D. J. Gross and A. Neveu, “Dynamical symmetry breaking in asymptotically free field theories”, *Physical Review D* **10**, 3235–3253 (1974).
- ¹⁷C. Boehmer and M. Thies, “Large N solution of generalized Gross-Neveu model with two coupling constants”, *Physical Review D* **80**, 125038 (2009).
- ¹⁸J. A. Gracey, “Large N_f quantum field theory”, *International Journal of Modern Physics A* **33**, 1830032 (2018).
- ¹⁹G. t’Hooft, “A planar diagram theory for strong interactions”, *Nuclear Physics B* **72**, 461 (1974).
- ²⁰P. Di Francesco, “2D quantum gravity, matrix models and graph combinatorics”, in *NATO Advanced Study Institute: Marie Curie Training Course: Applications of Random Matrices in Physics* (2004), pp. 33–88.
- ²¹R. G. Gurau, “Notes on tensor models and tensor field theories”, *Ann. Inst. H. Poincaré D Comb. Phys. Interact.* **9**, 159–218 (2022).
- ²²C. Jepsen and Y. Oz, “RG flows and fixed points of $O(N)^r$ models”, *Journal of High Energy Physics* **2024**, 35 (2024).
- ²³R. G. Gurău, ed., *Random Tensors* (Oxford University Press, 2016), <https://doi.org/10.1093/acprof:oso/9780198787938.001.0001>.
- ²⁴R. G. Gurau and G. Schaeffer, “Regular colored graphs of positive degree”, *Annales de l’Institut Henri Poincaré D* **3**, 257–320 (2016).
- ²⁵R. Delbourgo, A. C. Kalloniatis, and G. Thompson, “Dimensional renormalization: Ladders and rainbows”, *Physical Review D* **54**, 5373–5376 (1996).
- ²⁶D. J. Broadhurst and D. Kreimer, “Exact solutions of Dyson-Schwinger equations for iterated one-loop integrals and propagator-coupling duality”, *Nuclear Physics B* **600**, 403–422 (2001).
- ²⁷R. Delbourgo, D. Elliott, and D. S. McAnally, “Dimensional renormalization in Φ^3 theory: Ladders and rainbows”, *Physical Review D* **55**, 5230–5233 (1997).

- ²⁸D. Kreimer and K. Yeats, “An Etude in non-linear Dyson–Schwinger Equations”, *Nuclear Physics B - Proceedings Supplements, Proceedings of the 8th DESY Workshop on Elementary Particle Theory* **160**, 116–121 (2006).
- ²⁹O. Krüger and D. Kreimer, “Filtrations in Dyson–Schwinger equations: Next-to-j-leading log expansions systematically”, *Annals of Physics* **360**, 293–340 (2015).
- ³⁰O. Krüger, “Log expansions from combinatorial Dyson–Schwinger equations”, *Letters in Mathematical Physics* **110**, 2175–2202 (2020).
- ³¹J. Courtiel and K. Yeats, “Next-to-k Leading Log Expansions by Chord Diagrams”, *Communications in Mathematical Physics* **377**, 469–501 (2020).
- ³²J. Courtiel and K. Yeats, “Terminal chords in connected chord diagrams”, *Ann. Inst. H. Poincaré D Comb. Phys. Interact.* **4**, 417–452 (2017).
- ³³E. Panzer and K. Yeats, *Feynman symmetries of the Martin and c_2 invariants of regular graphs*, (2023) <http://arxiv.org/abs/2304.05299>, pre-published.
- ³⁴P.-H. Balduf and K. Shaban, “Predicting Feynman periods in ϕ^4 -theory”, *Journal of High Energy Physics* **2024**, 38 (2024).
- ³⁵D. Kreimer, “A remark on quantum gravity”, *Annals of Physics* **323**, 49–60 (2008).
- ³⁶H. Kibler, “Off-shell diagrammatics for quantum gravity”, *Physics Letters B* **816**, 136219 (2021).
- ³⁷M. Borinsky, “Renormalized asymptotic enumeration of Feynman diagrams”, *Annals of Physics* **385**, 95–135 (2017).
- ³⁸V. Bonzom, R. Gurau, A. Riello, and V. Rivasseau, “Critical behavior of colored tensor models in the large N limit”, *Nuclear Physics B* **853**, 174–195 (2011).
- ³⁹A. Pelissetto and E. Vicari, “Critical phenomena and renormalization-group theory”, *Physics Reports* **368**, 549–727 (2002).
- ⁴⁰B. G. Nickel, D. I. Meiron, and G. A. Baker Jr., “Compilation of 2-pt. and 4-pt. graphs for continuous spin models”, *University of Guelph Report* (1977), <http://users.physik.fu-berlin.de/~kleinert/nickel/guelph.pdf>.
- ⁴¹H. Kleinert and V. Schulte-Frohlinde, *Critical Properties of ϕ^4 -Theories* (World Scientific, 2001), 512 pp., <https://hagenkleinert.de/documents/phi4/phi4.pdf>.
- ⁴²J. A. Ellis-Monaghan, “New Results for the Martin polynomial”, *Journal of Combinatorial Theory, Series B* **74**, 326–352 (1998).
- ⁴³J. Thürigen, “Renormalization in Combinatorially Non-Local Field Theories: The Hopf Algebra of 2-Graphs”, *Math. Phys. Anal. Geom.* **24**, 19 (2021).
- ⁴⁴J. Thürigen, “Renormalization in Combinatorially Non-Local Field Theories: the BPHZ Momentum Scheme”, *SIGMA* **17**, 094 (2021).
- ⁴⁵A. Hock and J. Thürigen, *Combinatorial Dyson-Schwinger Equations of Quartic Matrix Field Theory*, (2024) pre-published.
- ⁴⁶R. Gurau, “Lost in translation: topological singularities in group field theory”, *Class. Quant. Grav.* **27**, 235023 (2010).
- ⁴⁷P. Martin, “Énumérations eulériennes dans les multigraphes et invariants de Tutte-Grothendieck”, thesis (Institut National Polytechnique de Grenoble - INPG ; Université Joseph-Fourier - Grenoble I, 1977), <https://tel.archives-ouvertes.fr/tel-00287330>.
- ⁴⁸R. Arratia, B. Bollobás, and G. B. Sorkin, “The interlace polynomial of a graph”, *Journal of Combinatorial Theory, Series B, Special Issue Dedicated to Professor W.T. Tutte* **92**, 199–233 (2004).
- ⁴⁹B. Bollobás, “Evaluations of the Circuit Partition Polynomial”, *Journal of Combinatorial Theory, Series B* **85**, 261–268 (2002).
- ⁵⁰J. A. Ellis-Monaghan, “Exploring the Tutte–Martin connection”, *Discrete Mathematics* **281**, 173–187 (2004).
- ⁵¹J. A. Ellis-Monaghan, “Identities for circuit partition polynomials, with applications to the Tutte polynomial”, *Advances in Applied Mathematics, Special Issue on the Tutte Polynomial* **32**, 188–197 (2004).
- ⁵²D. Kreimer, “On the Hopf algebra structure of perturbative quantum field theories”, *Adv. Theor. Math. Phys.* **2**, 303–334 (1998).
- ⁵³A. Connes and D. Kreimer, “Renormalization in quantum field theory and the Riemann-Hilbert problem II: the beta-function, diffeomorphisms and the renormalization group”, *Communications in Mathematical Physics* **216**, 215–241 (2001).
- ⁵⁴W. Zimmermann, “Convergence of Bogoliubovs method of renormalization in momentum space”, *Communications in Mathematical Physics* **15**, 208–234 (1969).

- ⁵⁵D. J. Broadhurst and D. Kreimer, “Knots and Numbers in ϕ^4 Theory to 7 Loops and Beyond”, *International Journal of Modern Physics C* **06**, 519–524 (1995).
- ⁵⁶O. Schnetz, “Quantum periods: A census of ϕ^4 -transcendentals”, *Communications in Number Theory and Physics* **4**, 1–47 (2010).
- ⁵⁷F. C. S. Brown, *On the periods of some Feynman integrals*, (2010) <http://arxiv.org/abs/0910.0114>, pre-published.
- ⁵⁸A. N. Vasilev, *The field theoretic renormalization group in critical behavior theory and stochastic dynamics* (Chapman & Hall, 2004), 704 pp.
- ⁵⁹J. Zinn-Justin, *Quantum Field Theory and Critical Phenomena*, 5th ed. (Oxford University Press, 2021), <https://doi.org/10.1093/oso/9780198834625.001.0001>.
- ⁶⁰P.-H. Balduf, “Dyson–Schwinger equations in minimal subtraction”, *Annales de l’Institut Henri Poincaré D*, **10.4171/aihpd/169** (2023).
- ⁶¹M. V. Kompaniets and E. Panzer, “Minimally subtracted six loop renormalization of $O(n)$ -symmetric ϕ^4 theory and critical exponents”, *Physical Review D* **96**, 036016 (2017).
- ⁶²O. Schnetz, “Numbers and Functions in Quantum Field Theory”, *Physical Review D* **97**, 085018 (2018).
- ⁶³O. Schnetz, “ ϕ^4 Theory at seven loops”, *Physical Review D* **107**, 036002 (2023).
- ⁶⁴L. N. Lipatov, “Divergence of the Perturbation Theory Series and the Quasiclassical Theory”, *Sov. Phys. JETP* **45**, 216–223 (1977).
- ⁶⁵E. Brézin, J. C. Le Guillou, and J. Zinn-Justin, “Perturbation theory at large order. I. The φ^{2N} interaction”, *Physical Review D* **15**, 1544–1557 (1977).
- ⁶⁶A. J. McKane, D. J. Wallace, and O. F. d. A. Bonfim, “Non-perturbative renormalisation using dimensional regularisation: applications to the ε expansion”, *Journal of Physics A: Mathematical and General* **17**, 1861–1876 (1984).
- ⁶⁷M. V. Komarova and M. Yu. Nalimov, “Asymptotic Behavior of Renormalization Constants in Higher Orders of the Perturbation Expansion for the $(4 - \epsilon)$ -Dimensionally Regularized $O(N)$ symmetric ϕ^4 theory”, *Theoretical and Mathematical Physics* **126**, 339–353 (2001).
- ⁶⁸H. Kinkelin, “Ueber eine mit der Gammafunction verwandte Transcendente und deren Anwendung auf die Integralrechnung.”, *Journal für die reine und angewandte Mathematik* **57**, 122–138 (1860).
- ⁶⁹M. Borinsky, “Generating Asymptotics for Factorially Divergent Sequences”, *The Electronic Journal of Combinatorics*, P4.1–P4.1 (2018).
- ⁷⁰D. Benedetti, R. Gurau, H. Keppler, and D. Lettera, “The Small-N Series in the Zero-Dimensional $O(N)$ Model: Constructive Expansions and Transseries”, *Annales Henri Poincaré* **25**, 5367–5428 (2024).
- ⁷¹R. L. Stratonovich, “On a Method of Calculating Quantum Distribution Functions”, *Soviet Physics Doklady* **2**, 416 (1958).
- ⁷²J. Hubbard, “Calculation of Partition Functions”, *Phys. Rev. Lett.* **3**, 77–80 (1959).
- ⁷³K. Byczuk and P. Jakubczyk, “Generalized Gaussian integrals with application to the Hubbard–Stratonovich transformation”, *American Journal of Physics* **91**, 840–846 (2023).
- ⁷⁴V. A. Novikov, M. A. Shifman, A. I. Vainshtein, and V. I. Zakharov, “Two-dimensional sigma models: Modelling non-perturbative effects in quantum chromodynamics”, *Phys. Rept.* **116**, 103 (1984).
- ⁷⁵J. A. Gracey, “Progress with large N_f β -functions”, *Nucl. Instrum. Meth. A, New Computing Techniques in Physics Research V* **389**, 361–364 (1997).
- ⁷⁶J. M. Cornwall, R. Jackiw, and E. Tomboulis, “Effective action for composite operators”, *Physical Review D* **10**, 2428–2445 (1974).
- ⁷⁷J. Berges, “N-particle irreducible effective action techniques for gauge theories”, *Physical Review D* **70**, 105010 (2004).
- ⁷⁸M. E. Carrington and Y. Guo, “Techniques for n -particle irreducible effective theories”, *Physical Review D* **83**, 016006 (2011).
- ⁷⁹F. W. J. Olver, “On an Asymptotic Expansion of a Ratio of Gamma Functions”, *Proceedings of the Royal Irish Academy. Section A: Mathematical and Physical Sciences* **95A**, 5–9 (1995), <https://www.jstor.org/stable/20490148>.
- ⁸⁰P. V. Pobylitsa, *Superfast convergence effect in large orders of the perturbative and ϵ expansions for the $O(N)$ symmetric φ^4 model*, (2008) <https://doi.org/10.48550/arXiv.0807.5136>, pre-published.

- ⁸¹P. V. Pobylitsa, *Anharmonic oscillator, negative dimensions and inverse factorial convergence of large orders to the asymptotic form*, (2008) <https://doi.org/10.48550/arXiv.0807.5032>, pre-published.
- ⁸²V. Bonzom, L. Lionni, and V. Rivasseau, “Colored Triangulations of Arbitrary Dimensions are Stuffed Walsh Maps”, *The Electronic Journal of Combinatorics*, P1.56–P1.56 (2017).
- ⁸³L. Lionni and J. Thürigen, “Multi-critical behaviour of 4-dimensional tensor models up to order 6”, *Nuclear Physics B* **941**, 600–635 (2019).
- ⁸⁴L. Lionni, *Colored Discrete Spaces: Higher Dimensional Combinatorial Maps and Quantum Gravity*, Springer Theses (Springer International Publishing, Cham, 2018), <http://link.springer.com/10.1007/978-3-319-96023-4>.
- ⁸⁵V. Rivasseau, “Loop vertex expansion for higher-order interactions”, *Letters in Mathematical Physics* **108**, 1147–1162 (2018).
- ⁸⁶I. R. Klebanov and A. M. Polyakov, “AdS dual of the critical $O(N)$ vector model”, *Physics Letters B* **550**, 213–219 (2002).
- ⁸⁷N. J. A. Sloane (editor), *The On-Line Encyclopedia of Integer Sequences*, (2023) <https://oeis.org>.
- ⁸⁸B. D. McKay and A. Piperno, “Practical graph isomorphism, II”, *Journal of Symbolic Computation* **60**, 94–112 (2014).
- ⁸⁹F. Brown and O. Schnetz, “Single-valued multiple polylogarithms and a proof of the zig-zag conjecture”, *Journal of Number Theory* **148**, 478–506 (2015).
- ⁹⁰M. Borinsky, H. J. Munch, and F. Tellander, “Tropical Feynman integration in the Minkowski regime”, *Computer Physics Communications* **292**, 108874 (2023).
- ⁹¹M. Borinsky, “Tropical Monte Carlo quadrature for Feynman integrals”, *Annales de l’Institut Henri Poincaré D* **10**, 635–685 (2023).